PolyPublie
Polytechnique Montréal

POLYTECHNIQUE MONTRÉAL
UNIVERSITÉ D'INGÉNIERIE

Titre: Title:	Solution Processable Semiconductor Thin Films: Correlation Between Morphological, Structural, Optical and Charge Transport Properties
Auteur: Author:	Dilek Isik
Date:	2013
Type:	Mémoire ou thèse / Dissertation or Thesis
Référence: Citation:	Isik, D. (2013). Solution Processable Semiconductor Thin Films: Correlation Between Morphological, Structural, Optical and Charge Transport Properties [Thèse de doctorat, École Polytechnique de Montréal]. PolyPublie. https://publications.polymtl.ca/1139/

Document en libre accès dans PolyPublie
Open Access document in PolyPublie

URL de PolyPublie: PolyPublie URL:	https://publications.polymtl.ca/1139/
Directeurs de recherche: Advisors:	Clara Santato, & Sylvain Turenne
Programme: Program:	Génie métallurgique

Ce fichier a été téléchargé à partir de PolyPublie, le dépôt institutionnel de Polytechnique Montréal
This file has been downloaded from PolyPublie, the institutional repository of Polytechnique Montréal

https://publications.polymtl.ca

UNIVERSITÉ DE MONTRÉAL

SOLUTION PROCESSABLE SEMICONDUCTOR THIN FILMS: CORRELATION BETWEEN MORPHOLOGICAL, STRUCTURAL, OPTICAL AND CHARGE TRANSPORT PROPERTIES

DILEK ISIK

DÉPARTEMENT DE GÉNIE PHYSIQUE

ÉCOLE POLYTECHNIQUE DE MONTRÉAL

THÈSE PRÉSENTÉE EN VUE DE L'OBTENTION

DU DIPLÔME DE PHILOSOPHIÆ DOCTOR

(GÉNIE MÉTALLURGIQUE)

MAI 2013

© Dilek Isik, 2013.

UNIVERSITÉ DE MONTRÉAL

ÉCOLE POLYTECHNIQUE DE MONTRÉAL

Cette thèse intitulée:

SOLUTION PROCESSABLE SEMICONDUCTOR THIN FILMS: CORRELATION BETWEEN MORPHOLOGICAL, STRUCTURAL, OPTICAL AND CHARGE TRANSPORT PROPERTIES

présentée par: ISIK, Dilek

en vue de l'obtention du diplôme de : Philosophiæ Doctor

a été dûment acceptée par le jury d'examen constitué de :

M. PETER Yves-Alain, Dr. Sc., président

Mme SANTATO Clara, Ph.D., membre et directrice de recherche

M. TURENNE Sylvain, Ph.D., membre et codirecteur de recherche

M. KYMISSIS Ioannis, Ph.D., membre

M. VETRONE Fiorenzo, Ph.D., membre

DEDICATION

I dedicate this work to my mother and father, Sacide and Ali Osman, and my sisters, Işıl and Meltem, who supported me throughout my life and education. No word can express how much I love you and how much I appreciate you.

"Bilmezdim şarkıların bu kadar güzel,

Kelimelerinse kifayetsiz olduğunu."

Orhan Veli Kanik

ACKNOWLEDGEMENTS

During the past five years, I have had the opportunity to interact with many invaluable colleagues at École Polytechnique de Montréal and with collaborators from other universities. Along the way, I have had the chance to build strong relationships, which I believe will be carried into the future. The process of obtaining my Ph.D. degree in Canada was an exquisite and rewarding experience, which I believe not only contributed to my scientific background and adaptation to a multicultural environment but also helped me in improving my interpersonal relationship and my leadership skills. Having interacted with a large group of people I owe many "Thank you!" for all the support I have received.

This Ph.D. thesis would not have been possible without the guidance of my supervisor Prof. Clara Santato. During the past five years, she was always there for me as a mentor to ensure high quality in our research. I would especially like to thank her for helping me realize my dream towards obtaining my Ph.D. and become an independent researcher and a scientist. I cannot fail to mention that she was always there to lend an ear when I needed one. I have been lucky with all the opportunities given to me for improving and developing my scientific skills. I am also proud to be the first Ph.D. student in her work group, which made my Ph.D. *journey* more interesting.

I would like to thank Prof. Sylvain Turenne for agreeing to be my co-supervisor for the completion of my Ph.D. degree in the Metallurgical Engineering program and for all the help and support he gave me during the past five years.

I would like to thank Prof. Fabio Cicoira, for all the support he gave me during my Ph.D.. I will always remember his contributions to my research and in the preparation of my thesis.

I would like to acknowledge our collaborators from Prof. John Anthony's and Prof. William Skene's groups for their contributions in the presented work.

I have been extremely lucky to learn the basics of semiconductor physics from Prof. R. Masut. I am grateful to him for being so helpful to me when I was trying to enter into the world of semiconductors. Also, I would like to mention Professors Yves-Alain Peter, Gilles L'Esperance, Jean Paul Bailon and Oumarou Savadogo for sharing their knowledge with me through classes or discussions. Many thanks to Prof. Sebastian Francoeur and Gabriel Éthier-

Majcher for their collaboration in obtaining photoluminescence spectra with upconverting materials (article in preparation).

Three summer students who worked with me contributed to the research for this thesis: Philippe Lefebvre, Jonathan Pison and Alexandre Labine. I would like to thank them all for all their work and their friendship in the laboratory.

To Jonathan Pison and Mathieu Maisonneuve, thank you for all the discussions on scientific issues and finally for helping me with the French translations. *Merci beaucoup, encore une fois!*

I would like to thank Ali Reza Mesgar for his friendship and the intellectual discussions we had at school. His expertise in microfabrication processes helped me in the successful completion of my microfabrication project with ITO.

With the help and dedication of Jeremy Lerner I have became an independent user of the PARISS fluorescence hyperspectral imaging system, which permitted to collect a significant part of my research at Ecole Polytechnique.

There are many people I would like to acknowledge who were behind the scenes during my Ph.D.: Dr. Khalid Laaziri, Marie-Hélène Bernier, Patricia Moraille, Jacqueline Sanchez, Christophe Clément, Yves Drolet, Jean Paul Lévesque, Joël Bouchard and Yves Leblanc.

My dear group friends (2008-2013), thank you all for all the useful discussions during group meetings and for your collaborations in the laboratory. I thank to all my friends for the laughter they brought into my life at Ecole Polytechnique. I will always remember them with their warm hearts and big smiles.

The ITO patterning process performed during the Ph.D. was supported by the Canadian Microelectronics Corporation (CMC).

RÉSUMÉ

Cette thèse de doctorat est le résultat d'un travail de recherche multidisciplinaire réunissant divers concepts fondamentaux comme l'ingénierie et la caractérisation des couches minces, l'électrochimie ainsi que la physique des dispositifs à base de couches minces semiconductrices.

L'objet des expériences menées lors du travail de thèse porte sur les couches minces semi-conductrices et leurs interfaces avec des matériaux électroniques ou des couches diélectriques. Le but ultime de la thèse est de mettre en corrélation la morphologie, la structure cristalline et la structure électronique des couches minces, ainsi que leurs propriétés fonctionnelles, avec le fonctionnement des dispositifs électroniques de type transistors utilisant ces mêmes couches minces en tant que matériau actif. En outre, de nouvelles stratégies fondées sur des phénomènes ayant lieu aux interfaces électrolyte/couche mince semiconductrice ont été explorées afin de contrôler la conductivité électrique au sein des couches minces.

Trois principaux systèmes chimiques ont fait l'objet d'études approfondies durant cette thèse: deux types de semiconducteurs organiques (oligomère et polymères dérivés d'azométhine-thiophènes et dérivés solubles de pentacène) et un semi-conducteur métal-oxyde (le trioxyde de tungstène, WO_3).

Dans le but d'explorer les propriétés morphologiques de couches minces à base de semiconducteurs organiques, les microscopies à force atomique et à fluorescence en mode hyperspectrale ont été employées. Grâce aux observations réalisées par ces techniques, des hypothèses de corrélation ont été formulées entre les caractéristiques morphologiques et les propriétés de transport des porteurs de charges au sein des couches minces. La diffraction par rayons X en configuration *glancing angle* (GIXRD, utilisant de la lumière de synchrotron) a été utilisée pour examiner la structure cristalline des couches mais aussi pour en apprendre plus sur l'organisation moléculaire au sein de ces dernières.

Pour les transistors en couches minces, une configuration de type *bottom contact* a été choisie. Les caractéristiques de transfert et de sortie ont été utilisées pour calculer la mobilité des porteurs de charges, le voltage de seuil du dispositif ainsi que le ratio I_{ON}/I_{OFF}.

Afin de contribuer à l'exploration de stratégies innovantes pour l'électronique de basse puissance basée sur des couches minces semiconductrices déposées à partir de méthodes en solution, tout en tirant parti de l'expertise du groupe de recherche dans la synthèse du WO_3, des transistors en couches minces de WO_3 utilisant un électrolyte en tant que *gating medium* ont été explorés durant ce travail de thèse. Le concept à la base de la stratégie est la formation d'une double couche électrique à l'interface électrolyte/couche mince de WO_3 suite à l'application d'un voltage aux bornes de l'électrode de grille immergée dans l'électrolyte, en contact avec la couche mince. La capacité de la double couche électrique a été mesurée par spectroscopie d'impédance électrochimique afin de calculer la mobilité des porteurs de charge dans la couche mince de WO_3.

L'ARTICLE 1 traite des propriétés de transport des porteurs de charge dans les couches minces à base de molécules organiques de type dérivé soluble de pentacène (préparé par le groupe de recherche du professeur John E. Anthony, de l'Université du Kentucky). Les résultats du GIXRD ont suggéré un arrangement moléculaire favorisant le transport des porteurs de charge entre les électrodes de *drain* et de *source*, principalement dû à l'interaction des orbitales π-π perpendiculaires au canal du transistor. Dans ce travail, des substrats de SiO_2 traités à l'HMDS ont été utilisés pour améliorer la capacité d'étalement des couches et pour limiter la densité des sites piégeant les porteurs de charge au niveau de l'interface couche mince/diélectrique. Ces résultats ont été confirmés par des mesures à l'AFM où une bonne couverture de la surface a été observée. La caractérisation des transistors a révélé un comportement des porteurs de charge de type ambipolaire (c'est à dire transport simultané de trous et d'électrons). L'ambipolarité des couches minces vient de la bonne correspondance entre la valeur du niveau de Fermi de l'or (électrodes de *source* et de *drain*) et les niveaux HOMO et LUMO du dérivé soluble du pentacène en étude.

Le travail discuté dans l'ARTICLE 2 concerne des matériaux organiques tels que le thiophèno-azométhines π-conjugués, sous forme d'oligomère et de polymère, ainsi que des matériaux analogues de type dérivé d'oligothiophène. Dans le premier cas, les matériaux utilisent l'agent de couplage azométhines (-N=C-) alors que dans le deuxième cas, ils utilisent un agent de couplage plus conventionnel, de type (-C=C-). L'effet de l'extension de la conjugaison sur les propriétés de transport des porteurs de charge a été étudié. Le point clé de ce travail a est que les matériaux utilisant le couplage de type azométhine induisent des propriétés de transport

électronique au sein du transistor en couche mince, et ce pour la première fois. La microscopie à force atomique couplée à celle de fluorescence en mode hyperspectrale a été utilisée pour examiner l'étalement aux échelles micrométrique et nanométrique des couches minces d'oligothiopheno-azométhines. La caractérisation des transistors a permis de conclure que les matériaux de type oligothiophèno-azométhine et l'oligothiophène se comportent comme des semiconducteurs de type p tandis que le polythiophèno-azométhine se comporte comme un semiconducteur de type ambipolaire. De plus, la mobilité des trous de l'oligothiophèno-azométhine calculée après traitement thermique est de trois ordres de grandeur au dessus de son analogue oligothiophène utilisant l'agent de couplage (-C=C-). Cette étude ouvre donc une nouvelle possibilité pour l'amélioration des semiconducteurs basés sur l'agent de couplage de type azométhine.

L'intérêt grandissant pour les liquides ioniques - sels fondus à température ambiante - provenant de leurs propriétés physiques remarquables telles que leur faible volatilité et leur non-inflammabilité, dans le contexte de l'ARTICLE 3 nous a mené à les choisir comme électrolytes pour le *gating* de transistors à base de couches minces de WO_3. Les couches minces de trioxyde de tungstène ont été déposées sur des électrodes préfabriquées d'ITO par gravure chimique. Les microscopies à balayage électronique et à force atomique ont révélé une structure nanocristalline interconnectée dans les couches minces de WO_3. Les transistors en contact avec le 1-butyl-3-methyl imidazolium bis (trifluoromethylsulfonyl) imide [BMIM] [TFSI], 1-butyl-3-methyl imidazolium hexafluoro phosphate [BMIM] [PF6] et 1-ethyl-3-methyl imidazolium bis (trifluoromethylsulfonyl) imide [EMIM] [TFSI] ont montré un comportement semiconducteur de type n. La possibilité d'obtenir des transistors à base de WO_3 apparait alors comme une excellente opportunité de produire de manière simple des transistors ayant des voltages d'opération faibles (au dessous de 1 Volts).

ABSTRACT

This Ph.D. thesis is a result of multidisciplinary research bringing together fundamental concepts in thin film engineering, materials science, materials processing and characterization, electrochemistry, microfabrication, and device physics.

Experiments were conducted by tackling scientific problems in the field of thin films and interfaces, with the aim to correlate the morphology, crystalline structure, electronic structure of thin films with the functional properties of the films and the performances of electronic devices based thereon. Furthermore, novel strategies based on interfacial phenomena at electrolyte/thin film interfaces were explored and exploited to control the electrical conductivity of the thin films.

Three main chemical systems were the object of the studies performed during this Ph.D., two types of organic semiconductors (azomethine-based oligomers and polymers and soluble pentacene derivatives) and one metal oxide semiconductor (tungsten trioxide, WO_3).

To explore the morphological properties of the thin films, atomic force microscopy was employed. The morphological properties were further investigated by hyperspectral fluorescence microscopy and tentatively correlated to the charge transport properties of the films. X-ray diffraction (Grazing incidence XRD, GIXRD) was used to investigate the crystallinity of the film and the effect of the heat treatment on such crystallinity, as well as to understand the molecular arrangement of the organic molecules in the thin film.

The charge transport properties of the films were evaluated in thin film transistor configuration. For electrolyte gated thin film transistors, time dependent transient measurements were conducted, in parallel to more conventional transistor characterizations, to explore the specific effects played on the gating by the anion and cation constituting the electrolyte. The capacitances of the electrical double layers at the electrolyte/WO_3 interface were obtained from electrochemical impedance spectroscopy.

In the context of ARTICLE 1, thin film transistors based on soluble pentacene derivatives (prepared by the research group directed by Professor J. Anthony, at the University of Kentucky) were fabricated and characterized. GIXRD results performed on the thin films suggested a molecular arrangement favorable to charge transport in the source-drain direction, with the π-π

stacking direction perpendicular to the channel. In ARTICLE 1, HMDS-treated SiO_2 substrates were used, to improve the surface coverage and to limit charge trapping at the dielectric surface. AFM showed good film coverage. The transistors showed ambipolar characteristics, attributed to the good matching between Au electrode work function and highest occupied molecular orbital (HOMO) and lowest unoccupied molecular orbital (LUMO) of the pentacene derivative.

The work reported in ARTICLE 2 deals with π-conjugated thiopheno-azomethines (both in oligomer and polymer form) and oligothiophene analogues. In the former case, couplings in the polymer are based on azomethine (-N=C-) moieties whereas in the latter case they are based on more conventional protocols (-C=C-). The effect of the coupling protocols on the corresponding thin film transistors behavior was studied. The key conclusion of this study was that thiopheno-azomethines thin films can be effectively incorporated into organic transistors: thin films of oligothiopheno-azomethines and the oligothiophenes exhibit p-type behavior whereas thin films of polythiopheno-azomethine exhibit an ambipolar behavior. The hole mobility of the heat-treated thin films of oligothiopheno-azomethines was three orders of magnitude higher compared to its oligothiophene analogue. AFM, coupled with hyperspectral fluorescence imaging, were used to investigate the micro- and nano-scale surface coverage. For the oligothiopheno-azomethine we were able to quantitavely deduce the surface coverage.

To contribute to the exploration of innovative strategies for low power consuming solution based electronics and capitalizing on the expertise of the group in the synthesis of solution deposited WO_3 films the electrolyte gating approach was explored in ARTICLE 3. Ionic liquids, that are molten salts at room temperature, were employed as the electrolyte. Ionic liquids are attractive for their low volatility, non-flammability, ionic conductivity and thermal and electrochemical stability. Thin films of WO_3 were deposited onto pre-patterned ITO substrates (source-drain interelectrode distance, 1 mm) prepared by wet chemical etching. SEM and AFM showed an interconnected film nanostructure. Electrolyte gated WO_3 thin film transistors making use of 1-butyl-3-methyl imidazolium bis(trifluoromethylsulfonyl)imide ([BMIM][TFSI]), 1-butyl-3-methyl imidazolium hexafluoro phosphate ([BMIM][PF6]), and 1-ethyl-3-methyl imidazolium bis(trifluoromethylsulfonyl)imide ([EMIM][TFSI]) showed an n-type transistor behavior. The possibility to obtain WO_3 electrolyte gated transistors represents an opportunity to

fabricate electronic devices working at relatively low operating voltages (about 1 V) by using simple fabrication techniques.

TABLE OF CONTENTS

DEDICATION III

ACKNOWLEDGEMENTS IV

RÉSUMÉ VI

ABSTRACT IX

TABLE OF CONTENTS XII

LIST OF TABLES XVI

LIST OF FIGURES XVII

LIST OF ABBREVIATIONS XXII

CHAPTER 1 INTRODUCTION 1

1.1 The interest and applications of large area electronic devices, solution processed 1

1.2 Solution deposition for large area thin film electronics 2

1.3 Objectives and organization of the thesis 3

CHAPTER 2 THEORETICAL BACKGROUND 5

2.1 Materials 5

2.1.1 Organic semiconductors 5

2.1.2 Tungsten trioxide 10

2.2 Analogies and differences between organic and inorganic semiconductors 11

2.3 Structure, components and operating mechanism of thin film transistors 12

2.3.1 Basic thin film transistor structure 12

2.3.2 Electrode/semiconductor interfaces 13

2.3.3 Gate dielectric 15

2.3.4 Organic thin film transistor operation 17

2.3.5 Mechanism of electrolyte gating 18

2.3.6 Transistor figures of merit 18

CHAPTER 3 EXPERIMENTAL METHODS AND TECHNIQUES 21

3.1 Sample preparation 21

3.1.1 Organic thin film transistors: device structure 21

3.1.2 Electrolyte gated thin film transistors: device structure 22

3.1.3 Ionic liquids 22

3.1.4 Cleaning and surface modification of transistor substrates 24

3.1.5 Solution preparation 25

3.1.6 Thin film deposition: spin coating and post-treatment 26

3.2 Transistor characterization 26

3.3 Morphological, Structural and optical characterization of thin films 27

3.3.1 Powder and thin film X-Ray Diffraction (XRD) and Grazing Incidence X-ray Diffraction (GIXRD) 27

3.3.2 Atomic force microscopy (AFM) 28

3.3.3 Fluorescence hyperspectral imaging 29

3.3.4 Scanning Electron Microscopy (SEM) and Energy Dispersive X-Ray Spectrometer (EDS) 30

3.4 Electrochemical Impedance Spectroscopy (EIS) 31

Capacitance measurements 31

CHAPTER 4 MOLECULAR AND THIN FILM ENGINEERING OF π-CONJUGATED PENTACENE DERIVATIVES 33

4.1 π-conjugated pentacene derivatives: Effect of the functionalization and the processing conditions on the thin film transistor performance 34

4.2 ARTICLE 1: Ambipolar organic thin film transistors based on a soluble pentacene derivative 36

4.2.1 Abstract 37

4.2.2 Introduction 37

4.2.3 Experimental 38

4.2.4 Results and Discussion 39

4.2.5 Conclusions 43

Acknowledgments 43

4.3 Correlation of charge transport properties with morphological and photophysical characteristics of solution processed pentacene derivatives 44

CHAPTER 5 CHARGE-CARRIER TRANSPORT IN THIN FILMS OF π-CONJUGATED THIOPHENO-AZOMETHINES 49

5.1 ARTICLE 2: Charge-Carrier Transport in Thin Films of π-Conjugated Thiopheno-Azomethines 50

5.1.1 Introduction 51

5.1.2 Experimental 53

5.1.3 Results and Discussion 58

5.1.4 Conclusions 70

Acknowledgements 70

CHAPTER 6 ELECTROLYTE-GATED TUNGSTEN TRIOXIDE THIN FILM TRANSISTORS MAKING USE OF IMIDAZOLIUM-BASED IONIC LIQUIDS 76

6.1 ARTICLE 3: Electrolyte-Gated Tungsten Trioxide Thin Film Transistors making use of Imidazolium-based Ionic Liquids 77

6.1.1 Abstract 78

6.1.2 Introduction 78

6.1.3 Experimental 80

6.1.4 Results and Discussion 81

6.1.5 Conclusions 86

6.2 Microfabrication of ITO microelectrodes 91

CHAPTER 7 CONCLUSIONS, PERSPECTIVES AND GENERAL DISCUSSION 99

REFERENCES 102

LIST OF TABLES

Table 2-1 Comparison of the physical, electrical and optical properties of c-Si, WO_3 and organic semiconductors 11

Table 2-2 Transistor parameters 20

Table 3-1 Transistor channel widths (W) and lengths (L) in organic thin film transistors investigated in this work. 22

Table 3-2 Gate dielectric properties for organic thin film transistors investigated in this work. 22

Table 3-3 Properties of the ionic liquids used for the characterization of electrolyte gated transistors. 23

Table 3-4 Summary of the solutions and preparation conditions for organic thin films investigated in thin film transistor configuration. 25

Table 4-1 HOMO and LUMO level location with respect to vacuum level and optical band gap of three soluble pentacene derivatives determined by cyclic voltammetry synthesized by the group of Prof. J. E. Anthony at the University of Kentucky. 44

Table 4-2 Mobilities of 2,3-CN2-TIPS-Pn, TIPS-F8 and TES-F8 as a function of temperature and deposition solution concentrations. 46

Table 5-1 Electrochemical and photophysical properties of compounds 1-3. 61

Table 6-1 Process steps for photolithography and etching of ITO substrates. 93

LIST OF FIGURES

Figure 2-1 Conjugated backbone of pentacene molecule with alternating single and double bonds. 6

Figure 2-2 C_2H_4, bonds and orbitals, showing the delocalized electron regions forming the π-bonding above and below the C atom plane. 6

Figure 2-3 Molecular energy structure of a conjugated molecule showing the bonding and anti-bonding orbitals. The gap between π-π* orbitals is the energy band gap of the molecule [71]. 7

Figure 2-4 Energy band diagrams for an ordered molecular crystal and a disordered molecular material [71], [87], [88]. 7

Figure 2-5 Chart showing molecular weights of oligomers and polymers together with the degree of polymerization. 8

Figure 2-6 Selected contributions in the molecular structure of an organic semiconductor that can affect its chemical and physical properties, for the specific case of the 2-Amino-5-[(3,4-bis(decyl)-5-formylthiophen-2-ylmethylene)-amino]thiophene-3,4 dicarboxylic acid diethyl ester molecule investigated in this Ph.D. work (Chapter 5) 8

Figure 2-7 Molecular structure of (a) pentacene (insoluble) (b) 6,13-bis (triisopropyl-silylethynyl) pentacene(TIPSpentacene,soluble),and(c)2,3dicyano6,13bis(triisopropylsilylethynyl)pentacene (2,3-CN2-TIPS-Pn, soluble). 9

Figure 2-8 The effect of the substituent groups on the HOMO-LUMO energy levels of (a) pentacene (E_g=2.29 eV) (b) 6,13-bis (triisopropyl-silylethynyl) pentacene (TIPS-pentacene, E_g=1.81 eV) , and (c) 2,3-dicyano-6,13-bis-(triisopropylsilylethynyl)pentacene (2,3-CN2-TIPS-Pn, E_g=1.81 eV). 10

Figure 2-9 Corner-sharing WO_3 octohedra. 11

Figure 2-10 Thin film transistor configuration: (left) bottom gate/bottom contact and (right) bottom gate/top contact. *W* is the channel width and *L* is the channel length. 12

Figure 2-11 Scheme of the metal/p-type semiconductor interface. The hole (electron) injection barrier, Φ_h (Φ_e), is the difference between HOMO (LUMO) level of the organic semiconductor and the Fermi level of the metal. Φ_h is small enough for hole injection. The effect of an applied bias at the gate electrode on the HOMO and LUMO levels at the interface is also shown by a small bending. GDOS is also shown. (Adapted from [71]).....14

Figure 2-12 ITO/WO_3 interface energy band diagram. The Φ_e for electron injection is <0.1eV. .15

Figure 2-13 Schematic illustration of organic thin film transistor operation. Circles in the semiconductor layer illustrate the holes during different stages of transistor operation. In (a) Cut-off, (b) Linear region and (c) the saturation region are illustrated. 17

Figure 2-14 General structure of an electrolyte gated transistor (left). Electrochemical mechanism (top right) and electrostatic mechanism (bottom-right) of doping during electrolyte gating. 19

Figure 3-1 Bottom contact-bottom gate (Si (n^+)) transistor substrate with interdigitated pre-patterned Au electrodes (30 nm thick) and SiO_2 (195 nm) gate dielectric coated with an organic semiconductor. 21

Figure 3-2 Electrolyte gated transistor built on a glass substrate with patterned ITO electrodes. The channel is in contact with the electrolyte, confined in a PDMS well on top of the channel. An electrode immersed into the electrolyte is used to gate the channel. 23

Figure 4-1 Molecular formulas of (a) triethylsilyl-octafluoropentacene, (b) Bis(triisopropylsilylethynyl)octafluoropentaceneand(c)Bis(triisopropylsilylethynyl)dicyanopentacene……..……33

Figure 4-2 Molecular structure of 2,3-CN2-TIPS-Pn (a); bottom gate/bottom contact FET structure used in this work (b); HOMO and LUMO levels of pentacene and 2,3-CN2-TIPS-Pn, with respect to the Au workfunction, Φ_{Au} (c).[100] 39

Figure 4-3 1 μm × 1 μm AFM topographical images of 2,3-CN2-TIPS-Pn film on HMDS-treated SiO_2. Inset: 5 μm × 5 μm AFM image of the same sample, rms = 1.56 nm. 40

Figure 4-4 TFT characteristics of 2,3-CN2-TIPS-Pn films: output curves (I_{ds} vs V_{ds}) for $|V_{gs}|$ = 0, 20, 40, 60 V in the p- and n-type regions (top); transfer curves (I_{ds} vs V_{gs}) at saturation for

V_{ds} = 60 V (bottom left); transfer curves at saturation for V_{ds} = -60 V (bottom right). Channel width/Channel Length = 10 μm/1880μm.....41

Figure 4-5 (a) Rietveld fit of one of the X-ray diffraction images collected at an incident angle of 2°. The principal spot is due to the (001) diffracting plane parallel to the sample surface. The bottom 2D pattern represents the experimental data; the recalculated pattern is on top. The three spots (001/002/003 reflections) are aligned in the diffraction plane normal to the sample surface. As we move out of it (moving vertically in the image), the strong texture causes a rapid decrease of the intensity. The inset reports the recalculated pole figure showing the strong 00l orientation (mrd: multiple of random distribution, values in log scale). (b) Proposed molecular arrangement of 2,3-CN2-TIPS-Pn on the substrate.....42

Figure 4-6 Absorption and fluorescence spectra (excitation wavelength 540 nm) of spin coated thin films heat treated at 100 °C on quartz slides.....45

Figure 4-7 TFT characteristics of spin coated and 100 °C annealed TIPS-F8 and TES-F8 films: output curves (I_{ds} vs V_{ds}) for $|V_{gs}|$ = 0, 20, 40, 60 V (a) TES-F8 and (b) TIPS-F8; transfer curves (sqrt I_{ds} vs V_{gs}) at saturation for V_{ds} = 60 V (c)TES-F8 and (d) TIPS-F8. Channel widths/Channel Length = 6 μm/1880μm and 10 μm/1880μm for TES-F8 and TIP-F8, respectively.....47

Figure 4-8 1μm×1μm height and phase AFM images of the three molecules in the as-prepared and 100 °C annealed conditions.....48

Figure 5-1. Cyclic voltammograms of **1** (black, bottom), **2** (red, middle) and **3** (blue, top) recorded in de-aerated dichloromethane with $TBAPF_6$ (0.1 M) using a saturated Ag/AgCl as reference electrode and a Pt wire as both the working and auxiliary electrode.....61

Figure 5-2 Powder X-ray diffraction of **1** (black, bottom), **2** (blue, middle) and **3** (red, top). The XRD powder data for **1** and **2** show diffraction peaks corresponding to a lamellar morphology (as per the inset sketch), consistent with π-stacking distance of 3.77 Å found from the single crystal data; the peak at $2\theta \approx 4.2°$ corresponds to an interlayer *d*-spacing of 21.2 Å, represented in the sketch in the inset.....63

Figure 5-3 50 μm×50 μm fluorescence hyperspectral images of spin-coated films of **1**-**3** on HMDS-treated SiO_2/Si FET substrates, after thermal treatment at 100 °C. Left: corresponding categorized images for **1** (a, λ_{exc} = 540 nm), **2** (b, λ_{exc}= 540 nm), **3** (c, λ_{exc} = 460 nm), Right: Histograms and collected spectral libraries of **1** (d), **2** (e), **3** (f), respectively. 65

Figure 5-4 AFM images of thin films of 1-3 on HMDS-treated SiO_2/Si FET substrates: (a) 5 μm × 5 μm and (b) 20 μm × 20 μm images of as-prepared films of 1; H range = 0-80 nm, rq = 8-9 nm. (c) 5 μm×5 μm and (d) 20 μm × 20 μm images of 100 °C-treated films of 1; H range = 0-100 nm, rq = 12.4-13 nm (rq 0.9 nm in the underlayer, see text). (e) 5 μm × 5 μm image of 2 treated at 100 °C; H range = 0-15 nm, rq ~1 nm. (f) 5 μm × 5 μm image of 3 treated at 100 °C; H range = 0-500 (see text for a discussion on rq). (b) and (d) have been taken on the transistor channel (electrode patterning visible in the images). 67

Figure 5-5 Output (left) and transfer (right) curves for FETs based on thin films of **1** (top) and **3** (bottom). In the output curves, V_{GS} were 0, -20, -40, -60 V. The transfer curves were recorded at V_{DS} = -60 V; the red line extrapolates the square root of I_{DS} at its maximum slope to obtain its intercept at y = 0, to calculate V_{TH}. 69

Figure 6-1 Device structure of the electrolyte gated WO_3 thin film transistor with the electrolyte confined by a PDMS well, on top of the WO_3 channel. The structures of the imidazolium-based ionic liquids for this work are also indicated. 79

Figure 6-2 Output characteristics of EG WO_3 transistors making use of ionic liquid electrolytes (W/L = 1000 μm/6000 μm) with V_{GS} increasing from 0 to 1 V with 0.2 V steps. (a) [EMIM][TFSI] WO_3 transistors. (b) [BMIM][PF6] WO_3 transistors. In the output curves, the hold time at a certain V_{GS} (before the acquisition of the current versus V_{DS} at a certain V_{GS}) is 600 sec. 83

Figure 6-3 Nyquist (a) and Bode (b) plots of two-electrode (WO_3/IL/Pt) electrochemical cells with [EMIM][TFSI] (E_{DC} = -1V), [BMIM][TFSI] (E_{DC} = -1 or -2V), [BMIM][PF6] (E_{DC} = -1V). (c) Capacitance versus E_{DC} plots for the three electrochemical cells making use of the above-mentioned ionic liquids. 85

Figure 6-4 Spin speed versus thickness curves for 4 inch Si-wafers spin coated with SPR 220 photoresists. The difference in the photoresist thickness for the Si wafer (red dashed line) and the ITO substrate (blue dashed line).....92

Figure 6-5 Mask layouts used for ITO patterning.....93

Figure 6-6 ITO substrate 93

Figure 6-7 Photoresist coated ITO substrate, thickness ~2,75 μm.....93

Figure 6-8 Hard contact (i-line, 365nm, exposure).....94

Figure 6-9 Patterned ITO glass 94

Figure 6-10 100 μm channel and developed 100 μm features of photoresist on ITO. Image taken under polarized light after 3 min 40 sec development, no photoresist was observed. 95

Figure 6-11 Developed photoresist cross section after 3 min 40 sec. Calibration correction 43% giving ~2.75 μm depth. 95

Figure 6-12 Optical images of step-by-step wet chemical etching. 96

Figure 6-13 SEM Images showing the fabricated (a) ITO electrodes, (b) 1000 μm channel. 97

Figure 6-14 A portion of the transistor substrate showing the chemical distribution of elements in and around the channel, as obtained from a EDX survey. After etching In and Sn are replaced by Si and O, i.e. ITO was etched and glass substrate was reached. 97

Figure 6-15 Spectra taken from different regions of the sample showing the presence of different elements in and near the transistor channel. These spectra clearly shows that no In or Sn residues were left in the channel after etching. 98

LIST OF ABBREVIATIONS

AFM Atomic force microscopy

CB Conduction band

CV Cyclic Voltammetry

EDX Energy-dispersive X-ray spectroscopy

EDL Electrical double layer

EG Electrolyte gated

EIS Electrochemical impedance spectrometry

HOMO Highest occupied molecular level

IL Ionic liquid

LUMO Lowest unoccupied molecular level

OSC Organic semiconductor

SEM Scanning electron microscope

TFT Thin film transistor

VB Valence band

XRD X-Ray diffraction

Φe electron injection barrier

Φh hole injection barrier

CHAPTER 1 INTRODUCTION

The underpinning of the present Ph.D. work is the investigation of the relationship between the solution based processing conditions of thin semiconductor films and the performance of devices based thereon.

1.1 The interest and applications of large area electronic devices, solution processed

Solution processed electronic devices are interesting for large area applications due to their low cost and compatibility with flexible substrates [1], [2], [3], [4], [5], compared to well established silicon based electronic devices [6].

Organic semiconductors and metal oxide semiconductors are the two classes of material groups that are commonly employed for solution processed large area device fabrication. Currently, semiconductor industry is dominated by silicon, with electron mobility (μ_e) ~ 1000 $cm^2/V \cdot sec$ in well established devices and ~ 600 $cm^2/V \cdot sec$ on plastic flexible substrates [7][8]. Amorphous silicon (a-Si) is widely used for high durability and relatively low mobility applications [9].

Organic semiconductors usually demonstrate electronic performances close to, and in some cases exceeding, that of a-Si. While the μ_e of a-Si thin film transistors (TFTs) was reported to be on the order of 1 $cm^2/V \cdot sec$ [10], hole mobility (μ_h) as high as 3.2 $cm^2/V \cdot sec$ and μ_e as high as 2 $cm^2/V \cdot sec$ for single crystal pentacene were reported [11] and μ_h 1.5 $cm^2/V \cdot sec$ for thin films of pentacene was reported [12]. A value of μ_e of 5.5 $cm^2/V \cdot sec$ for a single crystal of perylene was also reported [13].

Oxide semiconductor films yield mobility in the range 1-100 $cm^2/V \cdot sec$ [9], [14], [15]. In-Ga-Zn-O system yielded high μ_e in TFTs on plastic substrates, of 6-9 $cm^2/V \cdot sec$ [15].

While benchmark inorganic semiconductors can be operated at low operating voltages, this is not the case for many organic semiconductors, thus limiting the commercialization of organic electronic products, such as Radio Frequency Identification Devices (RFID) [16].

During the past decade, there has been an effort to tackle the high operating voltage issue by approaches based on replacing conventional gate dielectric such as SiO_2 (ε=3.9) by high-k materials such as Al_2O_3 and HfO_2 (ε=10-15) and reducing the thickness of the dielectric layer by the use of dielectric self-assembling monolayers [17], [18], [19, p. 2], [20]. An alternative approach is based on the concept of *electrolyte gating*, proven to reduce the operating voltages of transistors from dozens of volts to a few volts [21], [22], [23]. The first examples of electrolyte gating were proposed by Brattain et. Al [24]. Wrighton in the 1980s reported a number of electrolyte gated organic and inorganic transistors, thus preparing the basis for the advanced studies currently ongoing worldwide [25], [26], [27], [28], [29].

Application areas for organic electronics and oxide electronics can be listed as thin film transistors (TFTs) to be used in data storage, active matrix displays, flexible display devices [9], [30], [31], [32], RFID tags to replace barcodes [33], [34], [35, p. 56], solar cells [36], [37], [38], [39], gas-sensors and bio-sensors [25], [26], [40], [41], [42], [43], [44], [45], X-ray detectors [46] light-emitting diodes (LEDs) [47], [48], [49], [50], smart textiles (equipped with sensors, displays, solar cells and heaters) [51], [52], [53], e-paper [54].

1.2 Solution deposition for large area thin film electronics

Organic electronics stemmed from the discovery of conductive polymers by Alan J. Heeger, Alan G. MacDiarmid, and Hideki Shirakawa [55]. This discovery brought them the Nobel Prize in Chemistry in 2000 [56], [57], [58]. In the Nobel lecture, Alan J. Heeger summarized the discovery with these words: “Conducting polymers offered the promise of achieving a new generation of polymers: materials which exhibit the electrical and optical properties of metals or semiconductors and which retain the attractive mechanical properties and processing advantages of polymers”. Most organic semiconductors are indeed soluble in organic solvents such as chloroform, chlorobenzene, toluene and xylene.

Oxide semiconductors on the other hand, have been used in oxide thin films transistors since 1960s [59], [60], [61], [62], [63]. Semiconductor oxides can be prepared by the sol-gel technique, which is a solution based synthetic method [62], [64], [65], [66]. They are less prone, compared to organic semiconductors, to degradation upon contact with H_2O or O_2, such as they can be used

in contact with aqueous electrolytes for electrochromic and photoelectrochemical applications [67], [68], [69], [70, p. 3].

Manufacturing techniques i.e. roll-to-roll, doctor blade, inkjet printing and screen printing technologies allow production of electronic devices with dimensions from tens of micrometers to dimensions exceeding tens of meters [9], [71], [72], [73].

1.3 Objectives and organization of the thesis

The general objective of this thesis was to contribute to advance the knowledge in the field of structure-property relationships in semiconductor thin films deposited by solution based techniques with the aim to shed light on their functional properties and, afterwards, devices based thereon.

The research efforts whose results constitute this Ph.D. thesis work are multifaceted, indicated below as research efforts A-D.

A - Thin film engineering – In Chapters 4 and 5, we reported on new soluble organic materials (2,3-dicyano-6,13-bis-(triisopropylsilylethynyl)pentacene (2,3-CN2-TIPS-Pn), 2-amino-5-[(3,4-bis(decyl)-5-formylthiophen-2-ylmethylene)-amino]thiophene-3,4 dicarboxylic acid diethyl ester, thiopheno-polyazomethine and 2,5-Bis[(E)-2-(5-methylthiohene-2-yl)vinyl] thiophene) synthesized by organic chemists collaborators. We carried out systematic investigations on the thin film deposition conditions (substrate surface modification, solution concentration, solvent, thermal treatment conditions) to obtain homogeneous films with complete substrate surface coverage. We characterized the morphology of the organic thin films by atomic force microscopy and fluorescence hyperspectral imaging. The structure of the films was investigated by grazing incidence X-ray diffraction at the Elettra synchrotron facility (Trieste, Italy). In Chapter 6, the morphology and the structure of metal oxide solution processed thin films were followed by atomic force microscopy and scanning electron microscopy.

B - Microfabrication of transistor substrates hosting the thin films – The thin film engineering efforts were paralleled by the characterization of their charge carrier transport properties in thin film transistor configuration. The microfabrication of the transistor substrates

represents a relevant portion of the experimental efforts carried out within the context of this Ph.D. work (Chapter 6).

C – Characterization of the thin film transistors to study the electroactivity of the thin films, the polarity and the mobility of the charge carriers (Chapters 4, 5, 6). Device characterization was performed in controlled atmosphere conditions (vacuum 10^{-5} Torr or N_2 glove box atmosphere with O_2 and H_2O at about 1 ppm).

D – Exploration of an unconventional transistor gating approach (electrolyte gating) with metal oxide films (Chapter 6). With the aim to lower the operating voltages of the transistors the electrolyte gating approach was employed, making use of imidazolium-based room temperature ionic liquids. The formation of an electrical double layer at the ionic liquid/thin film interface underpins the effectiveness of the gating.

CHAPTER 2 THEORETICAL BACKGROUND

In this chapter, a theoretical background on the properties of the materials used in the Ph.D. is given. In addition, analogies and differences between organic and inorganic semiconductors are listed in Table 2-1 to clarify where organic and oxide semiconductors stand in terms of electronic applications, with respect to Si. Moreover, since during this Ph.D. work the transistor configuration was selected as a test-bed to study the charge-transport properties of the materials, a general view of transistor operation and characterization is proposed.

2.1 Materials

2.1.1 Organic semiconductors

Organic semiconductors possess a conjugated backbone i.e. carbon atoms form alternating single and double bonds, such as in pentacene (Figure 2-1). In a conjugated system, each C atom has 3 nearest neighbors with whom it forms 3 equivalent σ bonds. The bonds are built using the sp^2 hybridization of the three valence atomic orbitals of the carbon atom $2s$, $2p_x$ and $2p_y$. The fourth orbital, $2p_z$, lies perpendicular to the plane of the σ bonds. The overlap of the two out-of-plane $2p_z$ atomic orbitals give π bonds [74], with a delocalized electron density above and below the plane of the C atoms, as illustrated for the ethylene molecule in Figure 2-2 [75].

The difference in energy (E_g) between the bonding (π) and anti-bonding ($\pi*$) molecular orbitals are illustrated in Figure 2-3. The HOMO (Highest Occupied Molecular Orbital) and LUMO (Lowest Unoccupied Molecular Orbital) of organic semiconductors are analogous to valence (VB) and conduction band (CB) edges of inorganic semiconductors. In organic semiconductors, σ-bonds contribute to the stability of the molecular structure whereas π bonds enable charge transport.

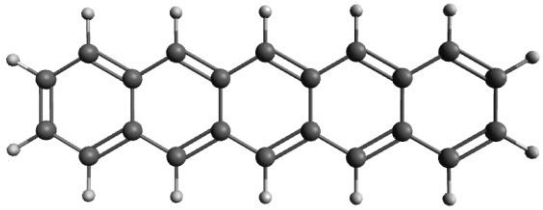

Figure 2-1 Conjugated backbone of pentacene molecule with alternating single and double bonds.

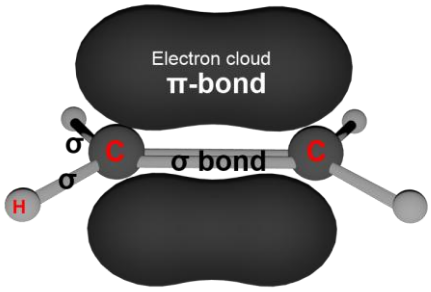

Figure 2-2 C_2H_4, bonds and orbitals, showing the delocalized electron regions forming the π-bonding above and below the C atom plane.

Because π–π Van der Waals intermolecular interactions are weaker compared to covalent interactions, in molecular thin films the electronic wave function is strongly localized to individual molecules [76], [77]. The variable range hopping model, where charge carriers hop between adjacent molecules, is commonly accepted as the charge carrier transport mechanism in organic semiconductors with room temperature mobility below 10^{-2} $cm^2/V \cdot sec$ [75], [78], [79], [80]. The fluctuations of the intermolecular spacings in organic semiconductors that lack long-range order lead to local variations of the wavefunction such that the HOMO and LUMO levels show an energetic distribution that can be approximated by a Gaussian density of states (GDOS). The difference in the DOS distribution between ordered molecular crystals and disordered organic materials is illustrated in Figure 2-4 [75], [81], [82]. There is also evidence of band-like transport for a number of organic semiconductors such as 6,13-bis(triisopropylsilylethynyl)-pentacene (TIPS-pentacene) and pentacene [83], [84], [85], [86].

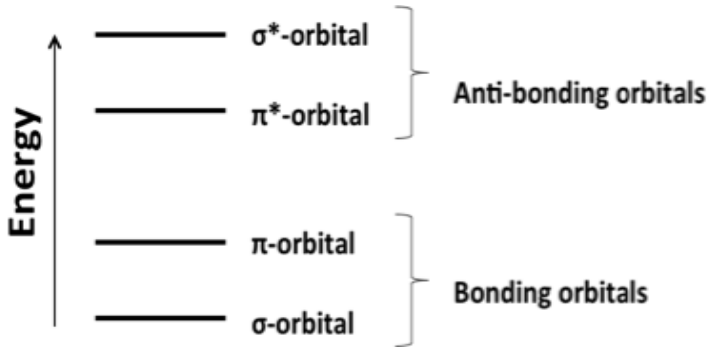

Figure 2-3 Molecular energy structure of a conjugated molecule showing the bonding and anti-bonding orbitals. The gap between π-π* orbitals is the energy band gap of the molecule [71].

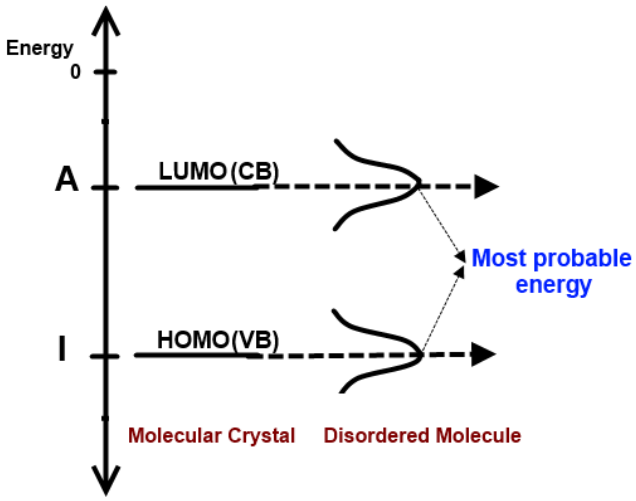

Figure 2-4 Energy band diagrams for an ordered molecular crystal and a disordered molecular material [71], [87], [88].

Organic semiconductors are found in the form of oligomers and polymers (Figure 2-5) [89]. Oligomers possess low-molecular weights that permit them to be vacuum-deposited. Conjugated polymers, on the other hand, have high-molecular weights and can be solution processed. The chemico-physical properties of organic semiconductor thin films are dramatically affected by molecular structure (Figure 2-6) as well as supramolecular arrangement in the film. Controlling the chemical structure through chemical synthesis and engineering the

supramolecular arrangement in the films can therefore promote specific, desirable functional properties in thin organic electronic films [90], [91], [92], [93], [94], [95].

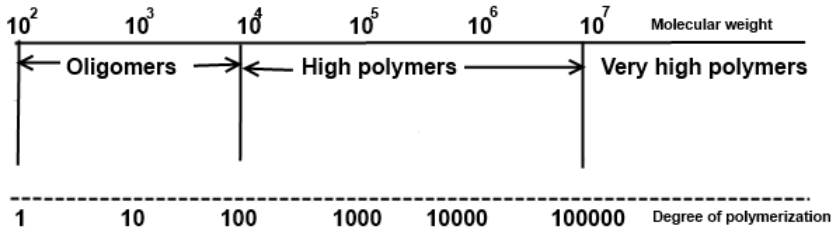

Figure 2-5 Chart showing molecular weights of oligomers and polymers together with the degree of polymerization.

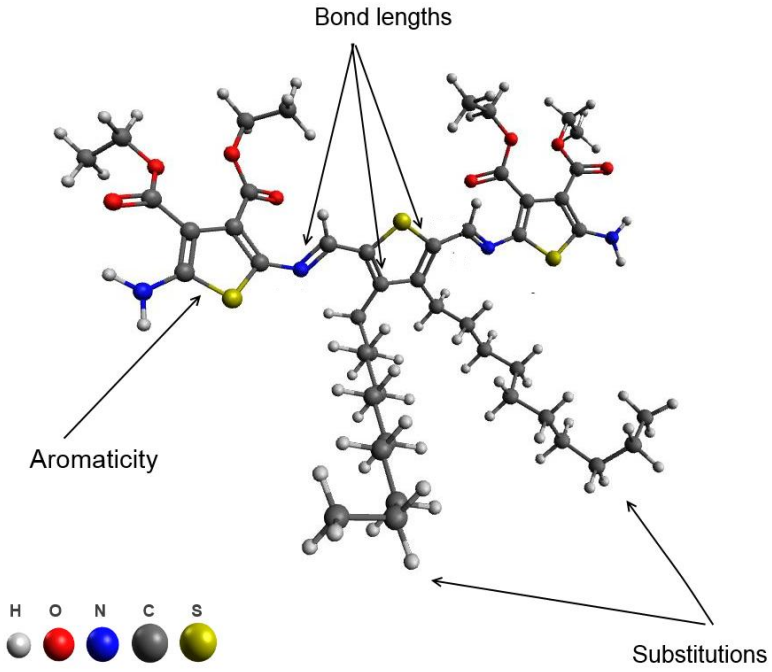

Figure 2-6 Selected contributions in the molecular structure of an organic semiconductor that can affect its chemical and physical properties, for the specific case of the 2-Amino-5-[(3,4-bis(decyl)-5-formylthiophen-2-ylmethylene)-amino]thiophene-3,4 dicarboxylic acid diethyl ester molecule investigated in this Ph.D. work (Chapter 5)

Acenes are a group of organic semiconductors that have been widely investigated [3]. Pentacene (Figure 2-7 a) and its derivative TIPS-pentacene (Figure 2-7 b) are two well-known acenes [3], [96]. The addition of specific substituents can influence the solubility of organic semiconductors such that while pentacene has very low solubility, TIPS-pentacene is highly soluble in common solvents due to the additional bulky side-on groups [97], [98], [99]. Additional electron withdrawing groups, such as cyano, fluoro, bromo groups, are known to increase the electron transport in organic semiconductors [90]. As an example, the 2,3-dicyano-6,13-bis-(triisopropylsilylethynyl)pentacene (2,3-CN2-TIPS-Pn) pentacene derivative exhibits n-type semiconductor properties beside the p-type properties well-established for the pentacene molecule (Article 1) (Figure 2-7 c) [5]. Fluorinated pentacene derivatives with n-type semiconductor properties were also studied in this Ph.D. work (Chapter 4). Figure 2-8 show energy level diagrams of pentacene, TIPS-Pn and 2,3-CN2-TIPS-Pn with respect to the Fermi level of gold, which is located at 4.4 eV with respect to the vacuum level [100].

In the field of novel materials for applications in organic electronics, besides conventional coupling protocols (-C=C) alternative protocols are investigated, e.g. based on the use of azomethines (-C=N-, length=1.279 Å, Chapter 5) [101][101], [102], [103]. The interest for azomethines stems from their synthesis that does not require stringent reaction conditions as well as the absence of undesired by-products during the synthesis (water is the unique side-product).

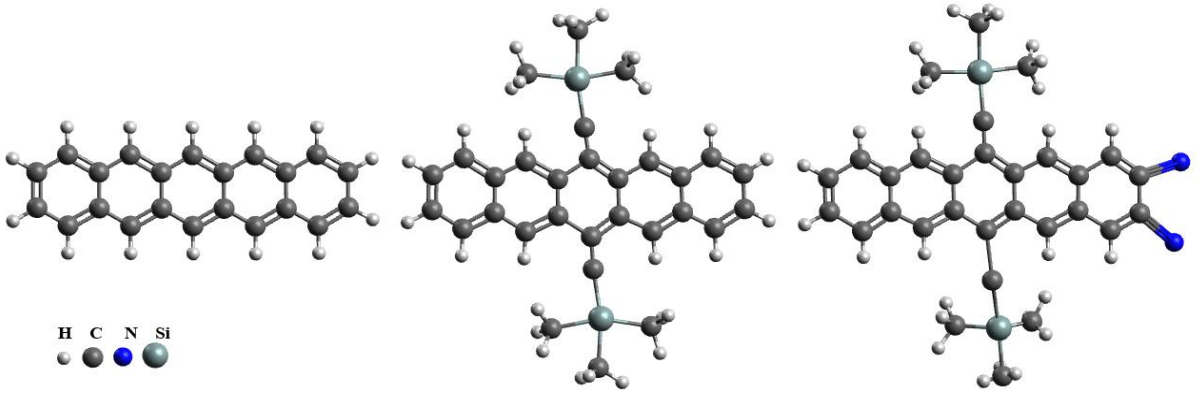

Figure 2-7 Molecular structure of (a) pentacene (insoluble) (b) 6,13-bis (triisopropyl-silylethynyl) pentacene (TIPS-pentacene, soluble), and (c) 2,3-dicyano-6,13-bis-(triisopropylsilylethynyl)pentacene (2,3-CN2-TIPS-Pn, soluble).

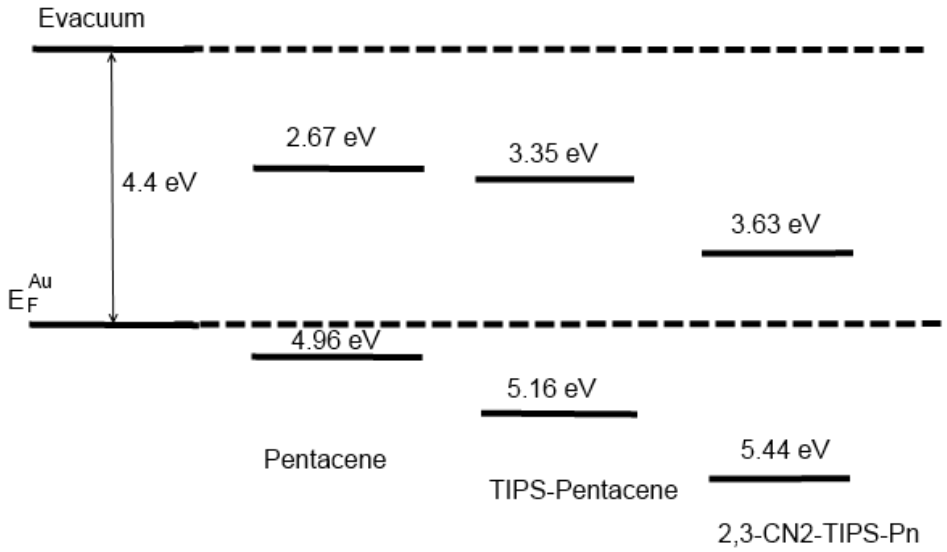

Figure 2-8 The effect of the substituent groups on the HOMO-LUMO energy levels of (a) pentacene (E_g=2.29 eV) (b) 6,13-bis (triisopropyl-silylethynyl) pentacene (TIPS-pentacene, E_g=1.81 eV) , and (c) 2,3-dicyano-6,13-bis-(triisopropylsilylethynyl)pentacene (2,3-CN2-TIPS-Pn, E_g=1.81 eV).

2.1.2 Tungsten trioxide

WO_3 is a transition metal oxide whose building blocks are WO_6 octahedra with tungsten being the central metal atom, surrounded by six oxygen atoms (Figure 2-10). The stoichiometric WO_3 is known to be formed by corner-sharing octahedra whereas the substoichiometric (oxygen-deficient) by a combination of corner-sharing and edge-sharing octahedral [104][104], [105], [106], [107], [108].

WO_3 is usually found in substoichiometric form, WO_{3-x}, behaving as n-type semiconductor[109], [110], [111], [112], [113], [114], [115], [116]. Depending on the value of x, the electrical properties of WO_3 change from insulator to highly conductive. WO_3 can have three different valence states, W^{4+}, W^{5+} and W^{6+}.

Reviews on the fabrication and application of nanostructured WO_3 materials are reported in [117], [118]. WO_3 is interesting for electrochromic displays [66], [105], gas sensors [119], [120], chemichromic biosensors [121], [122], and photocatalysis [123], [124], [125], [126]. WO_3 was

chosen due to the expertise of the group in the synthesis of solution deposited thin films and to contribute to the exploration of innovative strategies for low power consuming solution based electronics.

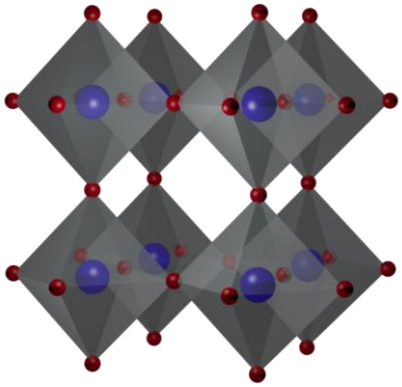

Figure 2-9 Corner-sharing WO_3 octohedra.

2.2 Analogies and differences between organic and inorganic semiconductors

Currently, electronics industry is mainly dominated by silicon as the semiconductor. However, oxide and organic semiconductors offer advantages in their processing (i.e. solution processability). Relevant analogies and differences between organic and inorganic semiconductors are reported in Table 2-1.

Table 2-1 Comparison of the physical, electrical and optical properties of c-Si, WO_3 and organic semiconductors

Property	**c-Si**	**WO_3**	**Organic semiconductors**
Bonding	Covalent bonds	Covalent bonds	Intermolecular Van der Waals bonds
Dielectric constant (static)	11.7	70 [127]	About 3-4
Energy gap, E_g [eV]	1.12	2.5-3.5 [65], [105], [128]	~2-3
Stability	Stable	Stable	Unstable in Air

2.3 Structure, components and operating mechanism of thin film transistors

2.3.1 Basic thin film transistor structure

Thin film transistors are three electrode-devices that are constituted of a gate electrode that is separated from the semiconductor by the gate dielectric, and source and drain electrodes. Application of a gate-source bias modulates the charge density in the channel. Upon application of a drain-source voltage charge carriers can be driven in the channel (Figure 2-10). Top and bottom contact electrode architectures are possible. For organic thin film transistors, top contact electrodes usually lead to better device performance; with bottom contact electrodes, high metal-semiconductor contact resistances and poor morphology at the vicinity of the electrodes are observed[129]. However, high performance bottom contact thin film transistors were also reported, e.g. for thermally evaporated pentacene[130].

Different transistor device structures can be prepared by changing the sequence of device fabrication (i.e. top contact-bottom gate or bottom contact-bottom gate). Each component of thin film transistors is important in establishing the performance of the device. In the following subsections, interfaces between metal electrode/organic semiconductor and ITO/WO_3 electrode are briefly discussed.

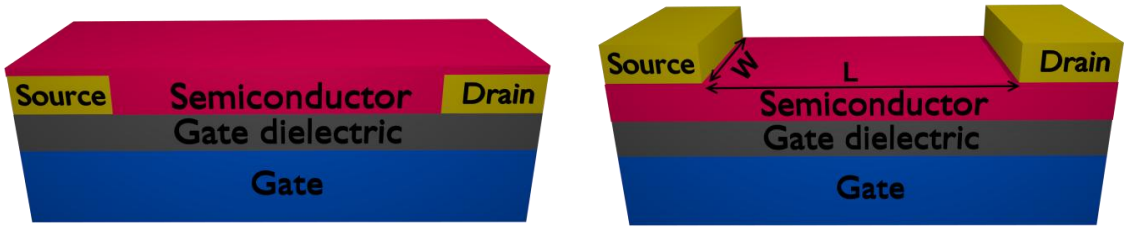

Figure 2-10 Thin film transistor configuration: (left) bottom gate/bottom contact and (right) bottom gate/top contact. *W* is the channel width and *L* is the channel length.

2.3.2 Electrode/semiconductor interfaces

Metal electrode/Organic semiconductor interfaces: The metal electrode/organic semiconductor interface is of high importance for thin film transistors operation. Metal electrode surfaces are prone to form dipoles even when they are stored in relatively dry inert gas atmosphere, leading to possible changes in the work function of the metal electrodes (Figure 2-11) [131]. Interface energetics are usually studied by spectroscopic techniques i.e. photoemission spectroscopy [132]. Because metal electrodes are used for extracting (injecting) charge carriers from the organic semiconductor, a good matching between the HOMO (LUMO) level of the semiconductor with the electrode work function is desired [77], [131], [132], [133], [134], [135], [136], [137], [138].

Ambipolar charge carrier transport, i.e. simultaneous electron and hole transport, is also possible under certain conditions e.g. with small energy band gap semiconductors ($E_g < 2$ eV) [5], [139], [140], [141]. N-type charge transport is rarely observed for organic semiconductors because of the unfavorable location of their LUMO level with respect to commonly employed metal electrode materials such as Au. In electrochemical terms, organic semiconductors usually have low electrochemical reduction potentials [142].

In this thesis, Article 3 reports ambipolar organic thin film transistors based on a soluble pentacene derivative. HOMO and LUMO levels of this novel pentacene derivative were compared with that of pentacene. The relative placement of the LUMO level of the new molecule was found to be closer to the Au work function leading to electron injection from the molecule to the metal electrode. In Article 4, p-type and ambipolar π-conjugated molecules making use of azomethines (–N = C–) compared to more conventional (–C = C–) coupling protocols are demonstrated. The position of the HOMO and LUMO levels with respect to Au electrode work function as well as the effect of electron donating groups in the molecular structure were discussed to explain the p-type and ambipolar behavior of the molecules [95]. We also studied the effect on the location of the HOMO and LUMO energy [4] of the oxidation level at the central sulfur in novel dithienothiophene oligomers. Although we did not observe an n-type behavior or ambipolarity for thin films prepared from these molecules, we observed p-type conductivity in the channel and the highest mobility was observed for oligomers with the lowest

hole injection barrier, i.e. with the smallest difference in energy between the location of the HOMO levels and the Fermi energy of the metal electrode.

WO_3/ITO interfaces: ITO is a commonly used transparent conductive oxide in display devices and photovoltaic cells with a Fermi level located at 4.7 eV with respect to vacuum [143]. The conduction band and valence band edges of WO_3 depend on the structure of the material and the experimental environment and they are approximately located at 4.6 and 7.3 eV (Figure 2-12) [144], [145], [146], [147], [148], [149].

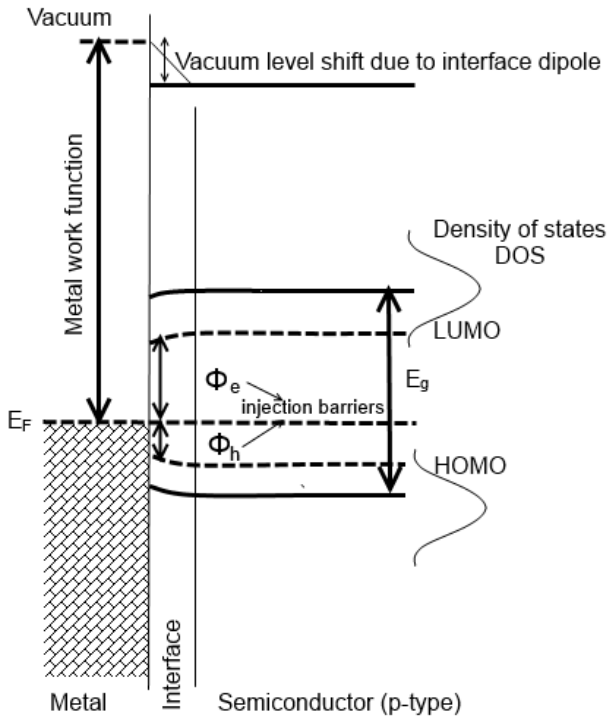

Figure 2-11 Scheme of the metal/p-type semiconductor interface. The hole (electron) injection barrier, Φ_h (Φ_e), is the difference between HOMO (LUMO) level of the organic semiconductor and the Fermi level of the metal. Φ_h is small enough for hole injection. The effect of an applied bias at the gate electrode on the HOMO and LUMO levels at the interface is also shown by a small bending. GDOS is also shown. (Adapted from [71])

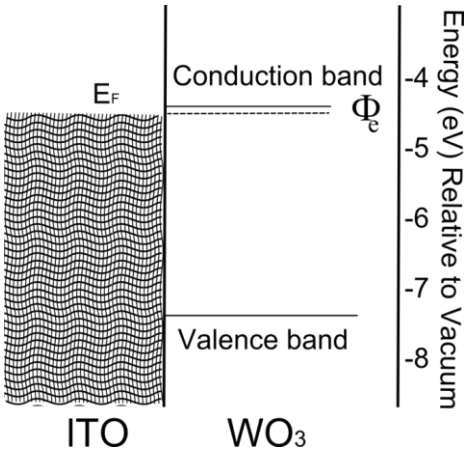

Figure 2-12 ITO/WO_3 interface energy band diagram. The Φ_e for electron injection is <0.1eV.

2.3.3 Gate dielectric

Semiconductor/gate dielectric interface is as important as the semiconductor/metal interface. The relative dielectric constant ε is related to the capacitance, C, of the material (Eqn 2-1):

$$C = \frac{\varepsilon_{\circ} \cdot \varepsilon \cdot A}{t} \qquad \textit{Eqn 2.1}$$

In this equation, $\varepsilon_{\circ}$ is the permittivity of free space (8.85×10^{-12} F/m), A is the surface area of the gate dielectric and t is its thickness. Gate dielectric selection criteria depend on dielectric constant and thickness, which needs to be as low as possible. Nevertheless, thin gate dielectrics can show high leakage current at the semiconductor gate electrode interface. Therefore the best dielectrics are those with high dielectric constants which can be deposited as very thin layers [150], [151].

Organic semiconductor/Gate dielectric interfaces: In organic thin film transistors the gate dielectric importance is two-fold: (i) functional properties of the films highly depend on the molecular ordering at this interface and (ii) the interfacial chemistry affects charge carrier trap density [152]. The arrangement of the molecules at the interface results in different

morphologies, structure and textures, i.e. π-π stacking vertical or parallel to the source and drain electrodes [5], [153], [154], [155], [156], [157], [158]. Considering that the field effect transistor operation depends on the first few nanometers at the vicinity of the organic semiconductor/gate dielectric interface, the importance of such interface can be easily understood [159]. Studies on benchmark pentacene and tetracene films showed that the gate dielectric surface roughness is an important parameter that affects the morphology, which in turn affects the transistors performance [130], [152], [160], [161]. A high roughness of the gate dielectric leads to smaller islands. The connectivity of the islands and the surface coverage play an important role in the performance of thin film transistors [152].

Second, the interfacial chemistry plays an important role in the charge carrier trap density at the semiconductor/gate dielectric interface. To improve the quality of this interface, passivating self assembled monolayers can be used [162], [163], [164]. In this Ph.D. work, SiO_2 gate dielectric was treated by hexamethyldisilazane (HMDS) [5], [95], [163], [165], [166]. A clear difference in device operation between HMDS treated and non-treated samples was observed, with low surface coverage observed for non-treated substrates [152], [167], [168].

WO_3/Ionic liquid interfaces: Electrolyte gating is an effective approach to lower the operating voltage of transistors. The structure of the electrical double layer forming at the semiconductor/electrolyte interface is one of the keys to the effectiveness of the gating [169], [170], [171], [172], [173][173]. The structure of the electrical double layer depends on a number of factors, such as the anion and cations constituting the electrolyte, the ionicity of the ionic liquid (i.e. the degree of dissociation of the ions) the applied electrical bias, the purity of the ionic liquid, the nature of the working electrode and the working electrode surface [174]. Because of the high capacitance values that can be achieved (eqn 2.1) using electrical double layers the amount of charge carriers accumulated in the semiconductor films is also remarkably high, for relatively low operating voltages [175], [176], [177][178].

2.3.4 Organic thin film transistor operation

Organic thin film transistors work most frequently in accumulation mode [30]. The operation of organic thin film transistors is generally described making use of the metal oxide insulator field effect transistor model.

The operation can be divided into three regions: cut-off, linear region and saturation region (Figure 2-13). This model assumes a long transistor channel length where the electrical field created by the gate electrode bias overcomes the transverse electrical field in the channel, i.e. the gradual channel approximation [179], [180].

Threshold voltage (V_{Th}) is defined as the minimum gate voltage that is required to electrostatically induce the channel [30], [181]. The current in the channel starts to flow in the transistor channel when the threshold potential is exceeded ($V_{GS}>V_{Th}$).

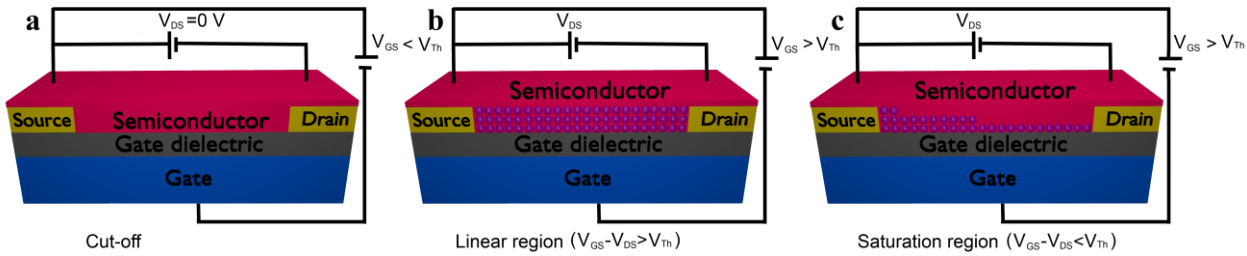

Figure 2-13 Schematic illustration of organic thin film transistor operation. Circles in the semiconductor layer illustrate the holes during different stages of transistor operation. In (a) Cut-off, (b) Linear region and (c) the saturation region are illustrated.

In cut-off conditions, where $V_{GS}<V_{Th}$ no or very low current flows in the transistor channel, which is called the off-current (Figure 2-13a).

In the linear region, at $V_{DS}< V_{GS}-V_{Th}$ and $V_{GS}>V_{Th}$ the Fermi energy level raises and the semiconductor energy bands bend upwards (Figure 2-13b). A thin sheet of mobile charge carriers is induced into the channel. At this point the transistor channel behaves like a resistor and the

current depends on the accumulation of positive charges as a function of the gate voltage. The resistance of the channel remains almost constant in this region, where the drain current I_{DS} is proportional to the V_{DS}. The current collected when the channel is open is called the on-current. At higher V_{DS} values, the amount of induced mobile charge carriers decreases and the slope of the I_{DS} vs V_{DS} curve starts to decrease because of increasing resistance. At $V_{DS} = V_{GS} - V_{Th}$ pinch-off occurs and the charge concentration at the drain electrode is said to become zero. In the saturation region, when $V_{DS} > V_{GS} - V_{Th}$ and $V_{GS} > V_{Th}$ the current in the channel saturates.

Figures of merit for transistor operation is further discussed in section 2.3.6 combined with electrolyte gated transistor characterization.

2.3.5 Mechanism of electrolyte gating

Low operating voltages can be achieved with thin gate dielectric layers and high dielectric constants [160], [182], [183] but also with more unconventional approaches such as electrolyte gating, which can take place by two different mechanisms: electrostatic (electric double layer) and electrochemical (Figure 2-14). In the electrostatic mechanism, the electrical double layer forming at the semiconductor/electrolyte interface upon the application of a gate voltage results in the electrostatic doping of the semiconductor [25], [26], [32], [72], [178], [184]. Electrical double layer capacitances per unit area are approximately 10 - 500 $\mu F\ cm^{-2}$ whereas the typical capacitance of a 200 nm-thick SiO_2 dielectric layer is of tens of $nF\ cm^{-2}$. In the electrochemical mechanism of electrolyte gating ion intercalation takes place [185], [186], [187]. In principle, the sizes of the ions constituting the ionic liquids are such that the electrochemical mechanism is unfavorable compared to the electrostatic.

2.3.6 Transistor figures of merit

Thin film transistor characteristics are mainly evaluated by acquisition of the output (I_{DS} vs V_{DS}) and transfer transistor characteristics (I_{DS} vs V_{GS}) [188], [189]. The parameters used in describing the transistor operation are listed in Table 2-2. Charge carrier mobility (μ_e and/or μ_h), threshold voltage (V_{Th}) and I_{ON}/I_{OFF} ratio of the transistor are the three basic parameters that needs to be reported after transistor characterizations.

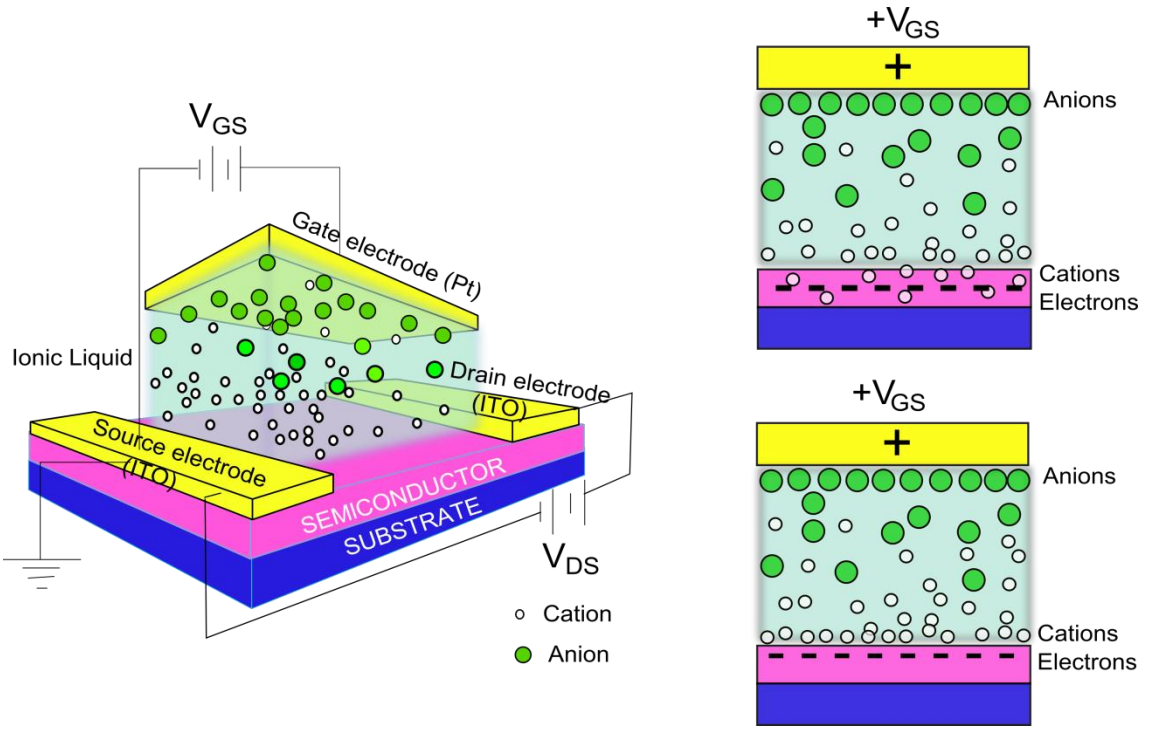

Figure 2-14 General structure of an electrolyte gated transistor (left). Electrochemical mechanism (top right) and electrostatic mechanism (bottom-right) of doping during electrolyte gating.

Charge carrier mobilities of devices in the linear (μ_{Lin}) and in the saturation (μ_{Sat}) region can be calculated by use of the equations 2.2 and 2.3:

$$\mu_{Lin} = \frac{L}{WC_i}\left(\frac{1}{V_{DS}} \cdot \frac{\partial I_{DS}}{\partial V_{GS}}\right) V_{DS=const} \qquad \textit{Eqn } 2.2$$

The mobility at saturation can be determined by substituting $V_{DS}=V_{GS}-V_{Th}$ in Eqn 2.2 and simplifying to:

$$\mu_{Sat} = \frac{2L}{WC_i}\left(\frac{\partial\sqrt{I_{DS}}}{\partial V_{GS}}\right)^2_{V_{DS}=const>V_{GS}-V_{Th}} \qquad \textit{Eqn } 2.3$$

V_{Th} is deduced from the maximum slope of the transfer curve (sqrt I_{DS} vsV_{GS}). I_{ON}/I_{OFF} ratio gives a hint on the ability of the device to switch on and off and is calculated by dividing the max I_{DS} value by the minimum I_{DS} value of the transfer curve ($LogI_{DS}$ vs V_{GS}).

Table 2-2 Transistor parameters

Parameter	**Symbol**	**Unit**
W	Channel width	μm
L	Channel length	μm
C_i C_{EDL}	Specific gate capacitance Electrical double layer capacitance	$\frac{F}{cm^2}$
I_D	Drain current	A
I_G	Gate current	A
I_S	Source current	A
V_{GS}	Gate-source voltage	V
V_{Th}	Threshold voltage	V
V_{DS}	Drain-source voltage	V
μ_e μ_h	Electron mobility Hole mobility	$\frac{cm^2}{V \cdot sec}$

CHAPTER 3 EXPERIMENTAL METHODS AND TECHNIQUES

3.1 Sample preparation

In this section of Chapter 3, a brief introduction to organic thin film transistor and electrolyte gated thin film transistor structures is given. Afterwards, the procedures for substrate cleaning and substrate surface modification processes are illustrated. Solution preparation and deposition by solution based techniques together with post-deposition steps are detailed. For electrolyte gated thin film transistors, an additional step for PDMS well preparation and ionic liquid confinement step is presented.

3.1.1 Organic thin film transistors: device structure

Organic semiconductors were tested on bottom contact/bottom gate transistor substrates making use of circular Au source and drain interdigitated electrodes photo-lithographically patterned on SiO_2 (195 nm-thick, $C_i = 1.77 \cdot 10^{-8}$ F/cm^2), thermally grown on heavily doped Si(n^+) wafers (resistivity 0.001-0.005 Ohm cm^{-1}) (Figure 3-1). Au has a Fermi level of 4.4 eV [100]. An advantage of using Au electrodes is that they do not get oxidized in ambient conditions as Ca, Mg, Al electrodes. Characteristics of the transistor structures used for organic thin film transistor studies are listed in Table 3-1 and Table 3-2 for the channel and the material, respectively.

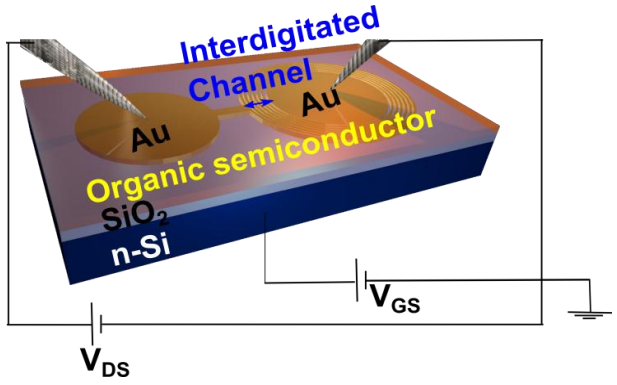

Figure 3-1 Bottom contact-bottom gate (Si (n^+)) transistor substrate with interdigitated pre-patterned Au electrodes (30 nm thick) and SiO_2 (195 nm) gate dielectric coated with an organic semiconductor.

Table 3-1 Transistor channel widths (W) and lengths (L) in organic thin film transistors investigated in this work.

	W (µm)	**L (µm)**
Interdigitated devices	6	41000
	20	41800
	40	18800

Table 3-2 Gate dielectric properties for organic thin film transistors investigated in this work.

SiO_2 Relative Dielectric Constant	3,9
SiO_2 Thickness [nm]	195
SiO_2 Absolute Dielectric Constant [F/m]	$8{,}854187818\times10^{-12}$
C_i [F/m^2]	$1{,}770837564\times10^{-4}$

3.1.2 Electrolyte gated thin film transistors: device structure

The effect of the electrolyte gating on the WO_3 thin films was tested in the electrolyte gated transistor configuration (Figure 3-2). In this configuration, the channel conductivity is controlled by a gate electrode that is immersed into the electrolyte that is confined by a PDMS well positioned in correspondence of the semiconductor channel.

3.1.3 Ionic liquids

Ionic liquids were used as electrolytes for electrolyte gated thin film transistors. During the work conducted in the frame of this thesis ionic liquids were selected as the gating medium (Table 3-3) due to their non-volatile and highly conductive nature. Ionic liquids also posses high chemical stability with relatively wide electrochemical windows [190]. The electrochemical window is defined as the voltage range in which the electrolyte is electrochemically stable. Ionic liquids are molten salts that do not contain any solvent; they are solely formed of anion and cation pairs.

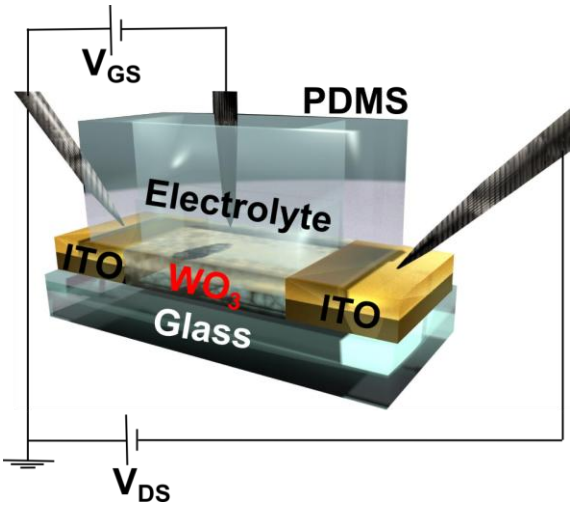

Figure 3-2 Electrolyte gated transistor built on a glass substrate with patterned ITO electrodes. The channel is in contact with the electrolyte, confined in a PDMS well on top of the channel. An electrode immersed into the electrolyte is used to gate the channel.

Table 3-3 Properties of the ionic liquids used for the characterization of electrolyte gated transistors.

Name (abbreviation)	**Viscosity (Poise)**	**Ionic Conductivity (mS/cm)**	**Electrochemical Window* (V)**		**Molecular structure** 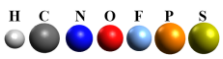
			Anodic limit	Cathodic limit	
1-Butyl-3-methylimidazolium hexafluorophosphate (BMIM:PF6)	310×10^{-2}	1.37	2.2	-1.8	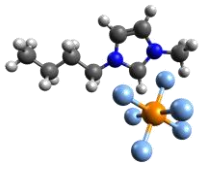
1-Butyl-3-methylimidazolium bis(trifluoromethylsulfonyl)imide, (BMIM:TFSI)	49×10^{-2}	3.41	2.6	-2.1	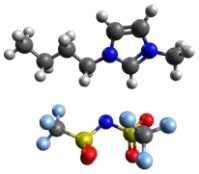
1-Ethyl-3-methylimidazolium bis(trifluoromethylsulfonyl)imide (EMIM:TFSI)	39×10^{-2}	6.63	2.5	-2.1	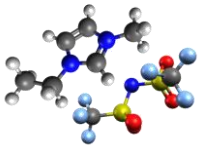

*Ag/AgCl reference electrode [191]

Other types of electrolytes were also reported to be used for electrolyte gating: aqueous electrolyte and non-aqueous electrolytes, ionic liquid gels, polyelectrolytes and polymer electrolytes. However, aqueous and non-aqueous electrolyte solutions are volatile due to the used solvents also aqueous electrolytes use is limited by the electrochemical window due to hydrolysis. Polyelectrolytes exhibit lower conductivity compared to ionic liquids and polymer electrolytes are non-volatile with relatively low ionic conductivities [178], [190], [192].

3.1.4 Cleaning and surface modification of transistor substrates

The interfaces between the semiconductor, the electrodes and the dielectric are of key importance in terms of device performance. The wetting properties of the film have an important role in its final structure and morphology. In organic semiconductors, film morphology and supramolecular organization strongly affect the charge transport properties of the films [160]. At the same time, the cleaning of the surface is also important considering the work function of the metal electrodes that can be affected by impurities present at the electrode surface, e.g. by dipole formation, with possible effects on the energy level alignment at the metal electrode/semiconductor interface [193].

Cleaning procedure:

The cleaning procedure used for the SiO_2 dielectric that was used in organic thin film transistors fabrication is the following one: Sonication in acetone to remove the photoresist (15min). This first sonication is followed by sequential sonication in isopropanol (IPA) (15min), acetone (15min), IPA (15min) and blow drying with nitrogen jet. A subsequent exposure to UV-Ozone treatment for 20 min or O_2 plasma for 3min (medium power) is conducted to remove organic residues from the surface.

For WO_3 transistors, pre-patterned ITO electrode-on glass substrates were cleaned by sonicating them in ALCONOX-distilled water solution for 15 min, followed by 15 min sonication in distilled water, blow drying and exposure to UV-ozone for 20 min [194], [195].

Surface modification of SiO_2:

Surface modification is usually needed for two reasons i) to reduce the charge carrier trapping sites at the dielectric/semiconductor interface and ii) to improve the wetting properties of the semiconductor film. SiO_2 surface modification was done by coating the cleaned substrates

with hexamethyldisilane (HMDS) and annealing them for 1 hr at 120 °C. The treatment by hexamethyldisilazane (HMDS) aims at replacing the hydroxyl groups, which are found on SiO_2, with apolar methyl groups, to improve the wettability of the surface. Substrates are stored in a glovebox with O_2 and H_2O < 1ppm for up to one week.

3.1.5 Solution preparation

Organic thin film transistors

Preparation of the solutions and the deposition of the films were carried out in a N_2 glove box (H_2O, O_2 < 1 ppm). Chlorobenzene (anhydrous) was chosen as the solvent. Used solution concentrations for different organic materials are summarized in Table 3-4.

Table 3-4 Summary of the solutions and preparation conditions for organic thin films investigated in thin film transistor configuration.

Organic semiconductor	**Concentration**	**Spin coating /Drop-cast**	**Post-treatment**
2,3-dicyano-6,13-bis-(triisopropylsilylethynyl)pentacene (2,3-CN2-TIPS-Pn)	*	Drop-cast and Coated from pre-heated chlorobenzene solutions (800 rpm for 15 s then 2000 rpm for 45 s)	With and without thermal treatment. Thermal treatment was performed for 1 hour at 100 °C, in a N_2 glove box.
Bis(triisopropylsilylethynyl) octafluoropentacene TIPS-F8	*		
Triethylsilyl octafluoropentacene TES-F8	*		
2-Amino-5-[(3,4-bis(decyl)-5-formylthiophen-2-ylmethylene)-amino]thiophene-3,4 dicarboxylic acid diethyl ester	5 mg/mL	The films were deposited by spin coating at 2000 rpm for 45 s at room temperature	
2,5-Bis[(E)-2-(5-methylthiohene-2-yl)vinyl] thiophene			
Thiopheno-polyazomethine			

** see Table 4-2*

Tungsten trioxide

Chemical precursor and thin film preparation: The chemical precursor to prepare the WO_3 thin films was obtained by a sol-gel method already reported in the literature, slightly modified by the use of the organic stabilizer poly(ethylene glycol) (PEG) 200 instead of PEG 300 [65]. The films were obtained by depositing on the patterned ITO substrate the chemical precursor, i.e. the tungstic acid stabilized by PEG 200, by spin coating (1500 rpm, in ambient conditions). WO_3 was spin coated onto the microfabricated, cleaned substrates and subsequently annealed in a tubular furnace under 100 sccm O_2 flow at ~500 °C during 30 min [105].

3.1.6 Thin film deposition: spin coating and post-treatment

Spin coating is a commonly applied deposition technique in research and development laboratories to prepare highly uniform thin films of the semiconductors. The spinning rate is the defining step in this deposition technique; increasing the spinning rate and lowering the viscosity of the solution decreases the thickness of the coated film. Pinholes, comets and non-uniform edges on the non-circular substrates are the frequently observed defects. Pinholes and comets can be prevented by filtering the solution.

Organic semiconductor thin films were separated into two groups as heat-treated and pristine. Heat treatment is a typical way of reorganizing the molecules on the SiO_2 dielectric surface. The effect of heat treatment is discussed in the chapters presented as articles.

3.2 Transistor characterization

Electrical measurements in thin film transistor configuration were performed using a semiconductor parameter analyzer (Agilent B1500A). Testing conditions were selected depending on the material properties.

Most organic semiconductors do not show long term stability when exposed to H_2O or O_2 therefore the measurements of the organic thin film transistors were carried out under vacuum, $P=10^{-6}$ Torr, in a micromanipulated probe station directly connected to the N_2 glove box where the film deposition was done.

For the electrolyte gated thin film transistors, the environment and the exposure to the light were also important. Ionic liquids that are used in this Ph.D. work are sensitive to H_2O and O_2. WO_3 is a well known photocatalyst that absorbs the near UV - blue portion of the electromagnetic spectrum therefore measurements were conducted in dark and in the N_2 glove box. All the measurements were done at room temperature.

3.3 Morphological, Structural and optical characterization of thin films

3.3.1 Powder and thin film X-Ray Diffraction (XRD) and Grazing Incidence X-ray Diffraction (GIXRD)

X-ray diffraction is used in the characterization of the crystal structure and orientation of crystals in a polycrystalline material [196]. When organic molecular materials are investigated, XRD can provide insight on molecular packing, which dramatically affect the charge carrier transport and optical properties of the films [5], [152], [154], [155], [197], [198]. The use of XRD is commonly applied in inorganic powders and thin films research, to determine the crystal structure and to understand how the crystallographic planes were aligned in the transistor channel [196].

Organic semiconductor films used in this Ph.D. work were usually ~100 nm thick (depending on the deposition technique, concentration of the solvent) and cannot be easily characterized by a conventional X-ray source and configuration. High intensity and a grazing incident beam are needed in order to reveal the structure and the molecular packing of the thin films. In collaboration with the research group of Professor Luca Lutterotti (Universita di Trento, Italy) structural data on organic thin films were collected , in particular on 2,3-CN2-TIPS-Pn , at the XRD1 beamline of the Elettra synchrotron (Trieste, Italy) [199]. A modified Rietveld refinement method was used to obtain the film texture and the phase from GIXRD data. In the GIXRD configuration the incident synchrotron beam is directed to the sample at a selected angle to limit the penetration (to prevent scattering from the substrate) and to scan to the full depth of the thin film. Reflected X-rays are detected with a 2D CCD camera that is set perpendicular to the incident beam. The data is first converted into 2D images showing in-phase and out-of-phase reflections and a 2D detector geometry is used for this purpose [200].

For the case of thiopheno-azomethines characterization was limited to the characterization of powders, at the Université de Montréal. X-ray powder diffraction patterns were obtained using a Bruker X-ray diffractometer with monochromatic Cu-K_α (1.54 Å) radiation (40 kV, 40 mA). Samples were mounted on a capillary tube sample holder and scanned in the 2θ range 1°- 25°, with a step size of 2θ = 0.01°.

For WO_3 thin films structural studies were already available in the literature. Using our synthetic procedure the polycrystalline films are known to have a high degree of orientation and a monoclinic structure [65].

3.3.2 Atomic force microscopy (AFM)

AFM is applied as a characterization method in thin film research to gain insight in the surface topography of a sample, including surface roughness. AFM signal detection loop comprises a micro cantilever a laser beam that is reflected into a position sensitive photon detector (PSPD), detecting the cantilever deflections during the entire scan) and a software to produce the surface profile map depending on the cantilever deflection. We used two different AFM instruments: the cantilever was scanned over the sample as in the Dimension 3100 (Digital Instruments) and the sample was scanned under the tip in the IIIa-MultiMode AFM (Digital Instruments).

AFM provides a 3D topographical image of the scanned area which reveals the surface profile and the surface roughness by the root mean square averaging (r_q) can be evaluated from the collected data by use of Nanoscope software. Height and phase images are used to correlate the topographical information to formed phases and directionality. Phase images (material property), in some cases can be used for advanced characterization such as determining preferred orientation of the molecules, to distinguish different phases. Phase images are obtained by processing the changes in the cantilever's oscillation amplitude. Height image and the phase image are collected simultaneously [201].

AFM is used commonly in tapping or contact mode. Tapping mode has certain advantages over the contact mode: i) with organic materials not hard enough to preserve their structure when brought into contact with a hard tip since some of the bonds at the surface may be broken or can

be totally scratched out of the substrate and ii) with a hard surface such as those of metal oxides where the microcantilever tip may be damaged when brought into contact with the surface. In tapping mode, the tip touches the sample surface lightly by an oscillating tip and the oscillation amplitude changes with sample surface. The tip plays an important role in the resolution of the AFM. In tapping mode etched single crystal Si cantilevers are preferred due their stiffness which creates higher resonance frequencies compared the SiN cantilevers that are used in contact mode [201].

Considering these advantages, tapping mode AFM was used to study the nanoscale morphology, surface coverage, roughness of the organic molecular thin films and WO_3 thin films, in the transistor channel. Samples were scanned in ambient conditions at room temperature in tapping mode using a IIIa-MultiMode AFM (Digital Instruments) or Dimension 3100 (Digital Instruments) and etched Si microcantilevers with a resonance frequency around ~500 kHz and tip radius of <10 nm. The two models enable the user to have high quality images with high spatial resolution in the nanoscale.

As a final note, the image resolution depends on the size of the area being scanned. AFM has imaging options in three different pixilation modes. The number of data points present in the image is determined by this choice in the X and Y scan direction512, 256, and 128. In order to have higher resolution 512 × 512 resolution is usually preferred. The smallest feature that can be imaged can be calculated as follows: For a 10μm × 10μm image, we divide 10 by 512 and find the primary cell size that is ~19.5 nm. This gives us the resolution.

3.3.3 Fluorescence hyperspectral imaging

Fluorescence Hyperspectral Imaging was performed with PARISS (Prism and Reflector Imaging Spectroscopy System by LightForm Inc., Asheville, NC, USA. Fluorescence Hyperspectral Imaging is used to study the optical properties of organic and inorganic semiconductors and is used as a tool to characterize fluorescent samples by collecting spectral information in a field of view (FOV). The FOV is formed by heterogeneously distributed components in the sample that have different spectral properties or a homogenous component with a unique spectrum. These are considered as "spectral fingerprints" of the fluorescent

components of the sample. The topography of the sample can subsequently be determined by building a fluorescent spectral map of the sample.

During this Ph.D. work, fluorescence hyperspectral imaging was used to characterize the optical properties and also to gain insight about the substrate coverage and the morphological properties of the thin films. Fluorescence microscopy also provided an insight in the morphology-charge transport relationship in thin films.

The hyperspectral images (spectral maps) were generated in the "push broom" mode by use of a wavelength-dispersive spectrometer collecting all wavelengths simultaneously at each location along the slit by translating the FOV underneath the spectrometer on an automated translation stage connected to the microscope[202]. The information was collected with PARISS 8 software with a minimum correlation coefficient (minCC) > 0.98, in realtime.

The image size and spatial resolution was calculated by dividing the slit height (5 mm) and slit width (25μm) to the magnification of the objective lens of the microscope.

All the images were obtained in ambient conditions, at room temperature. Grayscale referred to as “processed” images were further analyzed and the spectral libraries of each sample were collected and categorized into *classes*. Classes of spectra were given pseudocolor codes, which were correlated and *painted* onto the FOV in its associated pseudocolor, forming the classified image. By use of classified images we were able to quantitatively evaluate the percentile surface coverage of each fluorescent component. Fluorescence hyperspectral imaging was used for fluorescent molecules only (Chapter 5-section 5.2.7).

3.3.4 Scanning Electron Microscopy (SEM) and Energy Dispersive X-Ray Spectrometer (EDS)

Scanning electron microscopy (SEM) was used to investigate the morphological properties of the WO_3 thin films and to qualitatively characterize the formation of a channel between the ITO electrodes by using an Energy Dispersive X-Ray Spectrometer (EDS) coupled to the SEM. Images were collected by irradiating the region of interest with a focused electron beam; the interactions between the e-beam and the material results in secondary and backscattered electrons that carry information on the morphology and the chemical composition, respectively. Other

signals such as characteristic X-rays are also produced and during electron-material interaction and they are used for quantitative analysis of the chemical composition at the region of interest. SEM allows resolving nanometer size (1-5 nm) features (high spatial resolution) [203]. EDS analysis is usually limited by the thickness of the specimens and if the thin film has a thickness less than 1 μm the analysis would contain information from the substrate as well as the film.

Scanning electron microscopy images were obtained with a Hitachi S-4700 scanning electron microscope in the secondary electron mode using the upper and lower detectors in ultra high resolution mode (×150K magnification, at an accelerating potential of 10 kV and a working distance of 5 mm).

EDS analysis was done in the analysis mode at an accelerating potential of 10 kV and a working distance of 12 mm. X-ray mapping is a way of presenting the elemental constituents in a microstructure. Here, the colors were attributed to each element to show their location in the region of interest. By use of this method the removal of ITO after wet chemical etching was assessed (an electrical characterization of each pattern before the use of substrates by applying a few volts between the drain and source electrodes was also carried out to check the effectiveness of the removal).

3.4 Electrochemical Impedance Spectroscopy (EIS)

Capacitance measurements

Electrochemical impedance spectroscopy (EIS) measurements were performed on electrolyte gated transistors to explore the characteristics of the electric double layer formed at the semiconductor electrolyte interface upon application of a gate electrical bias.

The electric double layer capacitances of the semiconductor/electrolyte interfaces were investigated by analyzing impedance spectra at the frequencies from 10 mHz to 1 MHz as a function of the applied electrical bias (direct current potential, E_{DC}). Cells for the characterization were formed of a circular Pt disc as the counter electrode (the circular electrode area: was 0.070 cm^2) immersed in the ionic liquid [BMIM][TFSI], [EMIM][TFSI] and [BMIM][PF6] confined with a PDMS well on a WO_3 thin film as the working electrode that was coated onto an ITO/glass

substrate. The E_{DC} was varied between 0-2 V for the ILs with ΔE=0.25 V and a fixed E_{AC}=10 mV root mean square (alternating current potential) was applied during the measurements.

To prevent water intake and parasitic electrochemical reactions the measurements with ionic liquids were carried out in a glovebox (O_2, H_2O < 1 ppm) using a VersaSTAT 4 Electrochemical Impedance Spectrometer.

CHAPTER 4 MOLECULAR AND THIN FILM ENGINEERING OF π-CONJUGATED PENTACENE DERIVATIVES

FOREWORD

In this chapter, the impact of molecular engineering (e.g. by addition of substituent groups and moieties) on the charge carrier transport properties of soluble pentacene derivates is discussed. Three semiconductor pentacene derivatives with charge transport properties namely, Bis(triisopropylsilylethynyl) dicyanopentacene, Bis(triisopropylsilylethynyl) octafluoropentacene and Triethylsilyl-octafluoropentacene, were demonstrated (Figure 4-1). In Article 1, thin film transistors based on solution deposited films of a pentacene derivative, 2,3-dicyano-6,13-bis-(triisopropylsilylethynyl)pentacene (2,3-CN2-TIPS-Pn) was reported. The charge transport properties observed in these materials were explained according to the position of the highest occupied molecular orbital (HOMO) and lowest unoccupied molecular orbital (LUMO) with respect to the Fermi level of Au (4.4 eV with respect to vacuum) charge-injecting electrode and the arrangement of the molecules in the film, as deduced by grazing incidence X-ray diffraction analysis.

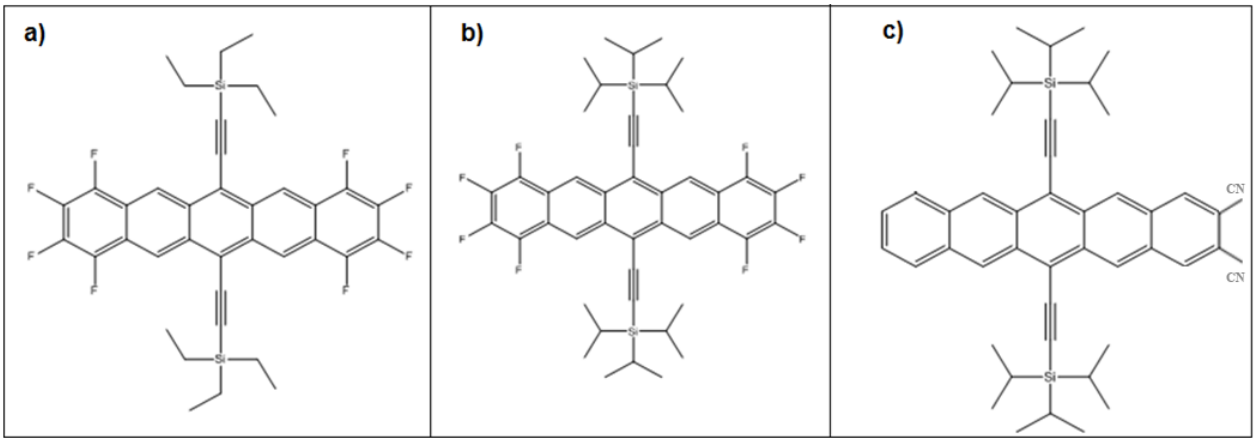

Figure 4-1 Molecular formulas of (a) triethylsilyl-octafluoropentacene, (b) Bis(triisopropylsilylethynyl) octafluoropentacene and (c) Bis(triisopropylsilylethynyl) dicyanopentacene

4.1 π-conjugated pentacene derivatives: Effect of the functionalization and the processing conditions on the thin film transistor performance

The interest in obtaining solution processable π-conjugated oligomers and polymers exhibiting appropriate charge transport, optical and intrinsic properties for use in thin film transistors, light emitting diodes, electrochromic devices and organic photovoltaics is the driving force for the organic electronics, a multidisciplinary field nourished by the mutual developments in synthetic chemistry, materials science, solid-state physics and electronics.

The motivation for processing pentacene derivatives lies in the possibility of manufacturing relatively high mobility electronic devices by solution based coating techniques. Pentacene is an insoluble organic semiconductor and requires vacuum techniques for thin film processing. At the same time its lacks photo-stability due to the low oxidation potential [99], [204]. When compared to many organic semiconductors pentacene has a relatively high mobility on the order of ~5 $cm^2/V \cdot sec$ on polymer gate dielectrics [205]. Pentacene shows a "herringbone" crystal structure in which the molecules are packed in two dimensional layers by edge-to-face stacking [210]–[212]. However, face-to-face stacking is believed to increase the charge carrier mobility in pentacene. In order to achieve face-to-face stacking most commonly applied approach is to use substitutional groups that would disrupt the herringbone motif of stacking. While disrupting the herringbone crystal structure substitutional groups would also improve the solubility. Also, it is important to mention the function of the carbon-carbon triple bond that is critical in the final crystal structure. The triple bond was reported to serve in holding the substituent away from the aromatic surface. This allows the face-to-face -stacking orientation of adjacent molecules [166]

In this Ph.D. thesis, the effect of alkyl groups in the solubility of pentacene derivatives and the HOMO-LUMO levels was explored. In addition, the effect of cyano- and fluoro- electron withdrawing moieties in tuning the HOMO-LUMO levels with respect to that of pentacene was explored. Use of electron withdrawing moieties such as bromo-, cyano-, and trifluoromethyl moieties was reported to improve the electrical conductivity in organic thin film transistors [98].

Among the three molecules bis-(triisopropylsilylethynyl) dicyanopentacene (2,3-CN2-TIPS-Pn), which is a modified form of 6,13-bis(triisopropylsilylethynyl)-pentacene (TIPS-pentacene) (Article 1), exhibits ambipolar charge carrier properties. Additional two cyano- groups at the two ends of the pentacene backbone are reported to be responsible for electron conductivity [5], [205], [206]. The other two fluorinated pentacene derivates, TIPS-F8 and TES-F8, exhibited n-type charge transport properties only. Experimental results for the extended work are reported in section 4.3.

4.2 ARTICLE 1: Ambipolar organic thin film transistors based on a soluble pentacene derivative

Dilek Işık[1], Ying Shu[2], Giuseppe Tarabella[3], Nicola Coppedè[3], Salvatore Iannotta[3], Luca Lutterotti[4], Fabio Cicoira[3], John Edward Anthony[2], Clara Santato[1]

[1]*École Polytechnique de Montréal, Département de Génie Physique, C.P. 6079, Succ. Centre Ville, Montréal, Québec H3C 3A7, Canada*

[2]*Department of Chemistry, University of Kentucky, Lexington, Kentucky, 40506, USA*

[3]*CNR-IMEM, Parco Area delle Scienze 37/A, 43100, Parma, Italy*

[4]*Dipartimento di Ingegneria dei Materiali e Tecnologie Industriali, Università di Trento, via Mesiano, 77, 38123, Trento, Italy*

Article published in Applied Physics Letters

Submitted on 2011

Published on 2011

4.2.1 Abstract

We report on ambipolar thin film transistors based on solution deposited films of a pentacene derivative, 2,3-dicyano-6,13-bis-(triisopropylsilylethynyl)pentacene (2,3-CN2-TIPS-Pn). The ambipolar charge transport observed in this material is well balanced: the values of the hole and electron mobility are both about $2 \cdot 10^{-3}$ $cm^2/V \cdot sec$. The position of the highest occupied molecular orbital (HOMO) and lowest unoccupied molecular orbital (LUMO) of 2,3-CN2-TIPS-Pn with respect to the work function of the Au charge-injecting electrode and the arrangement of the molecules in the film, as deduced by grazing incidence X-ray diffraction analysis, contribute to explain the charge transport properties of 2,3-CN2-TIPS-Pn films.

4.2.2 Introduction

Organic Thin Film Transistors (OTFTs) are of interest for low cost and flexible electronics [4], [139], [207]. Among the large number of organic semiconductors employed in OTFTs, pentacene stands out as a model compound, reaching a hole mobility (μ_h) as high as ~ 6 $cm^2/V \cdot sec$. Soluble pentacene derivatives for OTFTs have been demonstrated, with 6,13-bis(triisopropylsilylethynyl) exhibiting μ_h >1 $cm^2/V \cdot sec$ [166]. At present, there is an intense research effort to demonstrate ambipolar OTFTs based on soluble pentacene derivatives [3], [140], [208].

Ambipolar OTFTs, relevant for complementary circuits with low power consumption, require injection of holes (h^+) and electrons (e^-), which translates into a good matching between the energy levels of the organic semiconductor and the work function of the electrodes used for h^+ and e^- injection [139], [141], [209]. Since this matching is rarely observed, ambipolar OTFTs are usually based on blends or heterostructures (bilayers) of different p- and n-type semiconductors [80], [210].

In pentacene derivatives that already possess good hole transport properties, substitution with electron withdrawing groups, such as nitrile groups, is expected to lower the position of the lowest unoccupied molecular orbital energy level. In turn, this is expected to promote electron transport in bottom contact OTFTs, where metals with high work functions are typically used for source/drain electrodes.

Here, we demonstrate ambipolar transport in OTFTs based on solution processed 2,3-dicyano-TIPS-pentacene (2,3-CN2-TIPS-Pn), a cyano- substituted pentacene based on 6,13-bis(triisopropylsilylethynyl) (TIPS)-Pn (Figure 4-2a) [96], [211]. The observed ambipolar transport is in agreement with predictions from theoretical calculations [212]. We investigated the film forming properties of 2,3-CN2-TIPS-Pn and the structural properties of the resulting films by atomic force microscopy (AFM) and grazing incidence X-ray diffraction (GIXRD). We used a modified Rietveld method to obtain the film texture from GIXRD data. We propose a correlation between the electronic structure of 2,3-CN2-TIPS-Pn and the molecular packing in 2,3-CN2-TIPS-Pn films with the film charge carrier transport properties.

4.2.3 Experimental

Bottom contact/bottom gate 2,3-CN2-TIPS-Pn TFTs (Figure4-2b) were prepared on Au source and drain electrodes photolithographically patterned on SiO_2 (195 nm-thick, $C_i = 1.77 \cdot 10^{-4}$ F/m^2), thermally grown on heavily n-doped Si (resistivity 0.001-0.005 Ohm/cm), which served as the gate electrode. Prior to film deposition, TFT substrates, cleaned with standard solvent procedures and UV/ ozone exposure, were treated with hexamethyldisilizane (HMDS, Gelest). Films of 2,3-CN2-TIPS-Pn were spin-coated from 10 mg/ml pre-heated chlorobenzene solutions (800 rpm for 15 s then 2000 rpm for 45 s) and annealed for 1 hour at 100 °C, in a N_2 glove box. The TFT characteristics were measured in a vacuum probe station directly linked to the glove box, using a semiconductor parameter analyzer (Agilent B1500A). Film morphology was studied with a Veeco 3100 AFM, in tapping mode, in ambient conditions, using Si cantilevers. GIXRD images were collected at the XRD1 beamline of the Elettra Synchrotron (Trieste, Italy) at grazing angles from 0° to 13° (after that no diffraction figures were detectable), using a 165 mm CCD detector from MarResearch. Images were analyzed by a modified Rietveld method to obtain texture, crystal structure, and microstructure, accounting for absorption and geometrical effects at the specific grazing angle [213].

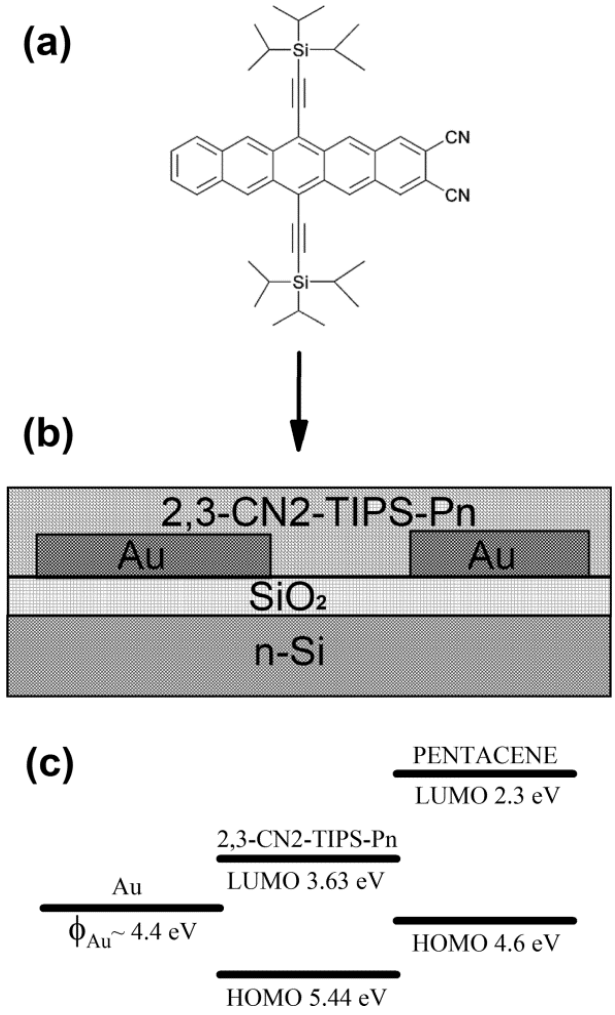

Figure 4-2 Molecular structure of 2,3-CN2-TIPS-Pn (a); bottom gate/bottom contact FET structure used in this work (b); HOMO and LUMO levels of pentacene and 2,3-CN2-TIPS-Pn, with respect to the Au workfunction, Φ_{Au} (c).[100]

4.2.4 Results and Discussion

4.2.4.1 Atomic Force Microscopy

AFM images of the thin film show that solution deposited 2,3-CN2-TIPS-Pn uniformly wets the HMDS modified substrate surface, a key requirement for the application of 2,3-CN2-TIPS-Pn films into TFT devices (Figure 4-3).

4.2.4.2 Thin Film Transistors Characterization

Output (I_{ds} vs V_{ds}) and transfer (I_{ds} vs V_{gs}) characteristics of 2,3-CN2-TIPS-Pn TFTs show well balanced ambipolar transport (Figure 4-4 a-c). The value of the mobility, as extracted from the transfer curves at saturation, was ~$2 \cdot 10^{-3}$ $cm^2/V \cdot sec$ for e^- and h^+. The threshold voltage, V_T, was 29 and -36.5 V, respectively for e^- and h^+ transport.

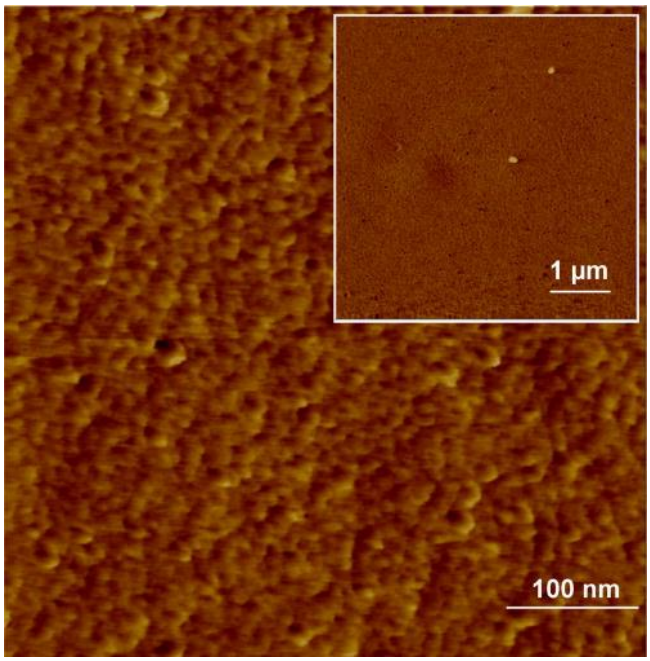

Figure 4-3 1 µm × 1 µm AFM topographical images of 2,3-CN2-TIPS-Pn film on HMDS-treated SiO_2. Inset: 5 µm × 5 µm AFM image of the same sample, rms = 1.56 nm.

Ambipolar transport in 2,3-CN2-TIPS-Pn can be explained, at least partially, by observing the position of the lowest unoccupied molecular orbital (LUMO) and highest occupied molecular orbital (HOMO) of 2,3-CN2-TIPS-Pn with respect to the work function of the Au injecting electrode ($\Phi_{Au,}$ about 4.4 eV) [100]. The LUMO and HOMO levels of 2,3-CN2-TIPS-Pn, deduced by cyclic voltammetry measurements, are located at about -3.63 and -5.44 eV [214], leading to injection barriers of about 0.77 eV for e^- and 1.04 eV for h^+. Clearly, e^- injection from Au is more favorable for 2,3-CN2-TIPS-Pn than for pentacene, where the injection barrier is

about 2.1 eV high. At the same time, the h^+ injection barrier, although larger than for pentacene, is low enough to permit h^+ injection, thus offering the possibility to observe ambipolar transport [215]. We would like to emphasize that in 2,3-CN2-TIPS-Pn OTFTs the ambipolar transport is balanced, differently to what frequently observed in ambipolar OTFT where h^+ and e^- mobility can differ by a few orders of magnitude.

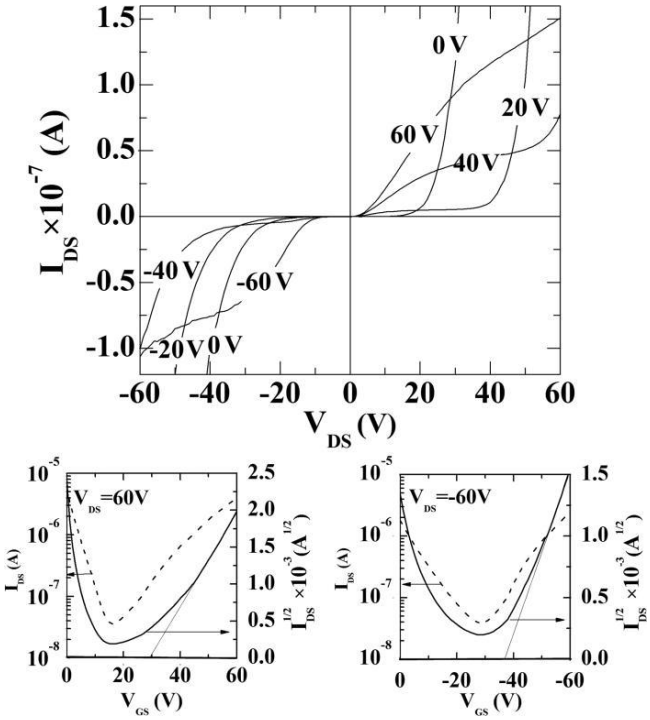

Figure 4-4 TFT characteristics of 2,3-CN2-TIPS-Pn films: output curves (I_{ds} vs V_{ds}) for $|V_{gs}|$ = 0, 20, 40, 60 V in the p- and n-type regions (top); transfer curves (I_{ds} vs V_{gs}) at saturation for V_{ds} = 60 V (bottom left); transfer curves at saturation for V_{ds} = -60 V (bottom right). Channel width/Channel Length = 10 μm/1880μm.

4.2.4.3 Grazing Incident X-Ray Diffraction

It is well recognized that the thin film structural properties play a primary role in establishing film transport properties [157], [216]. To gain insight into the structure and the

molecular arrangement in the crystalline domains forming the polycrystalline films, we carried out a GIXRD analysis (Figure 4-5 a).

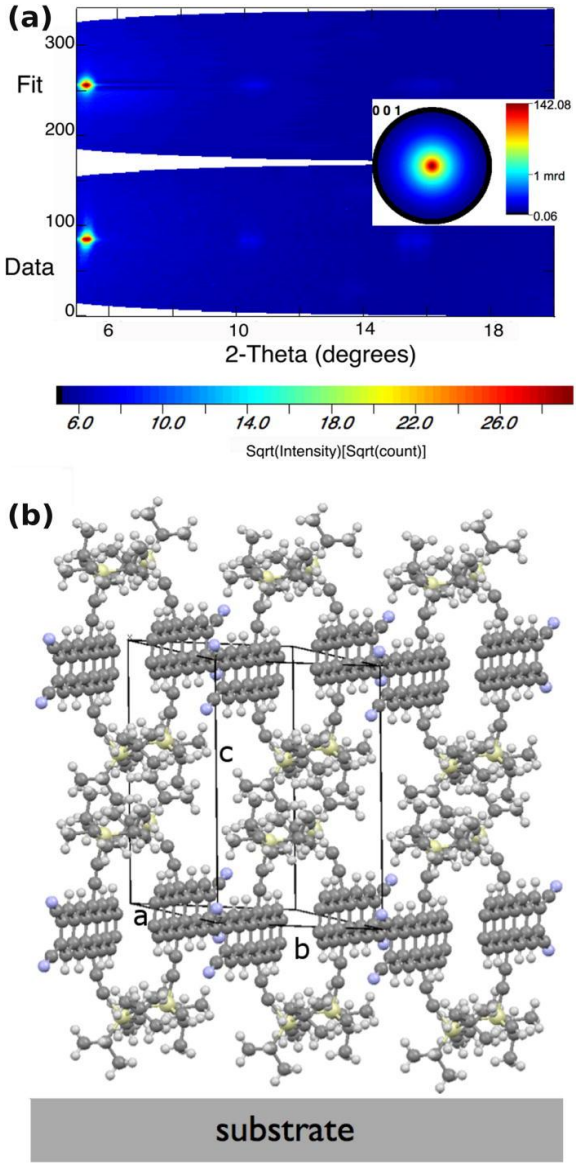

Figure 4-5 (a) Rietveld fit of one of the X-ray diffraction images collected at an incident angle of 2°. The principal spot is due to the (001) diffracting plane parallel to the sample surface. The bottom 2D pattern represents the experimental data; the recalculated pattern is on top. The three spots (001/002/003 reflections) are aligned in the diffraction plane normal to the sample surface. As we move out of it (moving vertically in the image), the strong texture causes a rapid decrease

of the intensity. The inset reports the recalculated pole figure showing the strong 00l orientation (mrd: multiple of random distribution, values in log scale). (b) Proposed molecular arrangement of 2,3-CN2-TIPS-Pn on the substrate.

The collected images were converted into 2D patterns. To obtain the phase content and texture, we further refined the images by use of the Rietveld methodology [213]. A triclinic structure was found with a strong fiber texture perpendicular to the film surface with (00l) planes aligned parallel to it. From the texture and molecule orientation we found that the pentacene backbone in the cell is located in a plane perpendicular to the substrate and that the long axis of the pentacene backbone is aligned parallel to the surface (Figure 4-5 b). The TIPS groups are pointing towards and away from the substrate. The observed molecular arrangement forms a highly semiconductor channel that is favorable for charge transport between source and drain electrodes [158], thus contributing to explain the good performance of 2,3-CN2-TIPS-Pn TFTs.

4.2.5 Conclusions

In conclusion, we demonstrated solution deposited ambipolar TFTs based on 2,3-CN2-TIPS-Pn films with balanced e^- and h^+ mobility, on the order of $2 \cdot 10^{-3}$ $cm^2/V \cdot sec$. The charge transport properties of 2,3-CN2-TIPS-Pn films show the effectiveness of TIPS-Pn functionalization with cyano- e^- withdrawing groups to promote e^- transport while maintaining equivalent h^+ transport. GIXRD characterization of the films revealed a favorable arrangement of the molecules in the TFT channel. We are currently fabricating 2,3-CN2-TIPS-Pn OTFTs using carbon nanotube electrodes, which are expected to improve electron and hole injection efficiency [217].

Acknowledgments

The authors are grateful to J. Bouchard for technical support. Part of this work was carried out at the Central Facilities of École Polytechnique/Université de Montréal. FC, NC, and GT acknowledge the Provincia Autonoma di Trento for financial support (projects FotoMINA and NanoSMART). JEA and YS thank the Office of Naval Research for support of synthesis efforts.

4.3 Correlation of charge transport properties with morphological and photophysical characteristics of solution processed pentacene derivatives

HOMO-LUMO levels and optical band gap of the three pentacene derivatives are listed in Table 4-1. Optical band gap of the three molecules was derived from the cut-off of the absorption spectra (Figure 4-6-left). The fluorescence spectra of the three pentacene derivatives are shown in Figure 4-6 (right). Although poorly, these molecules exhibited emission properties. 2,3-CN2-TIPS-Pn has an emission range wider and red-shifted compared to that of the TIPS-F8 and TES-F8. The HOMO and LUMO levels of 2,3-CN2-TIPS-Pn, TIPS-F8 and TES-F8 were deduced by cyclic voltammetry. The e^- and h^+ injection barriers with respect to Au were calculated as follows: for 2,3-CN2-TIPS-Pn, Φ_e=0.77 eV and Φ_h=1.04 eV; for TIPS-F8, Φ_e=0.79 eV and Φ_h=1.15 eV; for TES-F8, Φ_e=0.84 eV and Φ_h=1.15 eV.

Table 4-1 HOMO and LUMO level location with respect to vacuum level and optical band gap of three soluble pentacene derivatives determined by cyclic voltammetry synthesized by the group of Prof. J. E. Anthony at the University of Kentucky.

Molecule	Energy Levels	(eV)
Bis(triisopropylsilylethynyl) dicyanopentacene 2,3-CN2-TIPS-Pn	HOMO	5.44
	LUMO	3.63
	Optical Band gap	1.74
Bis(triisopropylsilylethynyl) octafluoropentacene TIPS-F8	HOMO	5.55
	LUMO	3.56
	Optical Band gap	1.90
Triethylsilyl octafluoropentacene TES-F8	HOMO	5.55
	LUMO	3.60
	Optical Band gap	1.90

The study reported in Article 1 was extended in a way to explore the effect of coating technique, post-treatment temperature and concentration. For 2,3-CN2-TIPS-Pn 15 mg/ml to 10 mg/ml and 7,5 mg/ml concentrations were experimented and 15mg/ml, 10mg/ml concentration of solutions for TIPS-F8 and TES F8 were prepared by dissolving the powders in chlorobenzene. Both, drop-casting and spin coating techniques were used.

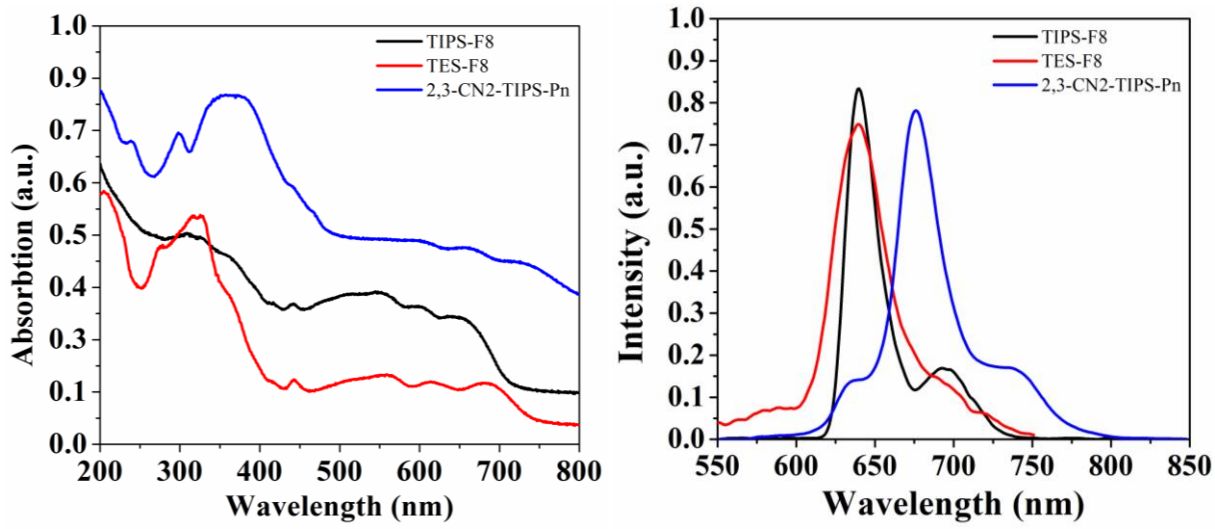

Figure 4-6 Absorption and fluorescence spectra (excitation wavelength 540 nm) of spin coated thin films heat treated at 100 °C on quartz slides.

Prepared samples were separated into two groups as as–prepared (25 °C) and 100 °C annealed. Drop-casted thin films post-treated at 100 °C and as-prepared samples demonstrated very poor electronic properties and are not presented in this thesis. On the other hand, spin-coated samples, although poor, showed ambipolar (2,3-CN2-TIPS-Pn) and n-type (TIPS-F8 and TES-F8) transistor characteristics (Figure 4-7). 100 °C annealed samples mobilities were one order of magnitude higher compared to that of the as-prepared samples. The increase in the mobility observed for the post-treated samples were attributed to the reorganization of the molecules for a more favorable arrangement in the channel. The increase in the charge carrier mobilities of organic semiconductors are often correlated to their morphologies, and higher crystallinity [218], [219], [220]. On the other hand the arrangement of the molecules in the channel plays a vital role in the charge transport properties of organic thin film transistors. An opposite case was also reported for poly(hexylthiophene) [221]. The effect of concentration can be viewed by looking at Table 4-3. The increase in the concentration leads to a decrease in the charge carrier mobilities for 2,3-CN2-TIPS-Pn and TIPS-F8, while no transfer properties were observed for thin films of TES-F8 deposited from 15mg/ml concentration solutions. Charge carrier mobilities for 2,3-CN2-TIPS-Pn decreases for lower concentration solution deposited samples as well. Also, an increase

in the V_{Th} with a decrease in the concentration of deposition solution for 2,3-CN2-TIPS-Pn and TES-F8 was observed. The output and transfer characteristics of n-type pentacene derivatives, TIPS-F8 and TES-F8 are presented in Figure 4-7. The general trend of the output and transfer curves points to an ambipolar charge transport however, it was not observed in our case, neither for drop-cast nor for spin coated samples.

Atomic force microscopy height and phase images of the three molecules are shown in Figure 4-8. A complete coverage of the sample surface was observed. Also, the roughnesses for as prepared and heat treated samples were calculated. A direct relation between the roughness and the heat treatment was observed, such that with increasing temperature the roughnesses of the three molecules were found to increase. Also, the morphology is affected by the thermal annealing.

In conclusion ambipolar and n-type pentacene derivatives for use in organic electronics are reported. The conducted study reveals the importance of the processing conditions in establishing high performing devices in the field of organic electronics. The relation between the thin film engineering, materials selection and the final performance were demonstrated in a systematical way.

Table 4-2 Mobilities of 2,3-CN2-TIPS-Pn, TIPS-F8 and TES-F8 as a function of temperature and deposition solution concentrations.

Molecule	**2,3-CN2-TIPS-Pn**		**TIPS-F8**	**TES-F8**
15mg/ml 100˚C sc	n-type	p-type		
Mobility	$4x10^{-5}$	$2x10^{-6}$		
V_{Th}	*1.6*	-6.8		
10mg/ml as prep sc				n-type
Mobility	1×10^{-4}	8×10^{-4}		9×10^{-4}
V_{Th}	28.8	- 42.2		19.7
10mg/ml 100˚C sc			n-type	
Mobility	2.1×10^{-3}	2.5×10^{-3}	1×10^{-3}	1.5×10^{-3}
V_{Th}	30.1	-37.2	18.3	25.8
7.5mg/ml 100˚C sc				
Mobility	4.7×10^{-4}	5×10^{-4}		
V_{Th}	30.1	-38.7		

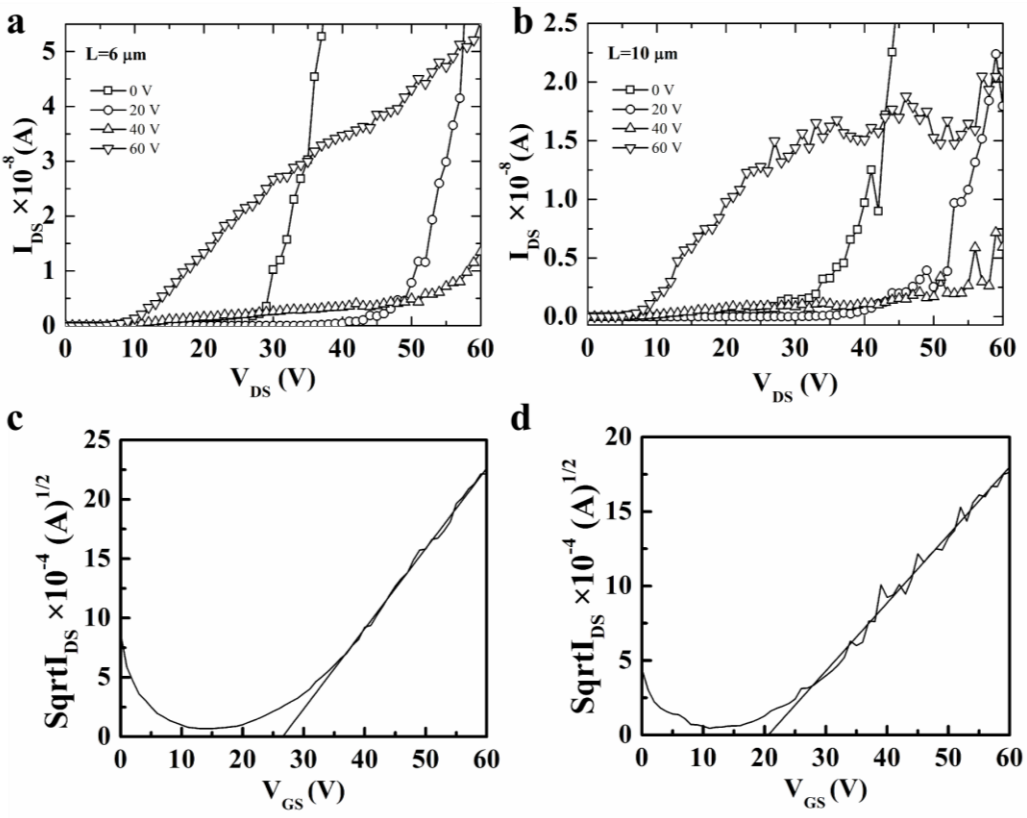

Figure 4-7 TFT characteristics of spin coated and 100 °C annealed TIPS-F8 and TES-F8 films: output curves (I_{ds} vs V_{ds}) for $|V_{gs}|$ = 0, 20, 40, 60 V (a) TES-F8 and (b) TIPS-F8; transfer curves (sqrt I_{ds} vs V_{gs}) at saturation for V_{ds} = 60 V (c)TES-F8 and (d) TIPS-F8. Channel widths/Channel Length = 6 µm/1880µm and 10 µm/1880µm for TES-F8 and TIP-F8, respectively.

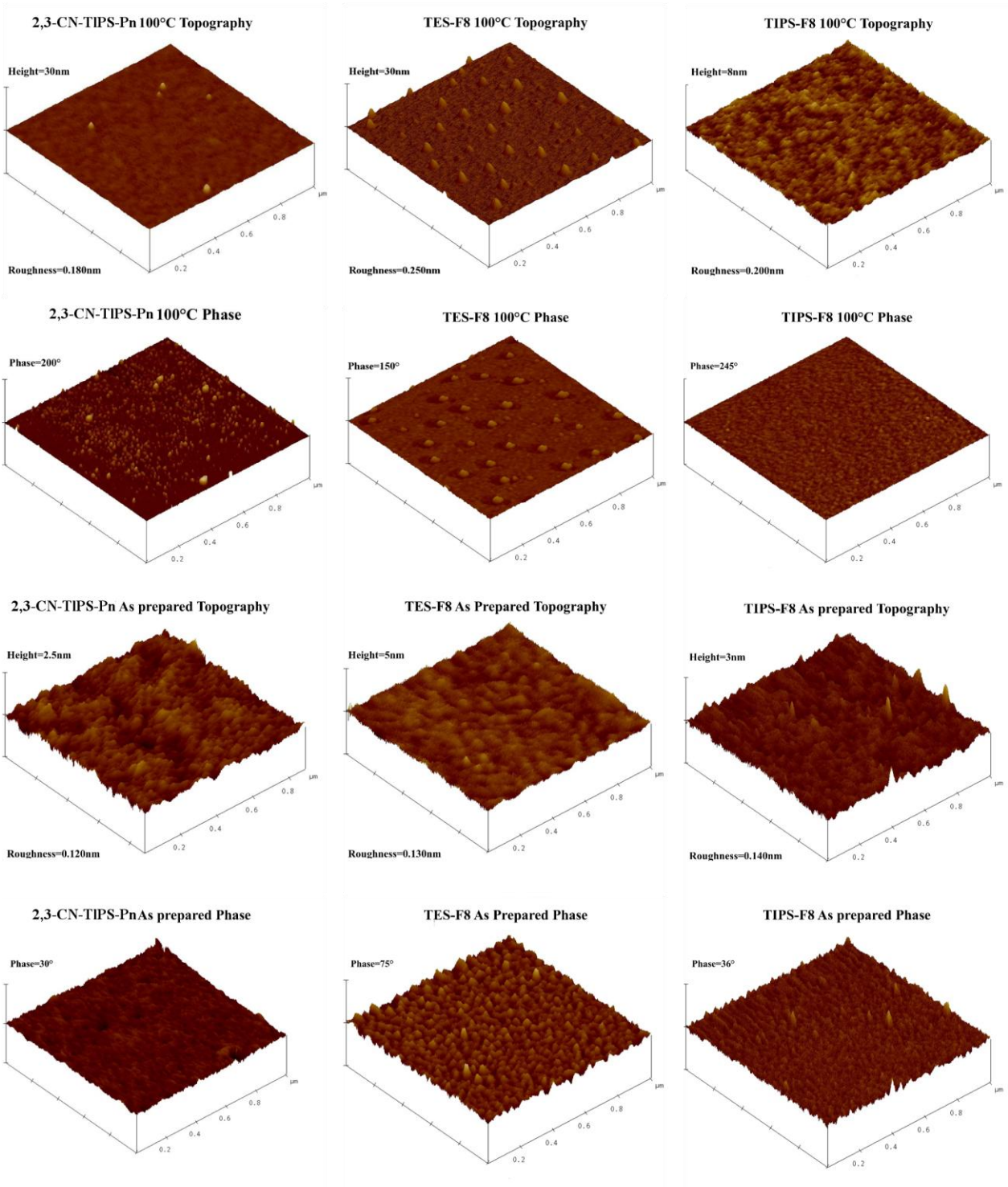

Figure 4-8 1μm×1μm height and phase AFM images of the three molecules in the as-prepared and 100 °C annealed conditions.

CHAPTER 5 CHARGE-CARRIER TRANSPORT IN THIN FILMS OF π-CONJUGATED THIOPHENO-AZOMETHINES

FOREWORD

In this chapter we report investigations on thin films of soluble thiopheno-azomethines, synthesized at Université de Montréal by the Prof. W. Skene research group.

The interest for thiopheno-azomethines stems from their straightforward synthesis that does not require stringent reaction conditions, unlike their carbon analogues. Furthermore, azomethines are advantageous because undesired by-products are not formed during the synthesis and water is the unique side-product.

In this chapter, besides organic thin film transistor characterization, fluorescence hyperspectral imaging and atomic force microscopy were used to shed light on the charge transport properties of the films.

5.1 ARTICLE 2: Charge-Carrier Transport in Thin Films of π-Conjugated Thiopheno-Azomethines

Dilek Işık,[1] Clara Santato,[1]* Satyananda Barik,[2] and W.G. Skene[2]*

[1]*École Polytechnique de Montréal, Département de Génie Physique, C.P. 6079, Succ. Centre-Ville, Montréal, Québec H3C 3A7, Canada.*

[2]*Laboratoire de caractérisation photophysique des matériaux conjugués, Département de Chimie, Université de Montréal, C.P. 6128, Succ. Centre-ville, Montréal, Québec, H3C 3J7, Canada.*

Article published in Organic Electronics

Submitted in June, 2012

Published in September, 2012

5.1.1 Introduction

In the rapidly evolving field of organic electronics [80], organic π-conjugated materials making use of azomethines (-N=C-) could be interesting alternatives to materials based on more conventional coupling protocols (i.e. -C=C). This is in part due to the straightforward synthesis of azomethines that does not require stringent reaction conditions, unlike their carbon analogues [222], [223]. Azomethines are advantageous because undesired by-products are not formed during the synthesis and water is the unique side-product. Therefore, relatively pure highly π-conjugated materials can easily be obtained both by minimal purification and mild reaction conditions. Organic π-conjugated materials making use of azomethine (-N=C-) couplings are additionally interesting because they withstand both chemical oxidation and reduction [222], [223], [224], [225], [226]. Moreover, their optical and electrochemical properties can readily be tailored contingent on the judicious choice of complementary heterocyclic amines and aldehydes [227].

Despite the synthetic advantages of azomethines, their use in the field of organic electronics has not yet been pursued. This is primarily because π-conjugated materials making use of azomethine couplings are misconceived to be hydrolytically and oxidatively unstable [228], [229]. This has been exacerbated by previously reported homoaryl azomethines that exhibited incompatible electrochemical and optical properties for use in organic electronics [230], [231], [232], [233]. These collective aspects have limited any interest in using azomethines as functional materials in organic electronics.

While cursory property evaluation of azomethines suggests that they have limited usefulness, they nonetheless have been exploited to prepare reversible dynamic materials [233]. The latter can undergo component exchange resulting in materials whose properties can be readily varied including their fluorescence emission, fluorescence yield, absorbance, and solubility in a given solvent [234], [235], [236]. Azomethines have further found uses as end-capping groups for oligothiophenes. The use of aryl azomethines increased the self-assembly of oligothiophenes and enhanced their charge transport properties [237]. Conjugated azomethines have also recently been used as a simple means to adjust the molecular wire spacing between gold contacts, leading to the discovery of different electron migration mechanisms from

"tunneling" to "hopping", in such wires [238], [239], [240]. Organic π-conjugated materials making use of azomethines have lately been used as the photoactive and emissive layers in organic photovoltaic devices and light-emitting diodes [241], [242], [243]. While the performance of these working devices was poor, it nonetheless successfully illustrates the compatibility of the heteroatomic materials properties for use in organic electronic devices. It would therefore be beneficial to identify the electronic processes that are responsible for the poor device performance. This knowledge could in turn be used to design and prepare new azomethines with improved device performance. For this reason, we were motivated to investigate the charge carrier transport properties of azomethines. Determining the transport properties is crucial for assessing the suitability of easily prepared thiopheno-azomethine based materials for use in organic electronic devices, especially given that they have optical and electrochemical properties that are compatible for use in organic electronics [226], [227], [244]. This is of particular interest given that previous studies exclusively examined homoaryl azomethines. The targeted thiopheno-azomethines (**1** and **2**, Scheme 1) should therefore possess enhanced electronic properties because of their high degree of conjugation owing to the intrinsic coplanarity of the heterocycles with the azomethine bond [227], [245]. This is in contrast to their homoaryl analogues that are highly twisted from planarity [246].

In this work, we present the charge carrier transport properties of thin films of thiopheno-azomethine, characterized in the field-effect transistor configuration. Both a thiopheno-azomethine oligomer (**1**) and an analogous polymer (**2**) were investigated. The transport properties of the films were correlated with their morphological properties that were assessed by fluorescence hyperspectral imaging and atomic force microscopy. We also investigated the effect of the degree of conjugation on the transport properties of the films by comparing the properties of the triad **1** versus its polymer counterpart, **2**. The transport properties of the azomethines were validated by measuring the hole mobilities of an all-carbon vinylene triad (**3**).

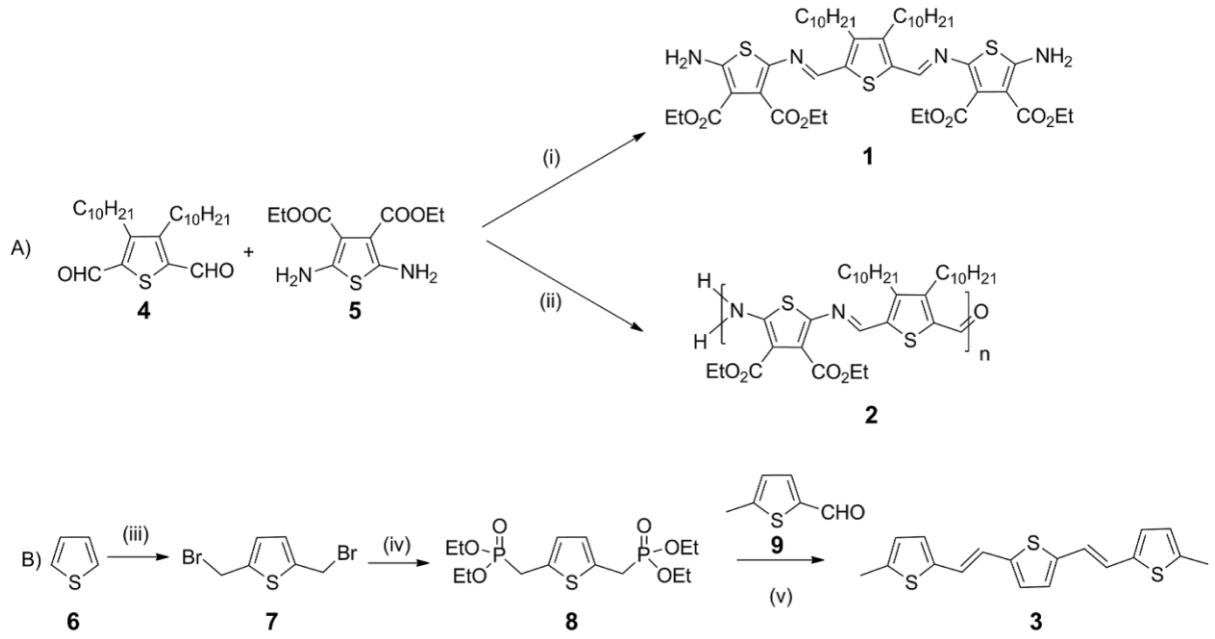

Scheme 5-1 Synthetic schemes for the preparation of **1-3** studied in this work: (i**)** ethanol, TFA, room temperature, 12 h; (ii) $CHCl_3$, 90 °C, 72 h; (iii) HBr, paraformaldehyde, acetic acid, 70 °C, 24 h; (iv) triethylphosphite, 150 °C, 24 h; (v) NaH, THF, room temperature, 24 h**.**

5.1.2 Experimental

5.1.2.1 Materials and general methods

Reagents and solvents were received from commercial sources and were used as received unless otherwise stated. Anhydrous and deoxygenated solvents were obtained with an activated alumina column system. ^{1}H and ^{13}C nuclear magnetic resonance (NMR) spectra were recorded at room temperature with a 400 MHz spectrometer. All the samples were dissolved in deuterated solvents and the spectra were referenced to the solvent line relative to Tetramethylsilane (TMS). The syntheses of **4, 5** and **7** were prepared according to reported procedures [222], [223].

5.1.2.2 Synthesis

2-Amino-5-[(3,4-bis(decyl)-5-formylthiophen-2-ylmethylene)-amino]thiophene-3,4 dicarboxylic acid diethyl ester (1) [247]. 3,4-Bis-decyl-thiophene-2,5-dicarbaldehyde **(4)** (200 mg, 0.47 mmol) and 2,5-diaminothiophene-3,4-dicarboxylic acid diethyl ester (**5)** (123 mg, 0.47 mmol) were dissolved in ethanol (40 mL), to which was later added a 1 M solution of trifluoroacetic acid (TFA) (50 mL) in ethanol. The solution was stirred at room temperature for 12 h. The solvent was evaporated and the product was extracted into ethyl acetate. The organic layer was washed with brine solution and dried over Na_2SO_4. After evaporating the solvent under reduced pressure, the crude product was purified by silica column chromatography with hexanes/ethyl acetate (30/70 % v/v). The product was obtained as a purple solid (320 mg, 88% yield). ^{1}H NMR (acetone) δ ppm: 8.16 (s, 2H), 7.51 (d, *J* = 5.5 Hz, 4H), 4.36 (q, *J* = 7.1 Hz, 4H), 4.21 (q, *J* = 7.1 Hz, 4H), 2.80 (t, *J* = 8.0 Hz, 4H), 1.57 (sext, *J* = 8.0 Hz, 1H), 1.48-1.19 (m, 40H), 0.87 (t, *J* = 6.8 Hz, 6H).^{13} C NMR (acetone) δ ppm: 164.9, 164.3, 161.5, 147.0, 144.1, 140.4, 133.4, 131.0, 102.2, 61.1, 60.1, 32.2, 32.0, 26.7, 22.9, 14.4, 14.1, 13.9. Mp = 129-133°C. HR-MS (+) calculated for $[C_{46}H_{69}O_8N_4S_3 + H]^+$ 901.4193, found 901.4192.

Thiopheno-polyazomethine (2) [248]. **4** (461 mg, 1.10 mmol) and **5** (283 mg, 1.10 mmol) were introduced into a pressure tube with chloroform (6 mL). A 1M solution of TFA (60 µL) in chloroform was then added. The tube was sealed and the mixture was heated to 90 °C for 72 hours. The solution was cooled to room temperature and the polymer was precipitated into a methanol/water (75/25) mixture. The precipitate was filtered and washed with methanol (3 × 20 mL), water (3 × 20 mL) and acetone (3 × 20 mL) to dissolve the residual oligomers. The desired polymer was quantitatively obtained as a dark blue solid. ^{1}H NMR (400 MHz, $CDCl_3$,) δ ppm: 10.1 (m, CHO), 8.08 (m, N=CH-), 4.25-4.45 (m, O-CH_2-), 2.71 (m, -C-CH_2), 1.3 (m, -CH_2-CH_2-), 0.88 (m, -CH_3). Gel permeation chromatography (GPC) molecular weight relative to polystyrene standards: M_n= 10 360 g/mol, DP_n=15.

2,5-Bis[(*E*)-2-(5-methylthiohene-2-yl)vinyl] thiophene (3). The title compound was prepared via the Horner-Emmons method. The phosphonic ester (**8,** 260 mg, 0.68 mmol) and 5-methyl-2-thiophenecarbaldehyde (**9**, 200 mg, 1.58 mmol) were dissolved in tetrahydrofuran (THF) (5 mL) under a nitrogen atmosphere. A dilute solution of NaH (40 mg, 1.6 mmol) in THF (2 mL) was

then added drop wise. The reaction mixture was stirred for 24 h at room temperature under nitrogen. The reaction mixture was then quenched with water and the crude product was extracted into dichloromethane. The organic layer was washed with water and brine solution (3 times) and then dried over Na_2SO_4. The solution was filtered and the solvent was removed under reduced pressure. The product was then purified by silica gel column chromatography using hexane/ethyl acetate (7:3) as an eluent. The product was obtained as an orange solid (340 mg, 61 % yield). ^{1}H NMR ($CDCl_3$, 400 mHz) δ ppm: 6.91 (s, 2H), 6.87 (d, 2H), 6.84 (s, 2H), 6.82 (d, 2H), 6.65 (d, 2H), 2.49 (s, 6H). ^{13}C NMR ($CDCl_3$, 400 mHz) δ ppm: 141.6, 140.8, 139.8, 127.0, 126.8, 126.3, 122.3, 120.7. HR-MS (+) calculated for $[C_{18}H_6S_3 + H]^+$ 329.0414, found 329.0415.

Tetraethyl-[thiophene-2,5-diylbis (methylene)] bis(phosphonate) (8). In a 2-necked flask were dissolved thiophene (**6**, 2.1 g, 25 mmol) and paraformaldehyde (5 g, 33 mmol) in ethanol. To the reaction mixture was added HBr (30 mL, 33% acetic acid) and the reaction was heated to 70 °C for 24 h under nitrogen. The reaction was cooled to room temperature and the crude product was extracted into diethyl ether (100 mL). The organic layer was washed with $NaHCO_3$ and dried over $NaSO_4$. The solution was filtered and the solvent was removed under reduced pressure. The crude oil was used without additional purification. Triethylphosphite (10 mL, 60 mmol) was added and the reaction mixture was heated to 150-160 °C for 24 h. The reaction was cooled to room temperature and water was added. The product was then extracted into dichloromethane and washed with a brine solution three times. The organic layer was dried over $MgSO_4$, filtered, and the solvent was removed under reduced pressure. The residue was purified by silica gel column chromatography using hexane/acetone (75/25 v/v %) as an eluent. The product was obtained as a colorless oil (1.3 g, 15%). ^{1}H NMR ($CDCl_3$, 400 mHz) δ ppm: 6.38 (2H, Th), 5.6 (d, 4H,-Th-CH_2-), 3.65 (dd, (8H, -O-CH_2-), 0.73 (12H, -CH_3). ^{13}C NMR ($CDCl_3$, 400 mHz) δ ppm: 132.4, 127.8, 61.1, 20.0, 14.2. HR-MS (+) calculated for $[C_{14}H_{26}O_6P_2S+H]^+$ 385.0959, found.385.0958.

5.1.2.3 Spectroscopic and electrochemical measurements

Absorption measurements were done with a Cary-500 spectrometer and fluorescence studies were carried out on an Edinburgh Instruments FLS-920 fluorimeter after de-aerating the samples thoroughly with nitrogen for 20 minutes. Cyclic voltammetry (CV) measurements were

performed with a Bio Analytical Systems EC Epsilon potentiostat. Compounds were dissolved in anhydrous and de-aerated dichloromethane at 10^{-4} M with 0.3 M tetra-*n*-butylammonium hexafluoride phosphate ($TBAPF_6$). A platinum electrode and a saturated Ag/AgCl electrode were employed as counter and reference electrodes, respectively. A platinum button electrode was used as the working electrode. Ferrocene was added after the measurements and the ferrocene/ferrocenium ion (Fc/Fc^+) reversible oxidation (E_{pa}= 460 mV vs the saturated calomel electrode (SCE) served as an internal reference for calibrating the measured redox potentials [249].

5.1.2.4 Molecular weight measurement

GPC analyses were performed with a Breeze system from Waters equipped with a 717 plus autosampler, a 1525 Binary High-performance liquid chromatography (HPLC) pump and a 2410 refractive index detector. Three Styragel columns HR3, HR4 and HR6 (7.8 mm × 300 mm) in series were used for resolving the different samples. The flow rate of the THF eluent was 1 mL/min. The temperature of the columns was 33°C. The polymer molecular weight was determined from a calibration curve prepared using ten polystyrene standards from a Shodex kit SM-105 .

5.1.2.5 Powder and thin film X-ray diffraction

X-ray powder diffraction patterns were obtained using a Bruker X-ray diffractometer with monochromatic Cu-K_α (1.54 Å) radiation (40 kV, 40 mA). Samples were mounted on a capillary tube sample holder and scanned in the 2θ range 1°- 25°, with a step size of 2θ = 0.01°.

5.1.2.6 Thin film deposition

Thin films for fluorescence hyperspectral imaging, atomic force microscopy and charge transport studies were deposited onto bottom contact/bottom gate transistor substrates making use of Au circular source and drain electrodes photolithographically patterned on SiO_2 (195 nm-thick, C_i= $1.77 \cdot 10^{-8}$ F/cm^2), thermally grown on heavily doped Si(n+) wafers (resistivity 0.001-0.005 Ohm·cm^{-1}). Typical transistor channel lengths (L) of 6, 10, and 40 μm and corresponding channel

widths (W) of 42,000, 41,800 and 18,000 μm were used. The films were deposited by spin coating at 2000 rpm at room temperature from 5 mg/mL chlorobenzene solutions.

Before spin coating, the patterned substrates were cleaned by sequential sonication in isopropanol, acetone, and isopropanol, blow-dried with nitrogen, and finally exposed during 20 min to UV/ozone treatment. Cleaned substrates were modified by spin coating a self-assembled monolayer of hexamethyldisilizane (HMDS, Gelest), to improve the wetting properties of the films. As-prepared and 100 °C thermally-treated films were investigated. The preparation of the solutions and the deposition of the films were carried out in a N_2 saturated atmosphere glove box (H_2O, O_2 about 1 ppm).

5.1.2.7 Fluorescence hyperspectral imaging

Fluorescence Hyperspectral Imaging was performed with PARISS (Prism and Reflector Imaging Spectroscopy System by LightForm Inc., Asheville, NC, USA), an imaging spectrometer coupled to a cooled scientific CCD camera to record the spectra.

The hyperspectral images (spectral maps) were generated in the "push broom" mode by use of a wavelength-dispersive spectrometer collecting all wavelengths simultaneously at each location along the slit by translating the field of view (FOV) underneath the spectrometer on an automated translation stage connected to the microscope [202]. The information was collected with PARISS 8 software with a minimum correlation coefficient (minCC) > 0.98, in realtime.

The image size and spatial resolution was calculated by dividing the slit height (5 mm) and slit width (25μm) to the magnification of the objective lens of the microscope. All the images were obtained in ambient conditions, at room temperature. Fluorescence images were collected from samples excited at λ_{exc}= 540 nm (**1** and **2**) and 460 nm (**3**). Grayscale referred to as “processed” images were further analyzed and the spectral libraries of each sample were collected and categorized into *classes*. Classes of spectra were given pseudocolor codes, which were correlated and *painted* onto the FOV in its associated pseudocolor, forming the classified image.

5.1.2.8 Atomic force microscopy (AFM)

AFM images were obtained in ambient conditions at room temperature in tapping mode using a IIIa-MultiMode AFM (Digital Instruments) or Dimension 3100 (Digital Instruments) and etched Si cantilevers with a resonance frequency around ~500 kHz and tip radius of <10 nm^{-1}.

5.1.2.9 Electrical measurements

Electrical measurements in field-effect transistor (FET) configuration were performed using a semiconductor parameter analyzer (Agilent B1500A). Measurements were carried out in N_2 atmosphere using a micromanipulated probe station, directly connected to the N_2 glove box where the film deposition was done.

FET mobility, μ_{FET} ($cm^2/V \cdot sec$), was calculated in the transistor saturation regime using the transfer characteristics (i.e. the drain-source current, I_{DS}, vs gate-source voltage, V_{GS}, curves obtained at a fixed drain-source voltage, V_{DS}). The threshold voltage, V_{TH}, was calculated from the intercept at y = 0 of the square root of I_{DS} plotted against V_{GS}, extrapolated at its maximum slope. I_{ON}/I_{OFF} was calculated by dividing I_{DS} ON (obtained at $|V_{DS}| = |V_{GS}| = 60$ V) by the I_{DS} OFF (obtained at $V_{GS} = 0$ V and $|V_{DS}| = 60$ V), obtained from the transfer curves.

5.1.3 Results and Discussion

5.1.3.1 Materials synthesis

The synthesis of the targeted thiopheno-azomethines was done according to the methods outlined in Scheme 1. The preparation of both materials was done by judicious control of the stoichiometry of the common reagents and the solvent. For example, a 2:1 stoichiometry of **5** and **4**, respectively, in ethanol selectively led to the triad **1** in high yield. Similarly, the polymer **2** was obtained in high yield with a 1:1 stoichiometry of **4** and **5** in chloroform. It should be noted that both of the products **1** and **2** were obtained with minimal purification for their one-step preparation. This is in contrast to the vinylene analogue **3** that required extensive purification for each of three-steps required for its preparations.

Although a more appropriate all-carbon analogue of **1** would include the same electron withdrawing groups in the 3,4-positions, such an analogue is synthetically challenging to prepare and is outside the scope of the current work. We then considered the triad **3** as the representative reference against which compare the properties of **1**. In addition to the synthetic advantage of **3**, it was further expected to be highly crystalline and hence lead to high mobilities courtesy of the favorable cofacial π-stacking (vide infra). Vinylenes such as **3** are further known to have hole transport properties [250], [251]. It was expected that the their hole mobilities would be similar to those of the targeted azomethines. **3** was therefore selected as a benchmark against which to measure the transport properties of **1** and **2** and to validate the device testing protocols. Vinylene are known to have hole transport properties. **3** was subsequently prepared by the Horner-Emmons method from the diethyl phosphate **8** and 2-methyl-thiophene-3 carboxyaldehyde [244]. This route was selected over the classic Wittig route as the preferred *E*-isomer was exclusively obtained and separation of the *cis*/*trans* isomers was not required. The Wittig reaction affords both regioisomers that can in principle be separated by standard chromatographic means. However, isomerization of the desired *trans* to the unwanted *cis* regioisomer is often problematic when separating the isomers by column chromatography. The *E*-regioisomer is desired for evaluating its properties relative to **1**. The required phosphate ester **8** for the Horner-Emmons reaction was therefore prepared by the Arbuzov reaction with triethylphosphite with the alkyl bromide **7**. The latter was obtained directly from thiophene with paraformaldehyde and bromic acid. The overall yield for the preparation of **3** was 61 % in contrast to near quantitative yields for **1** and **2**.

5.1.3.2 Electrochemistry and UV-visible spectra

Cyclic voltammetry measurements were performed on **1-3**. The cyclic voltammograms of **2** and **3** (Figure 5-1) show a one-electron oxidation at about 800 mV. The two terminal electron-donating groups of **1** lower the anodic potential (E_{pa}) to less positive values, compared to **2** and **3** (Table 5-1). Meanwhile, the increased degree of conjugation of **2** counter balances the electron withdrawing effect of the multiple azomethine bonds such that its E_{pa} is increased by 80 mV relative to **1**. The E_{pa} of **1** was found to be 100 mV higher than **1**. The collective effects of the

heteroatomic bonds and electron withdrawing esters vary on the oxidation potential by only ca. 100 from the corresponding all-carbon counterparts (Table 5-1).

The impact of incorporating the nitrogen atom into the conjugated framework is more noticeable on the spectroscopic properties. For example, the absorbance of both **1** and **2** is bathochromically shifted by more than 100 nm compared to their carbon counterparts. Given the similar E_{pa} values of the azomethines and their carbon analogues, the spectroscopic shifts observed with the heteroatomic compounds are most likely from intramolecular charge transfer [252]. This is not surprising given the intrinsic electron withdrawing behavior of the azomethine that leads to a donor-acceptor arrangement along the conjugated backbone. Meanwhile, the large Stokes shift observed for **1** would imply that its excited state is more polar than its counterpart **3**. This could be the result of intramolecular charge transfer involving the electron donating terminal amines in the excited state.

Interestingly, a second oxidation was observed with **3**, corresponding to the formation of its dication, while the azomethines exhibited a single oxidation. Meanwhile, the reduction processes of **1**-**3** were contingent on electronic effects. The less negative cathodic potential (E_{pc}) was found for **2**. This is a result of the collective effect of the large number of electron withdrawing azomethines and increased degree of conjugation that lower the LUMO energy level. In contrast, the E_{pc} of **1** is the most negative, and therefore more difficult to reduce, owing collectively to the limited number of azomethine bonds and the strong electron donating amines. The electrochemical data suggest that **1**-**3** could have p-type charge carrier transport properties. Meanwhile, the low cathodic potential observed for **2** implies that the polyazomethine would also exhibit n-type charge carrier transport properties. The collective p- and n-type expected transport properties of **3** would lead to an ambipolar transistor behavior providing the LUMO energy level of the polymer matches with the work function of the electrode in the transistor.

Table 5-1 Electrochemical and photophysical properties of compounds 1-3.

Compound	**λ_{max} (nm)[a]**	**λ_{PL} (nm)[b]**	**E_g^{opt} (eV)[c]**	**E_{pa}^{onset} (V)[d]**	**E_{pc}^{onset} (V)[e]**	**HOMO (eV)[f]**	**LUMO (eV)[f]**	**E_g^{el} (eV)[g]**
1	514	683	2.11	0.70	-0.86	-5.10	-3.54	1.56
2	660	791	1.54	0.78	-0.55	-5.18	-3.85	1.33
3	420	498	2.62	0.80 (1.12)	-0.69	-5.20	-3.71	1.49
Poly (thienylene vinylene)[h]	513	624	1.77	0.90	-0.75	-5.30	-3.65	1.65

[a] Absorption maximum at room temperature. [b] Photoluminescence maximum at room temperature. [c] Optical energy gap taken from the absorption onset. [d] Oxidation potential relative to SCE. [e] Reduction potential relative to SCE. [f] Relative to the vacuum level. [g] Electrochemically derived energy gap. [h] Taken from literature [251].

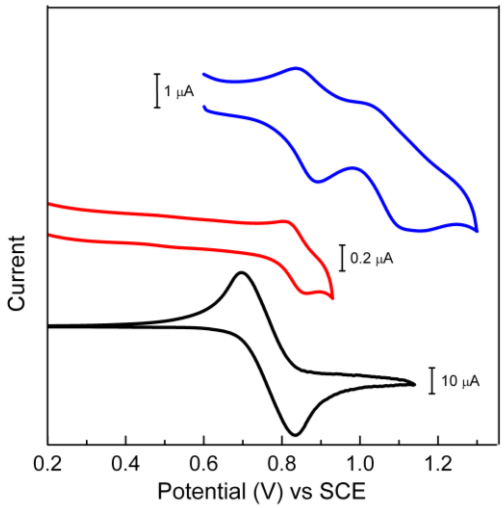

Figure 5-1. Cyclic voltammograms of **1** (black, bottom), **2** (red, middle) and **3** (blue, top) recorded in de-aerated dichloromethane with $TBAPF_6$ (0.1 M) using a saturated Ag/AgCl as reference electrode and a Pt wire as both the working and auxiliary electrode.

The HOMO and LUMO energy levels were calculated from the electrochemical oxidation and reduction onsets, respectively, according to the following standard methods [253]. The HOMO energy level was calculated from the oxidation onset (E_{pa}^{onset}) according to the following relation: E_{HOMO} = -e(E_{pa}^{onset} (SCE) - 4.4), where E_{pa}^{onset} is the oxidation potential onset in Volt versus SCE. The LUMO energy level was similarly determined from the cathodic potential onset (E_{pc}^{onset}) according to E_{LUMO} = -e(E_{pc}^{onset} (SCE) - 4.4). The difference between these two values affords the HOMO-LUMO energy difference (E_g). E_g for **1** was calculated to be approximately 1.5 eV, which is comparable to its analogue **3** (Table 5-1). The energy-gap of **2** was the lowest owing to the collective electron withdrawing capacities of the greater number of azomethine and ester groups taken together with its higher degree of conjugation relative to **1**.

5.1.3.3 X-ray powder diffraction

Room temperature powder X-ray diffraction (XRD) analyses on **1-3** were done to gather intermolecular information on the structural properties of the materials. This was to better understand the intermolecular packing of the materials and to correlate it to the transport properties (vide infra). The ideal structure that favors high charge carrier transport mobilities taking place by inter-chain hopping shows ordered cofacial aromatic π-stacking [254], [255]. The diffraction patterns of **1** showed well distinguishable diffraction peaks consistent with what was observed from the single crystal X-ray diffraction data (Figure 5-2) [247]. **1** additionally showed one distinct diffraction peak at **2**θ ≈ 4.2°, corresponding to the *d*-spacing of 21.2 Å. The two diffraction peaks at 6.7° and 8.7° for **1** correspond to the second and third order lamellae reflections. Only a weak diffraction peak at 2θ≈ 21.5° was observed, which is attributed to intermolecular π–π stacking. Diffraction peaks similar to **1** were also observed for **2**. The diffraction patterns for **1** and **2** were consistent with a polycrystalline, lamellar morphology. No lamellar diffraction peaks were observed for **3**. The weak diffractions observed at wide diffraction angles suggest there is little intermolecular π-stacking for both **1** and **2**. This is not surprising because of the disorder caused by the intermolecular entanglement of the long C_{10}-alkyl chains. Unalkylated derivatives of **1** and **2** would be beneficial for increasing the desired π-stacking. Unfortunately, their alkylation is required to make them soluble. Meanwhile, the strong diffraction peaks at 19.7° and 23.0° for **3** correspond to *d*-spacing of 4.36 and 3.77 Å,

respectively. The values are consistent with intermolecular π-stacking distances that are typically on the order of ≈ 3.8-3.9 Å for P3HT and other polymers [153], [256], [257]. The powder XRD data confirm that both **1** and **2** have limited cofacial π-stacking compared to **3** at room temperature.

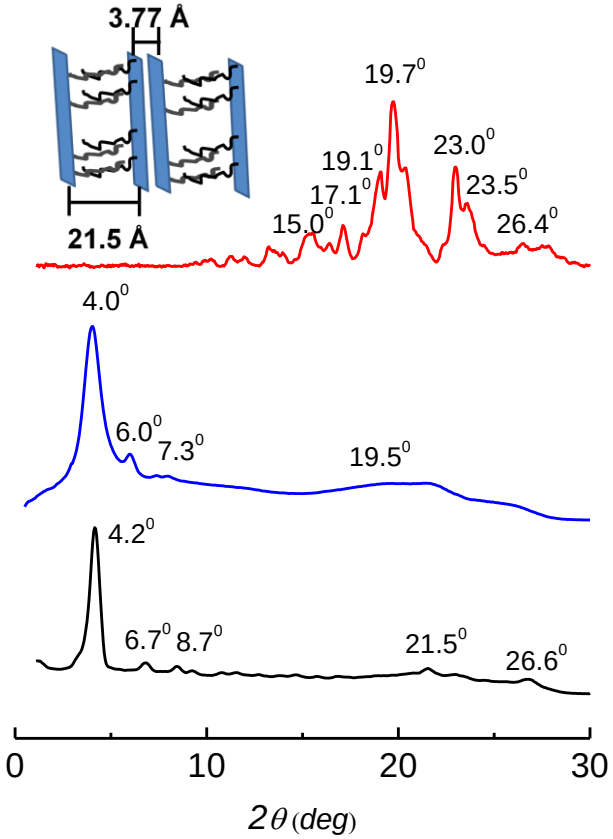

Figure 5-2 Powder X-ray diffraction of **1** (black, bottom), **2** (blue, middle) and **3** (red, top). The XRD powder data for **1** and **2** show diffraction peaks corresponding to a lamellar morphology (as per the inset sketch), consistent with π-stacking distance of 3.77 Å found from the single crystal data; the peak at 2θ ≈ 4.2° corresponds to an interlayer *d*-spacing of 21.2 Å, represented in the sketch in the inset.

5.1.3.4 Fluorescence hyperspectral imaging

Fluorescence hyperspectral imaging is a platform to characterize fluorescent samples by collecting spectral information in a field of view (FOV). The FOV is formed by heterogeneously distributed components in the sample that have different spectral properties. These are considered as "spectral fingerprints" of the fluorescent components of the sample. The topography of the sample can subsequently be determined by building a fluorescent spectral map of the sample. Given that **1-3** fluoresce, albeit weakly, fluorescence hyperspectral imaging was used to gain insight about the substrate coverage and the morphological properties of the thin films (Figure 5-3). This was further undertaken to provide understanding about the morphology-charge transport relationship. For films of **2** and **3**, it was possible to quantitatively evaluate the surface coverage using the collected spectral libraries of the films and their corresponding histograms. For **1**, this same evaluation was not possible due to its weaker fluorescence. Colors used for classifying the images do not necessarily indicate the real color of the emission. They are merely used for visualization the portions of the films having different fluorescence intensities. The bright field gray scale image of **1** shows fiber-like structures, 0.5-2.5 μm wide and ~10 μm long (Figure 5 SI-1a). The corresponding fluorescence categorized image (Figure 5-3a) permits the mapping of the fluorescence on the substrate. **1** has an emission maximum located at λ_{PL} = 635 nm, as shown in the classified spectra obtained with minCC of 0.9 (Figure 5-3d). This is blue shifted by ~50 nm compared to its fluorescence in solution. The bright field gray scale image of **2** indicates an almost featureless, smooth surface (Figure 5 SI-1b). A continuous film was indeed observed for **2** in the fluorescence categorized image (Figures 5-3b). The histogram of the spectral library obtained using a minCC of 0.9 showed ~98% substrate surface coverage, particularly favorable for thin film applications in devices (Figure 5-3e). **2** showed an emission maximum at λ_{PL} = 790 nm, similar to what was observed in solution.

Films of **3** were made of 0.5-1.5 μm sized structures (Figure 5-SI-1c), overgrown on a layer of **3**. The histogram obtained at minCC of 0.9 from the categorized fluorescence images, showed that ~80% of the surface was covered (Figure 5-3 c-f). **3** was characterized by a maximum emission located at λ_{PL} = 524 nm and by three emission shoulders respectively located at 559, 607, and 639 nm.

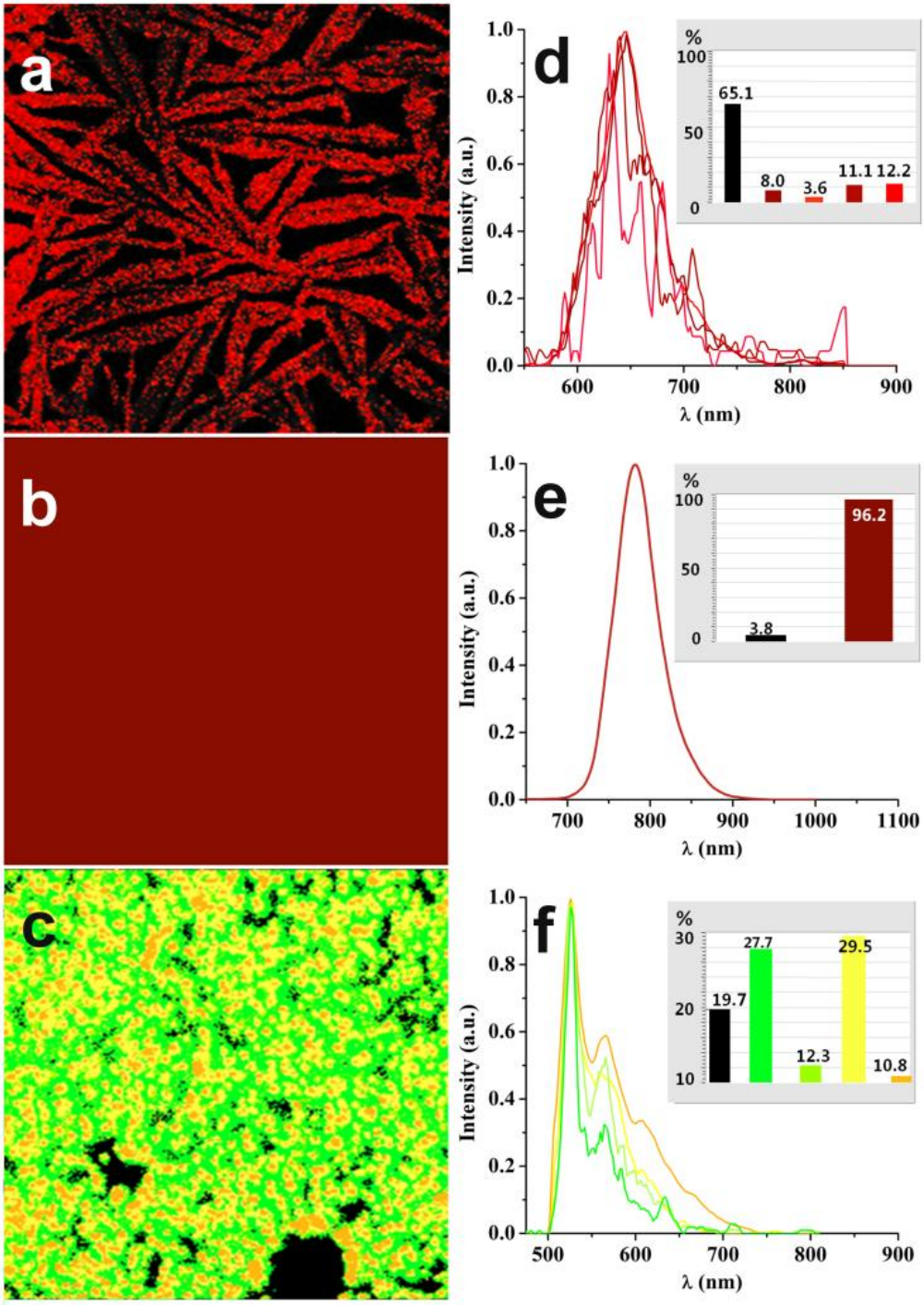

Figure 5-3 50 μm×50 μm fluorescence hyperspectral images of spin-coated films of **1**-**3** on HMDS-treated SiO_2/Si FET substrates, after thermal treatment at 100 °C. Left: corresponding categorized images for **1** (a, λ_{exc} = 540 nm), **2** (b, λ_{exc}= 540 nm), **3** (c, λ_{exc} = 460 nm), Right: Histograms and collected spectral libraries of **1** (d), **2** (e), **3** (f), respectively.

5.1.3.5 Atomic force microscopy (AFM)

AFM was used to study the nanoscale morphology of the thin films of **1**-**3** within the transistor channel. Together with the fluorescence hyperspectral imaging, AFM was used to correlate the morphological and charge transport properties of the thiopheno azomethine observed in thin films.

AFM images of the as-prepared films of **1** showed the presence of two types of structures: elongated (~100 nm wide, ~400 nm long) and round-shaped (~100 nm diameter) (Figures 5-4a-b). The RMS surface roughness (r_q) of the surface was 8-9 nm. On the other hand, AFM images of thermally treated films showed elongated structures with widths in the range of ~0.5-3 μm and variable lengths, in the micron scale (Figures 5-4c-d). In between the elongated structures, r_q was 0.9 nm, slightly higher than for HMDS treated-SiO_2 surfaces (r_q about 0.3 nm). A smooth layer of **1** is therefore assumed to form at the interface with the HMDS-treated SiO_2 substrate. This is certainly relevant for the application of thin films of **1** in transistors. The elongated structures were observed even in the absence of a patterned substrate surface, i.e. their nucleation is specific to the interface between **1** and the HMDS treated-SiO_2 surface (i.e. it is not induced by the electrode patterned substrate).

In contrast to **1**, the AFM images of **2** (Figure 5-4e) revealed a smooth (r_q ~1 nm) polymer surface. The homogenous and smooth layer qualities of **2** are in agreement with the hyperspectral fluorescence images and confirm a good surface coverage. The reference oligomer **3** formed structures with a maximum height of ~260 nm, after thermal treatment (Figure 5-4f). The roughness of the surface measured in regions between these large structures was about 0.8 nm. The latter value suggests the presence of a layer of **3** beneath the large structures, similar to what previously observed with **1**. This is in agreement with the results on the surface coverage properties of **3**, obtained by fluorescence hyperspectral imaging (Figure5-3c), and confirm the applicability of thin films of **3** for transistor applications.

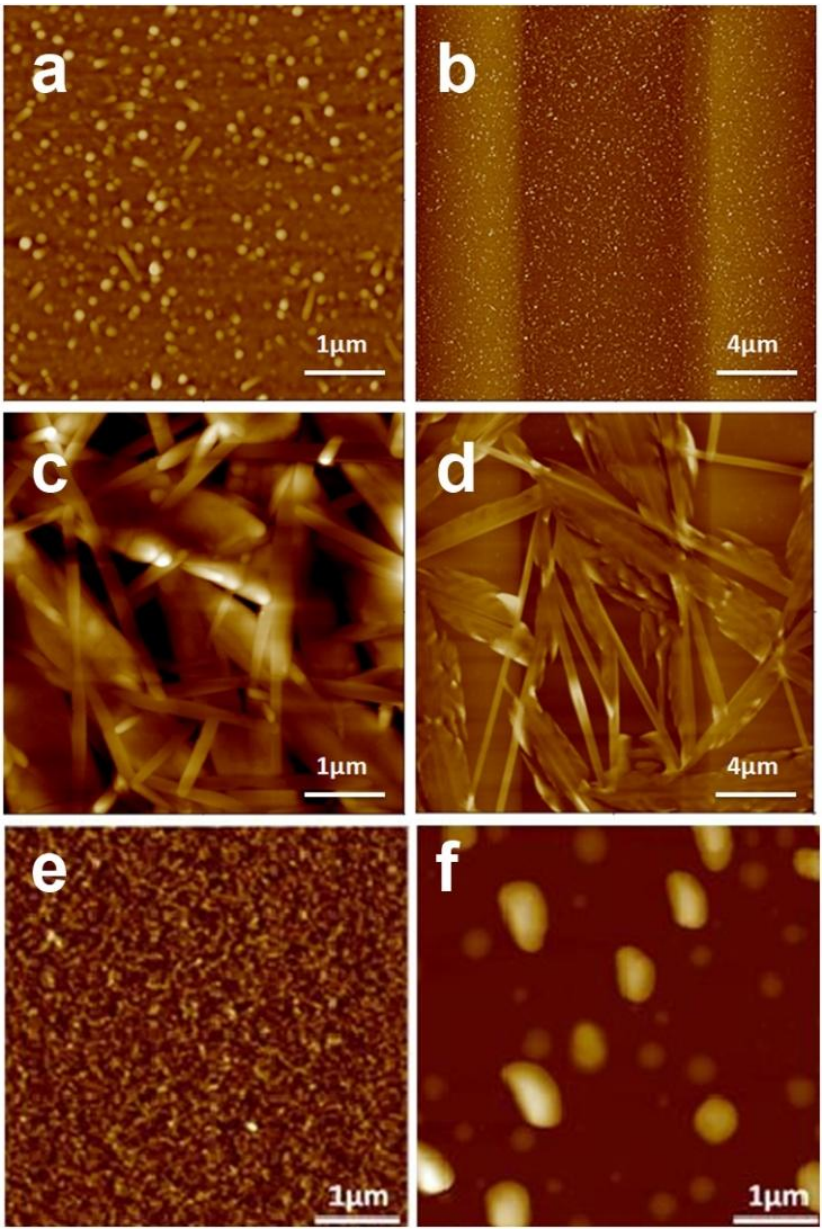

Figure 5-4 AFM images of thin films of 1-3 on HMDS-treated SiO_2/Si FET substrates: (a) 5 µm × 5 µm and (b) 20 µm × 20 µm images of as-prepared films of 1; H range = 0-80 nm, rq = 8-9 nm. (c) 5 µm×5 µm and (d) 20 µm × 20 µm images of 100 °C-treated films of 1; H range = 0-100 nm, rq = 12.4-13 nm (rq 0.9 nm in the underlayer, see text). (e) 5 µm × 5 µm image of 2 treated at 100 °C; H range = 0-15 nm, rq ~1 nm. (f) 5 µm × 5 µm image of 3 treated at 100 °C; H range = 0-500 (see text for a discussion on rq). (b) and (d) have been taken on the transistor channel (electrode patterning visible in the images).

5.1.3.6 Thiopheno-azomethine-based field-effect transistors

The charge carrier transport properties of thin films of **1**-**3** were characterized, before and after thermal treatment at 100 °C, in field-effect transistor configuration. Thin films of **1** and **3** showed a p-type (hole transport) transistor behavior. Output (drain-source current, I_{DS}, vs drain-source voltage, V_{DS}, for increasing gate-source voltage, V_{GS}) and transfer characteristics of transistors based on thin films of **1** and **3** are shown in Figure 5-5. The values of the hole mobility, μ_h, for thermally treated films of **1** and **3** were $\sim 3 \cdot 10^{-5}$ and $\sim 3 \cdot 10^{-8}$ $cm^2/V \cdot sec$, respectively.. While the absolute μ_h for **1** is low compared to extended thiophenylenes or regioregular oligothiophenes [156], [258], [259], the measured mobilities nonetheless confirm that the heterocyclic triad **1** has transport properties. This is contrast to previously investigated azomethines that had lower hole mobilities than the values measured for the as-cast film of **1** [260]. For transistors based on **1** and **3**, V_{TH} were -4 and -16 V and I_{ON}/I_{OFF} were $\sim 10^4$ and $\sim 10^2$, respectively. The fact that the mobility of transistors based on as-prepared films of **1** (with V_{TH} = -15 V) was one order of magnitude lower compared to thermally treated films of **1** is attributable to the formation of larger grains in the film, after thermal treatment (Figures 5-4 a-d). The formation of larger grains, paralleled by a decrease in the density of grain boundaries where charge carrier traps can be located, is usually favorable for charge transport [156], [259], [260], [261]. Normally good hole transport properties are observed with materials with cofacial π-overlap[262]. This is not the case with the as-cast film of **1**, according to the XRD powder data (vide supra). Thermally treating the film of **1** therefore most likely increases π-stacking, contributing to the observed increased transport behavior. While the exact structure change and the mechanism responsible for the increased mobility upon thermal treatment cannot unequivocally be assigned, the measured hole mobility of **1** value is among the highest reported value for such these compounds.

For films of **2**, we observed a weak and balanced ambipolar charge carrier transport with $\mu_h \sim \mu_e \sim 10^{-7}$ $cm^2/V \cdot sec$ (Figure 5-SI-2). The ambipolarity can be explained by the positions of the HOMO and LUMO levels with respect to the position of the work function of the Au electrode (φ_{Au} ~ -4.4 eV) [100]. HOMO and LUMO levels of **2**, as deduced from cyclic voltammetry

measurements are located at -5.2 and -3.9 eV, respectively. As a consequence, the energy barriers for injection are as low as ~0.8 eV for holes and ~0.5 eV for electrons [4], [5], [263].

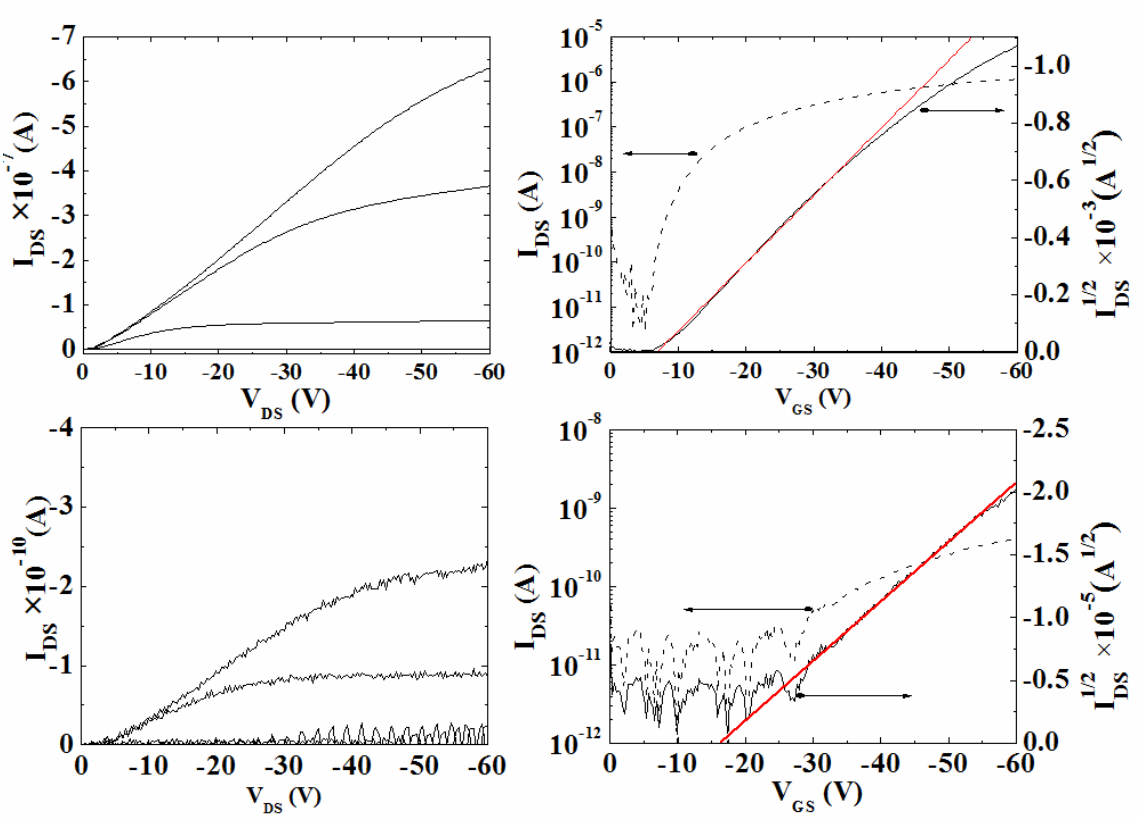

Figure 5-5 Output (left) and transfer (right) curves for FETs based on thin films of **1** (top) and **3** (bottom). In the output curves, V_{GS} were 0, -20, -40, -60 V. The transfer curves were recorded at V_{DS} = -60 V; the red line extrapolates the square root of I_{DS} at its maximum slope to obtain its intercept at y = 0, to calculate V_{TH}.

The enhanced p-type transport properties observed in thin films of **1** and **3,** relative to **2**, is attributed to the amino and methyl electron donating groups at the end of **1** and **3**, respectively. The poor p-type transport properties of **2** are most likely a result of weak degree of cofacial overlap observed in the solid state and its increased number of electron withdrawing moieties.

5.1.4 Conclusions

Thin films of **1**-**3** deposited on HMDS-treated SiO_2 substrates showed interesting charge carrier transport properties. Transistor characterization of the three compounds in thin film form indicated that **1** and **3** have p-type semiconductor behavior. On the other hand, **2** showed ambipolar behavior. The hole mobility of **1**, compared to its carbon analogue **3** is three orders of magnitude higher. Thermal treatment of the films prepared from **1** improved the charge transport properties. Overall, the results show that azomethines have charge transport properties. While the measured transport properties of the thiopheno-azomethines are appreciably lower than their aryl-aryl counterparts such as poly(3-hexylthiophene), higher values are expected by improving the self-assembled π-stacking of the thiophene segments. This desired configuration is expected to be favored by modifying the length and/or type of the alkyl segments, which is currently being explored.

Acknowledgements

The authors acknowledge financial support from the Natural Sciences and Engineering Research Council of Canada for Discovery, Strategic Research, and Research Tools and Instruments grants, the Canada Foundation for Innovation, the Centre for Self-Assembled Chemical Structures (CSACS) and the Regroupement Québecois sur les Matériaux de Pointe (RQMP). WGS thanks the Humboldt Foundation and the Royal Society of Chemistry for fellowships allowing the manuscript to be drafted. Dr. A Alouhabi is acknowledged for initial contributions. Part of this work was carried out at the central facilities of École Polytechnique and Université de Montreal.

Appendix 1. Supplementary data

Thin film bright field grey scale fluorescence images, transistor current-voltage plots for **2,** calorimetry plots, GPC elugram, cathodic cyclic voltammograms, NMR spectra of the compounds.

Supplementary Information-Article 2

Charge Carrier Transport in Thin Films of π-Conjugated Thiopheno-Azomethines

Dilek Işık,[1] Clara Santato,[1]* Satyananda Barik,[2] and W.G. Skene[2]*

[1]École Polytechnique de Montréal, Département de Génie Physique, C.P. 6079, Succ. Centre-Ville, Montréal, Québec H3C 3A7, Canada.

[2]Laboratoire de caractérisation photophysique des matériaux conjugués, Département de Chimie, Université de Montréal, C.P. 6128, Succ. Centre-ville, Montréal, Québec, H3C 3J7, Canada.

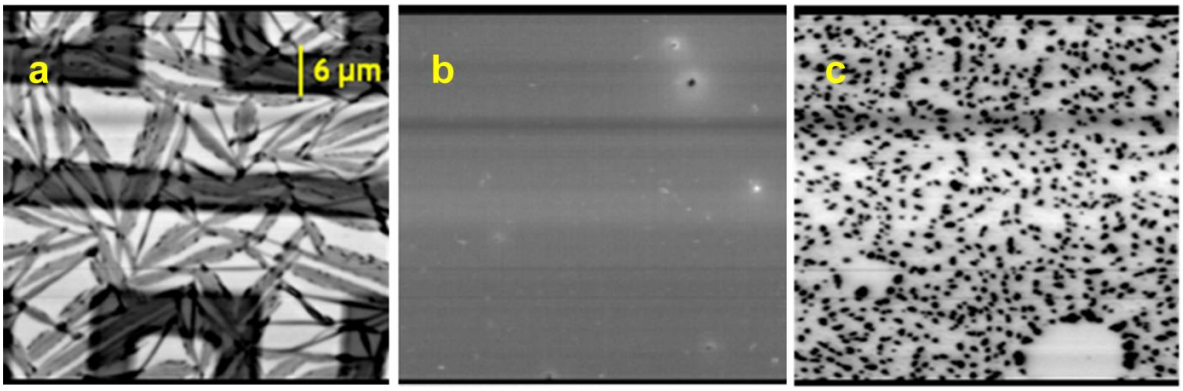

Figure SI 5-1 50 µm×50 µm bright field, gray scale, processed images of spin-coated films of **1-3** on HMDS-treated SiO_2/Si FET substrates, after thermal treatment at 100 °C for **1** (a), **2** (b), **3** (c).

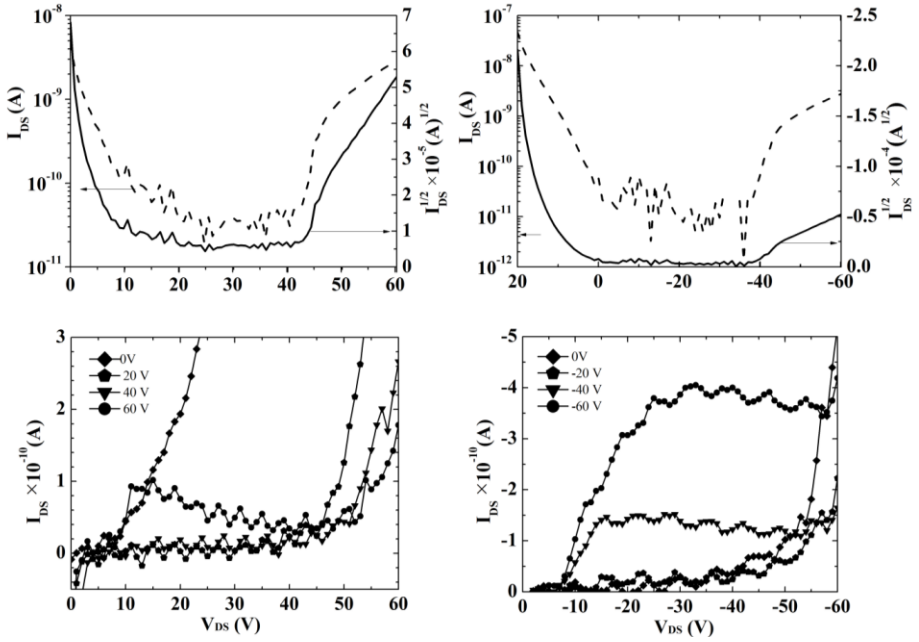

Figure SI 5-2 I_{DS} vs V_{GS} (top, $|V_{DS}| = 60$ V) and I_{DS} vs V_{GS} (bottom, V_{GS} indicated in the figures) characteristics of field-effect transistors based on thin films of 2 showing ambipolar charge carrier transport in such films (i.e. simultaneous holes and electron transport).

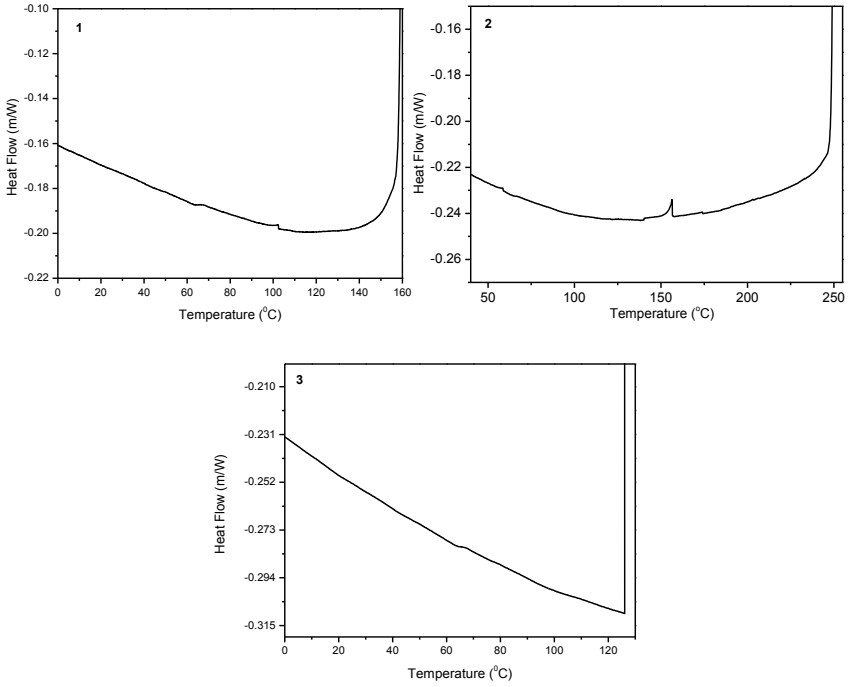

Figure SI 5-3 Differential scanning calorimetry of **1**-**3** (from left to right). Glass transition temperature of **1** T_g=65 °C; **2** is T_g =153°C; **3** is T_g=64 °C**.**

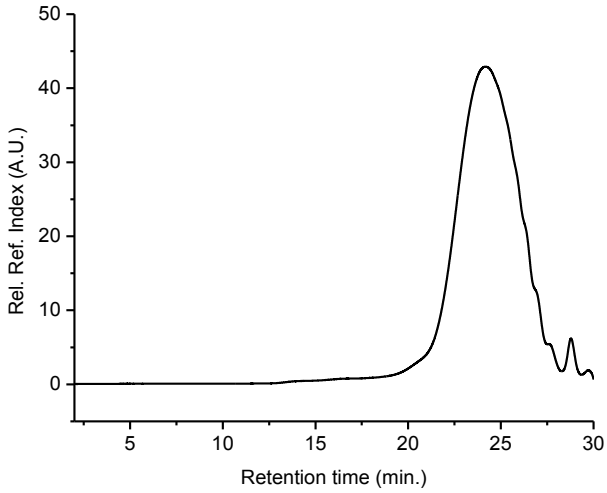

Figure SI 5-4 GPC elugram of **2** in THF.

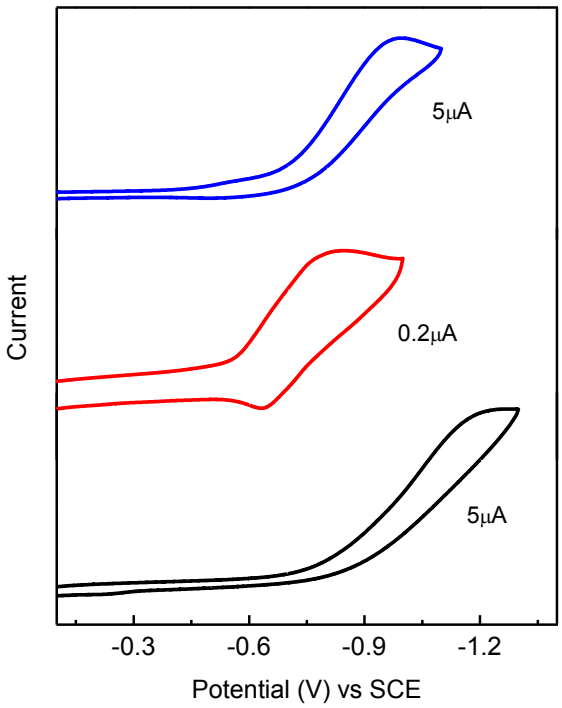

Figure SI 5-5 Cathodic cyclic voltammograms of **1** (black, bottom), **2** (red, middle) and **3** (blue, top) recorded in de-aerated dichloromethane with $TBAPF_6$ (0.1 M) using a saturated Ag/AgCl as reference and a Pt wire as both the working and auxiliary electrode.

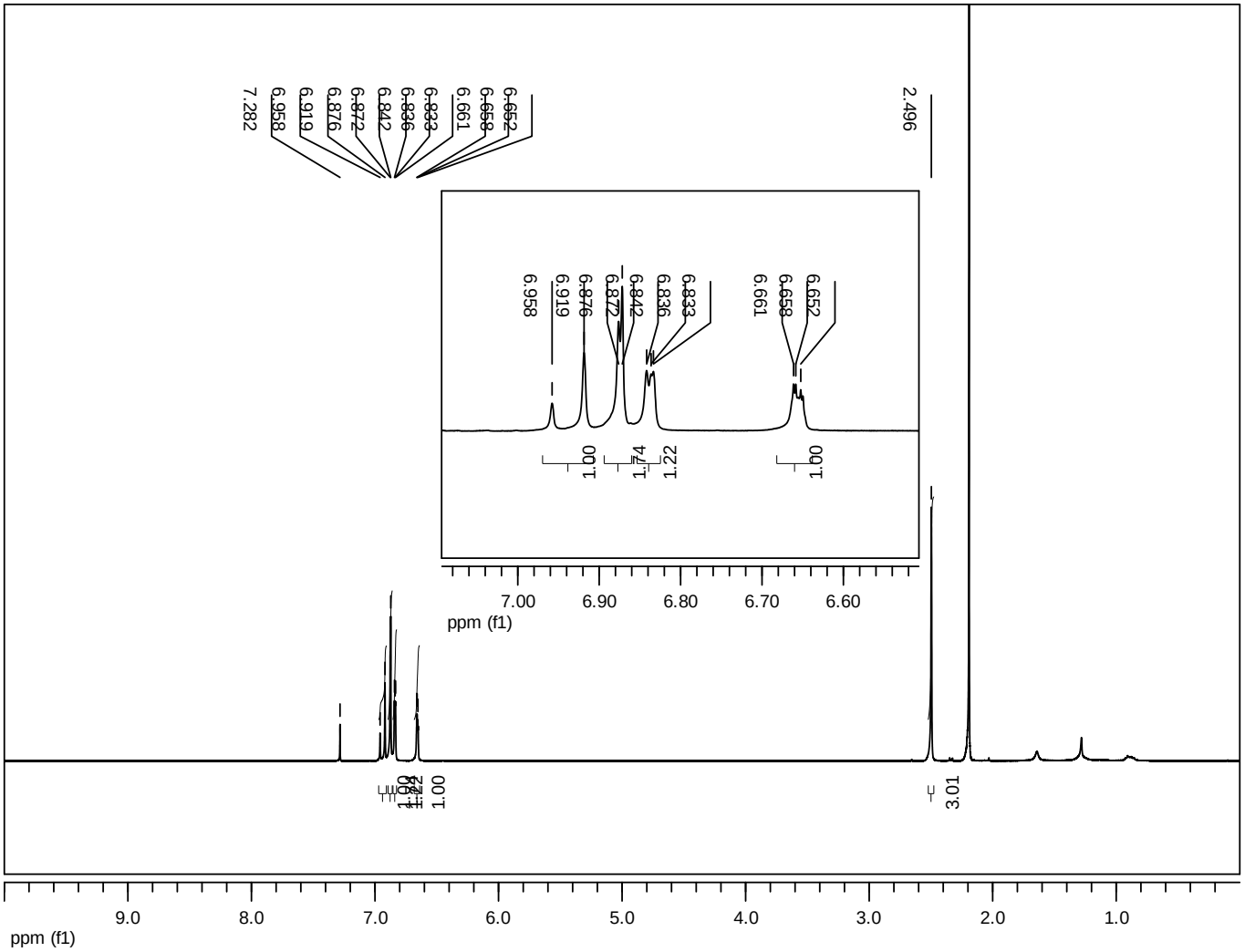

Figure SI 5-6 ^{1}H NMR spectrum of 3.

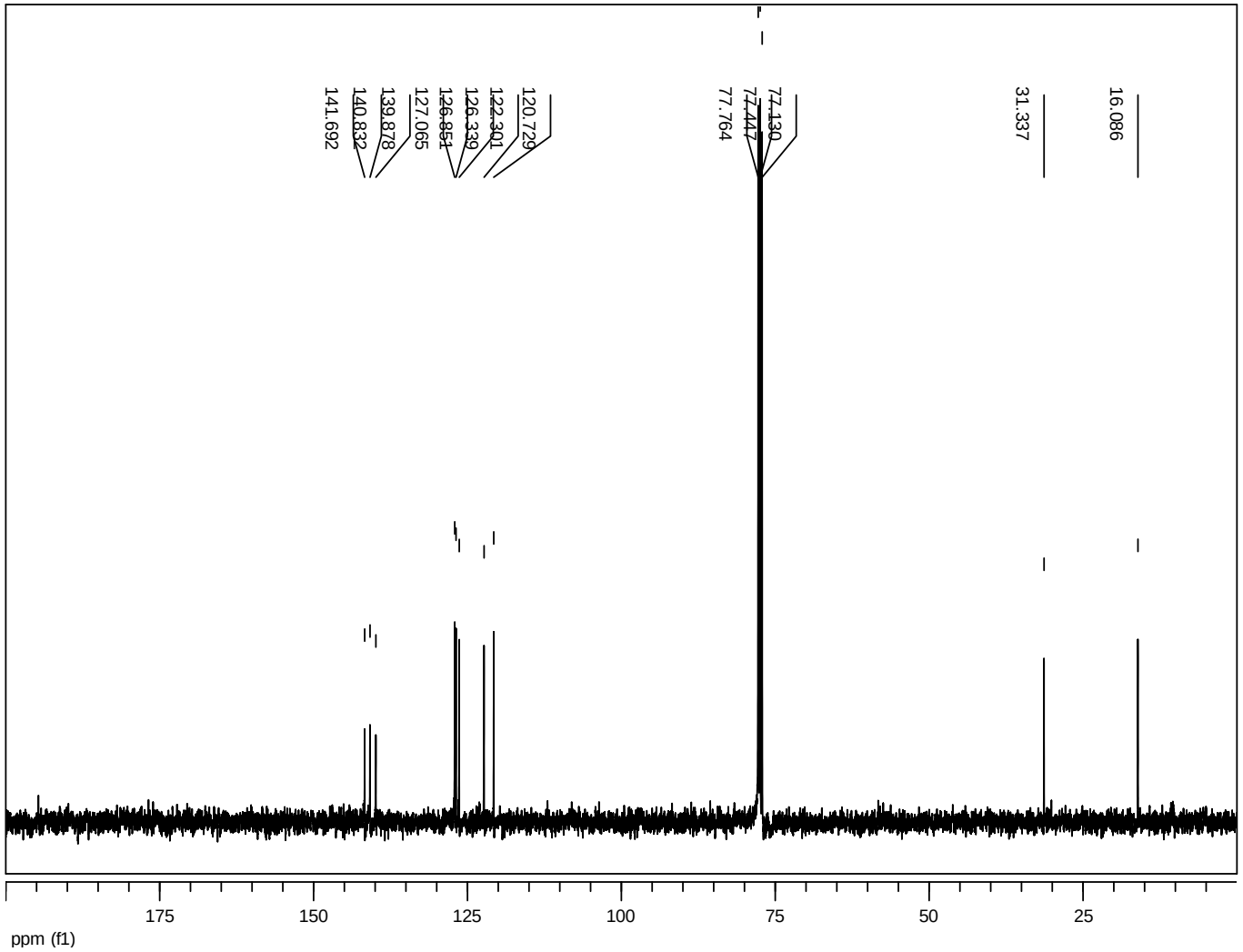

Figure SI 5-7 ^{13}C NMR spectrum of **3**.

CHAPTER 6 ELECTROLYTE-GATED TUNGSTEN TRIOXIDE THIN FILM TRANSISTORS MAKING USE OF IMIDAZOLIUM-BASED IONIC LIQUIDS

FOREWORD

Research on solution processable, large area and flexible devices working at low operating voltages is attracting large interest. Electrolyte gating is one of the most attractive approaches to produce thin film transistors working at low operating voltages. We specifically considered, in this Ph.D. work, the case of imidazolium-based ionic liquids to gate transistors based on sol-gel WO_3 thin films. WO_3 is an n-type semiconductor that is widely explored for its electrochromic, gas sensing and photocatalytic properties and thin films of WO_3 can be prepared by relatively easy solution processing methods making it an attractive material.

6.1 ARTICLE 3: Electrolyte-Gated Tungsten Trioxide Thin Film Transistors making use of Imidazolium-based Ionic Liquids

Dilek Işık[1], Dominic Rochefort[2], Francesca Soavi[3], Clara Santato[1,a]

[1] *Département de génie physique, École Polytechnique de Montréal, CP 6079, Succ. Centre-Ville, Montréal, Québec, Canada H3C 3A7*

[2] *Département de chimie, Université de Montréal, CP 6128, Succ. Centre-Ville, Montréal, Québec, Canada H3C 3J7*

[3] *Dipartimento di Chimica "Giacomo Ciamician", Università di Bologna, 40126 Bologna, Italy*

Article submitted to Applied Physics Letters, 7th May 2013

6.1.1 Abstract

Electrolyte gating is an approach to produce thin film transistors operating at low voltage (about 1 V). Here we report electrolyte-gated transistors based on solution-processable WO_3 thin films. As the gating medium, transistors make use of 1-butyl-3-methylimidazolium bis(trifluoromethylsulfonyl)imide ([BMIM][TFSI]), 1-butyl-3-methylimidazolium hexafluorophosphate ([BMIM][PF6]), and 1-ethyl-3-methylimidazolium bis(trifluoromethylsulfonyl)imide ([EMIM][TFSI]). The electrical double layer capacitances, obtained by electrochemical impedance spectroscopy, were used to calculate the electron mobility in the WO_3 films. The ionic conductivity and the viscosity of [EMIM][TFSI], together with the limited effect of faradic reactions at the [EMIM][TFSI]/WO_3 interface, explain the superior performance of [EMIM][TFSI]-gated WO_3 transistors.

6.1.2 Introduction

Electrolyte-gated thin film transistors, where electrolytes are used as gating media to change the conductivity of semiconductor thin films, have been intensively investigated for low power electronic applications[32], [186], [264], [265], [266], [267]. In the 1950s, electrolyte gating was used in the development of the first transistor [268]. In the 1980's, electrolyte gating was used to demonstrate microelectrochemical, pH-sensitive, WO_3 thin film transistor [26].

The underpinning of electrolyte-gated thin film transistors is the formation of an electrical double layer at the electrolyte/semiconductor interface, upon application of an electrical bias to the gate electrode immersed in the electrolyte, in contact with the semiconductor film (Figure 6-1). In electrolyte-gated transistors, electrical double layers at the electrolyte/semiconductor interface with capacitances (C_{EDL}) of a few $\mu F/cm^2$ replace more conventional dielectrics, such as thermally evaporated 100-200 nm-thick SiO_2 layers, whose capacitances are of ~ 10 nF/cm^2.

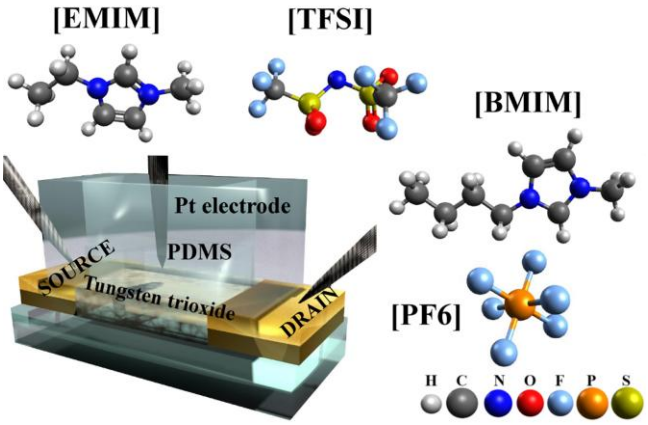

Figure 6-1 Device structure of the electrolyte gated WO_3 thin film transistor with the electrolyte confined by a PDMS well, on top of the WO_3 channel. The structures of the imidazolium-based ionic liquids for this work are also indicated.

The electrolyte gating approach has proven to dramatically reduce the operating voltage of transistors based on organic and inorganic, e.g. metal oxides, thin films. [32], [186], [266], [267].

Metal oxides are considered promising candidates for next-generation flexible thin film transistors [9]. Among metal oxides, WO_3 (an n-type semiconductor with a band gap of about 2.6 eV) stands for its electrochromic, sensing and photoelectrochemical properties [65], [66], [148].

A wide range of electrolytes has been considered to gate semiconductor films: aqueous and organic electrolytic solutions, ionic liquids, polymer electrolytes, and polyelectrolytes [264]. Ionic liquids are interesting for their low-volatility, non-flammability, relatively high ionic conductivity and hydrophobicity. Furthermore, they can have electrochemical stability windows compatible with the operating voltage of transistors [269].

At present, the effectiveness of the gating obtained using ionic liquids as the electrolytes it is not easily predictable because factors governing the formation of the electrical double layer at the ionic liquid/semiconductor interface are largely undiscovered. Therefore, there is a need to investigate different ionic liquid/semiconductor interfaces to understand how factors such as ionic conductivity, size and shape of the ions affect the gating process.

In this work, we fabricated and characterized electrolyte-gated WO_3 thin film transistors able to operate at about 1 V making use, as the electrolyte, of imidazolium-based ionic liquids, namely 1-butyl-3-methylimidazolium bis(trifluoromethylsulfonyl)imide ([BMIM][TFSI]), 1-butyl-3-methylimidazolium hexafluorophosphate ([BMIM][PF6]), and 1-ethyl-3-methylimidazolium bis(trifluoromethylsulfonyl)imide ([EMIM][TFSI], (Figure 6-1). Imidazolium-based ionic liquids exhibit relatively good ionic conductivity, low viscosity and low melting points with respect to other families based on, e.g., pyrrolidinium, ammonium and phosphonium. WO_3 thin films were solution-deposited by a sol-gel method on Indium Tin Oxide (ITO) patterned substrates. The conduction band edge of WO_3 lies at about 4.6 eV with respect to the vacuum level, thus properly matching the ITO work function for electron injection [148]. By electrochemical impedance spectroscopy, using two electrode-cells (Pt/ionic liquid/WO_3), we deduced the electrical double layer capacitance of the ionic liquid/WO_3 interface, to calculate the electron mobility of the electrolyte-gated WO_3 thin film transistors. We interpreted the observed results considering the ionic conductivity, viscosity and electrochemical stability of the three electrolytes investigated.

6.1.3 Experimental

ITO substrates were photolithographically patterned to define the source and drain electrodes by chemical etching (channel length (L) and width (W) were 1000 and 6000 μm, see supplementary material, Figure 6 SI-1, Ref [270]). The chemical precursor to prepare the WO_3 thin films was obtained by a sol-gel method already reported in the literature, slightly modified by the use of the organic stabilizer poly(ethylene glycol) (PEG) 200 instead of PEG 300 [65]. Films were spin coated on patterned ITO substrates at 1500 rpm, in ambient conditions, and annealed at 480-500 °C. Prior to spin coating, substrates were cleaned by sequential sonication (detergent solution in water, DI water, isopropanol, acetone, and isopropanol), blow-dried with N_2 and finally exposed for 20 min to UV/ozone. [EMIM][TFSI], [BMIM][TFSI], and [BMIM][PF6] (Iolitec Inc., chemical purity >99%) were purified under vacuum ($\sim 10^{-5}$ Torr) at 80 °C, for about 24 h, and directly transferred into the N_2 glove box (O_2, H_2O<1 ppm) for transistor characterization. Transistor measurements, performed using a semiconductor parameter analyzer (Agilent B1500A) and a micromanipulated electrical probe station, were done in the

order: transient, transfer and output curves. Transient curves were obtained by measuring the drain-source current, I_{DS}, and the gate-source current, I_{GS}, vs time at constant V_{DS}, for different gate-source voltages, V_{GS}, using a rectangular wave voltage with increasing amplitude. V_{GS} was applied for an interval of 182 sec. The acquisition time for each point was 2 sec. Transfer curves were obtained at a sweeping rate of 0.8 mV/sec; for each point the acquisition time was 60 sec. Output characteristics were acquired by modulating V_{GS} from 0 to 1 V with 0.2 V steps with a hold time at a certain V_{GS} (before the acquisition of the transistor current versus V_{DS} at a certain V_{GS}) of 600 sec; the acquisition time for each point was 200 msec. Electrochemical impedance spectroscopy (EIS) measurements were performed in the N_2 glove box with a two-electrode electrochemical cell. A Pt disc (0.07 cm^2) was used as the counter electrode in contact with the ionic liquid. WO_3 on ITO was the working electrode (0.07 cm^2). Impedance spectra were recorded over the 10^{-1} – 10^4 Hz frequency range, at applied DC voltages (E_{DC}) between 0 and 2 V, using 0.25 V steps, with a VersaSTAT 4 impedance spectrometer. The AC voltage (E_{AC}) was set to 10 mV root mean square (rms). System parameters such as cell resistance and double layer capacitance were obtained fitting the impedance data to an appropriate equivalent circuit (using the Windows-based application ZSimpWin).

6.1.4 Results and Discussion

6.1.4.1 Morphology of WO_3 films

Atomic Force Microscopy images of the WO_3 films, taken in the transistor channel region, show that films are nanostructured and have a relatively smooth surface (root mean square roughness, Rq, 2.2 nm, see supplementary material, Figure SI-2a, Ref [270]). Scanning Electron Microscopy images of the films show that they are constituted of well-interconnected particles, ~50 nm-sized (see supplementary material, Figure SI-2, Ref [270]).

6.1.4.2 Electrolyte Gated Transistors Characterization

To assess the possibility to gate the WO_3 thin films using the electrolyte gating approach, I_{DS} and I_{GS} were initially collected as a function of time upon application of increasing values of V_{GS}, at fixed V_{DS}, for the three ionic liquids (see supplementary material, Figure SI-3, Ref [270]).

Transient measurements clearly show that, even for relatively low values of V_{GS} (<1 V), gate modulation is possible. Transient measurements also show that the values of I_{DS} are about 1 order of magnitude higher than the corresponding steady state values of I_{GS} (except for [BMIM][TFSI]-gated WO_3 transistors at V_{GS}>1 V) thus indicating the limited effect of possible faradic processes taking place at the gate electrode. The measurement of I_{DS} vs time at V_{DS}=V_{GS}=1 V shows that a well-defined steady state condition for I_{DS} is not achieved even after 16 hours of continuous electrical biasing; after 40 minutes of biasing a *quasi*-steady state is observable (see supplementary material, Figure SI-4, Ref [270]).

For [EMIM][TFSI] and [BMIM][PF6], the output curves of the EG WO_3 transistors show a typical n-type behavior (Figure 2). The threshold voltage, V_{Th}, as deduced from the transistor transfer curves at saturation by extrapolating at y = 0 the square root of I_{DS}, has similar values for [EMIM][TFSI] and [BMIM][PF6], about -0.81 V and -0.77 V (see supplementary material, Figure SI-5, Ref [270]). The I_{ON}/I_{OFF} ratio (calculated between V_{GS}=0 and 1 V, for V_{DS}=1 V) is about 6 for transistors gated with [EMIM][TFSI] and 2 for transistors gated with [BMIM][PF6]. WO_3 transistors gated with [BMIM][TFSI] showed poor transistor performance (see supplementary material, Figure SI-5c, Ref [270]). For the case of [BMIM][TFSI], the application of higher electrical biases (≥2 V) resulted in significant faradic currents, compromising the transistor behavior (see supplementary material, Figure SI-3d and Figure 5c, Ref [270]).

To understand the factors governing the performance of the electrolyte-gated WO_3 thin film transistors, the physico-chemical properties of the ionic liquids have to be considered [271], [272]. The ionic conductivity of [EMIM][TFSI] is twice than that of [BMIM][TFSI] (6.63 and 3.41 mS/cm, at 20 °C) and five times higher than [BMIM][PF6] (1.37 mS/cm at 20 °C). Furthermore, the viscosity of [EMIM][TFSI] (39×10^{-2} Poise, 20 °C) is lower than that of [BMIM][TFSI] (49×10^{-2} Poise at 20 °C) and [BMIM][PF6] (310×10^{-2} Poise at 20 °C). On the basis of the ionic conductivity and viscosity, [EMIM][TFSI] is therefore is to lead to transistors with better performance with respect to [BMIM][TFSI] and [BMIM][PF6], as we indeed observed. On the other hand, the poor performance of [BMIM][TFSI]-gated transistors is tentatively attributed to relatively rapid faradic reactions involving [BMIM][TFSI] and water (present, in limited amount, in the N_2 glove box) or other impurities, at the WO_3 surface. Indeed,

water uptake for [BMIM][TFSI] is more significant with respect to other ionic liquids, such as [EMIM][TFSI] [267].

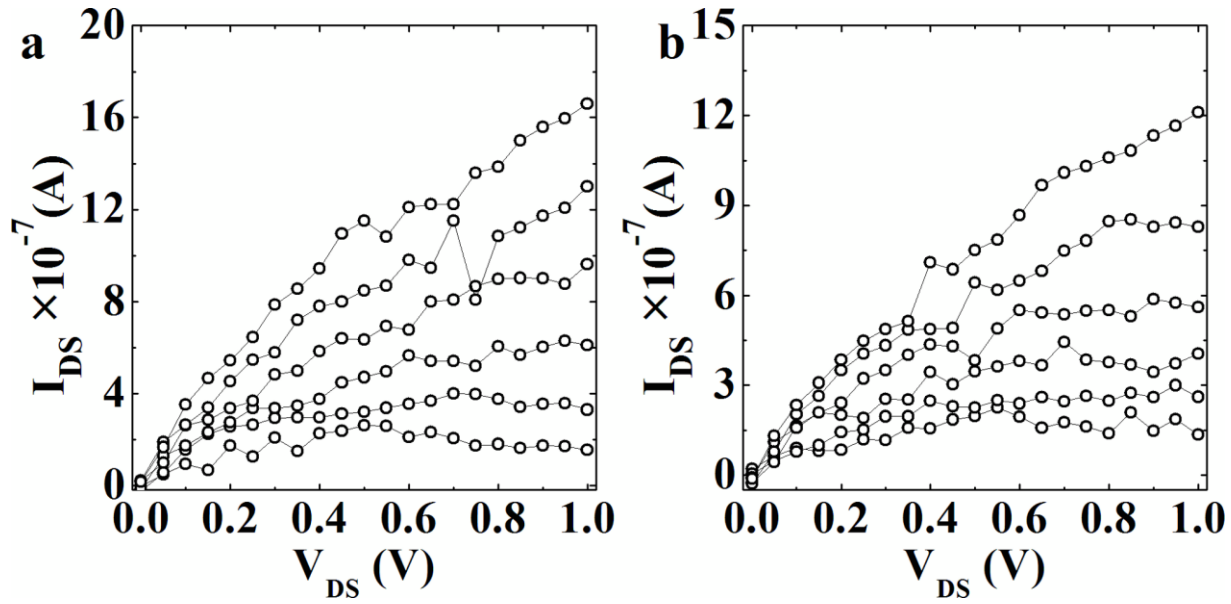

Figure 6-2 Output characteristics of EG WO_3 transistors making use of ionic liquid electrolytes (W/L = 1000 µm/6000 µm) with V_{GS} increasing from 0 to 1 V with 0.2 V steps. (a) [EMIM][TFSI] WO_3 transistors. (b) [BMIM][PF6] WO_3 transistors. In the output curves, the hold time at a certain V_{GS} (before the acquisition of the current versus V_{DS} at a certain V_{GS}) is 600 sec.

6.1.4.3 Electrochemical Impedance Spectroscopy

The capacitances of the electrical double layers were obtained by electrochemical impedance spectroscopy measurements performed on two-electrode (WO_3/ionic liquid/Pt) cells, with the three ionic liquids [EMIM][TFSI], [BMIM][PF6] and [BMIM][TFSI]. To explore the effect of the direct current potential (E_{DC}) applied to the (WO_3 on ITO) working electrode on the formation of the electrical double layer, the measurements were performed at E_{DC} = 0, -0.25, -0.5, -0.75, -1 V. Exclusively for [BMIM][TFSI], values of E_{DC} = -1.25, -1.5, -1.75, and -2 V were also investigated. Nyquist plots (Figure 6-3) show that for the three ionic liquids in the low frequency region (> 1 Hz) the lines are almost parallel to the imaginary axis at E_{DC}= -1V and they

can therefore be assigned to capacitive processes. For [BMIM][TFSI] at E_{DC}= -2 V, a semicircle was observed, indicating that a charge-transfer controlled process becomes dominant. At E_{DC}=-1 V, the electrochemical impedance of the cell can be modeled by a double-layer capacitance of the cell (C_{EDL}) in series with the cell resistance, including ionic and electronic contributions coming from the electrolyte and the electrodes, thus suggesting a finite diffusion process. At E_{DC}=-2 V, reactions occurring at the ionic liquid/electrode interface are responsible of the charge transfer resistance arising in parallel with C_{EDL}.[273], [274] For the three ionic liquids, the Bode plots show that at E_{DC}=-1 V the reorganization of the electrical double layer at the ionic liquid/electrode interface takes place and limiting capacitance values are achieved at frequencies < 10 Hz (Figure 3b). The EDL reorganization starts earlier at the [EMIM][TFSI]/electrode interfaces, suggesting a faster time constant of the double layer charging process (Figure 3b). For [BMIM][TFSI] at E_{DC}= -2 V, the phase angle decrease at low frequencies suggests the occurrence of undesirable redox reactions (Figure 3a-b), in agreement with the values of I_{GS} observed in the transient characteristics (see supplementary material, Figure SI-3d, Ref [270]). The C_{EDL} vs E_{DC} plots of the three electrochemical cells were deduced from the electrochemical measurements (Figure 3c). Making the assumption that the WO_3 electrode capacitance (C_{WO3}) limits the overall cell capacitance, ($C_{WO3} \approx C_{EDL}$) we calculated C_{EDL}= 6.63, 5.28, 7.33 μF/cm^2 for the [EMIM][TFSI]/WO_3, [BMIM][PF6]/WO_3 and [BMIM][TFSI]/WO_3 interfaces. Afterwards, the electron mobility in the saturation regime was calculated using the C_{EDL} obtained from the electrochemical impedance spectroscopy analysis.[275] We obtained similar values of the electron mobility for WO_3 transistors gated with [EMIM][TFSI] and [BMIM][PF6] at V_{DS}=1 V, in saturation conditions, i.e. 1.9×10^{-3} and 2.1×10^{-3} cm^2/V·s. The electron mobility was not calculated for [BMIM][TFSI]-gated WO_3 thin films because of the poor transistor performance.

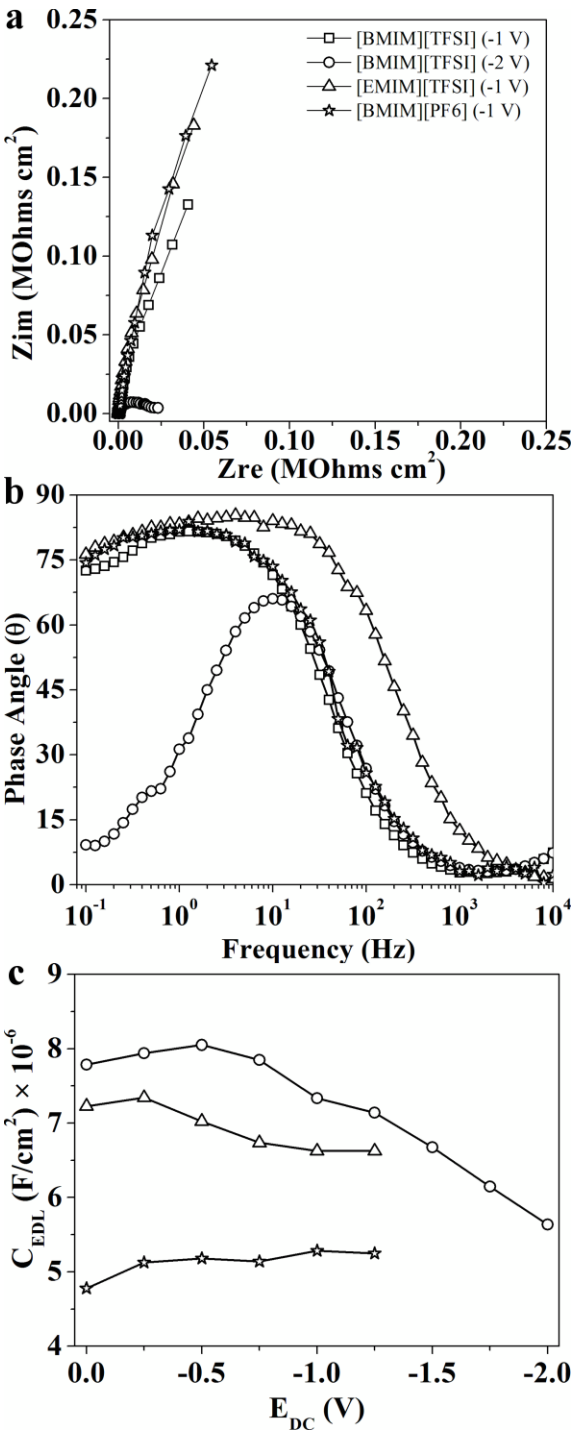

Figure 6-3 Nyquist (a) and Bode (b) plots of two-electrode (WO_3/IL/Pt) electrochemical cells with [EMIM][TFSI] (E_{DC} = -1V), [BMIM][TFSI] (E_{DC} = -1 or -2V), [BMIM][PF6] (E_{DC} = -1V). (c) Capacitance versus E_{DC} plots for the three electrochemical cells making use of the above-mentioned ionic liquids.

6.1.5 Conclusions

In conclusion, we adopted the electrolyte-gating approach to demonstrate transistors based on solution-processed WO_3 thin films operating at low voltages (about 1 V) making use of imidazolium-based ionic liquids as the gating medium. [EMIM][TFSI] gave better transistor performance with respect to [BMIM][PF6] and [BMIM][TFSI], attributable to a favorable combination of relatively high ionic conductivity, low viscosity, and absence of faradic reactions at the [EMIM][TFSI]/WO_3 interface. Electrolyte-gated transistors based on thin films of WO_3 and TiO_2, metal oxides of primary interest for photoelectrochemical applications, making use of relatively short channel lengths, to increase the mobility in the devices, are presently investigated.

C.S. acknowledges NSERC (Discovery Grant) and FQRNT (Équipe) for the financial support of this work. We thank Prof. F. Cicoira for fruitful discussions.

Supplementary Information-Article 3

Electrolyte-Gated Tungsten Trioxide Thin Film Transistors making use of Imidazolium-based Ionic Liquids

Dilek Işık[1], Dominic Rochefort[2], Francesca Soavi[3], Clara Santato[1,a]

[1] Département de génie physique, École Polytechnique de Montréal, CP 6079, Succ. Centre-Ville, Montréal, Québec, Canada H3C 3A7

[2] Département de chimie, Université de Montréal, CP 6128, Succ. Centre-Ville, Montréal, Québec, Canada H3C 3J7

[3] Dipartimento di Chimica "Giacomo Ciamician", Università di Bologna, 40126 Bologna, Italy

Article submitted to Applied Physics Letters, 7th May 2013

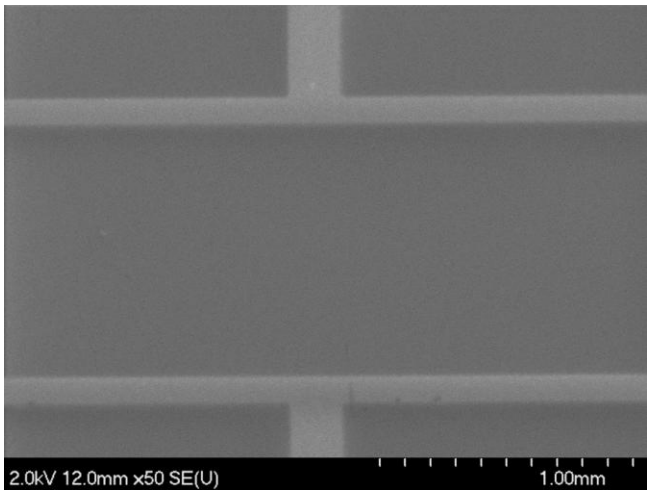

Figure SI 6-1 SEM image of a transistor channel after wet chemical etching with HCl:H_2O (5.5 M), at 35 °C, of ITO substrates (~125 nm-thick ITO, 15 Ω cm^{-1}). The positive photoresist SPR-220.3 was used as protective mask during the etching. Thin (100 μm-wide) ITO electrodes were

prepared to minimize the electrode area in contact with the electrolyte. Geometry of the channel: L=1000 μm and W=6000 μm.

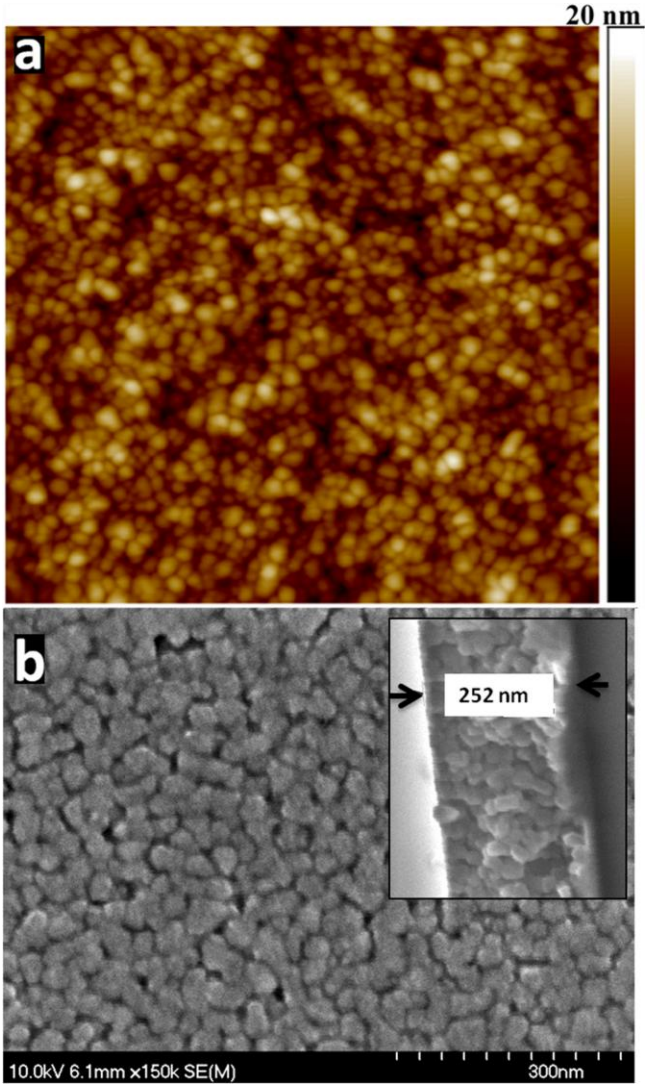

Figure SI 6-2 WO_3 film annealed at about 500 °C: (a) Atomic Force Microscopy (AFM) image (1 μm × 1 μm) root mean square roughness, R_q, ~ 2.2 nm; (b) Scanning Electron Microscopy (SEM) image. Inset: cross-section of the film showing that it is ~ 250 nm-thick, with an interconnected nanoparticle structure. AFM images were obtained in ambient conditions, at room temperature, in tapping mode, using a Dimension 3100 (Digital Instruments) microscope and etched Si cantilevers, with a resonance frequency ~500 kHz and tip radius <10 nm. SEM images were obtained with a Hitachi S-4700 microscope in the secondary electron mode using the upper and

lower detectors in ultra high-resolution mode (×150k magnification, accelerating voltage of 10 kV, working distance of 5 mm).

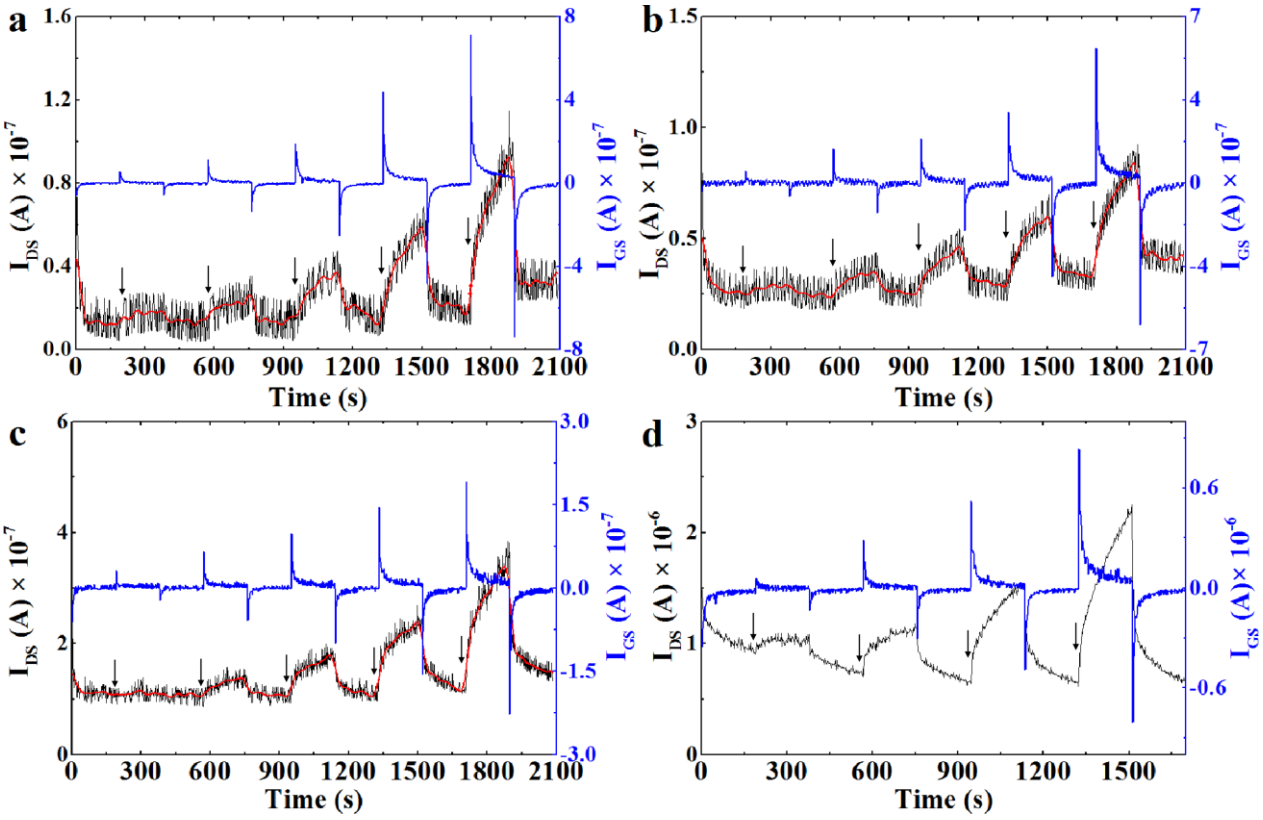

Figure SI 6-3 Transient characteristics for electrolyte gated WO_3 transistors making use of different ionic liquids (L=1000 µm and W=6000 µm). (a) [EMIM][TFSI], V_{DS} = 1 V and V_{GS} = 0, 0.2, 0.4, 0.6, 0.8, 1 V. (b) [BMIM][PF6] V_{DS} = 1V and V_{GS} = 0, 0.2, 0.4, 0.6, 0.8, 1 V. (c) [BMIM][TFSI] V_{DS} = 0.8 V and V_{GS} = 0, 0.2, 0.4, 0.6, 0.8, 1V. (d) [BMIM][TFSI] V_{DS} = 1V and V_{GS} = 0, 0.5, 1.0, 1.5, 2.0, 2.5 V. For every V_{GS} step, V_{GS} has been applied for an interval of 182 sec, followed by an interval of 182 sec at rest. In (a), (b), and (c), the red lines indicate the smoothened values of the currents by use of the FFT filter by Origin 8.5 data visualization software.

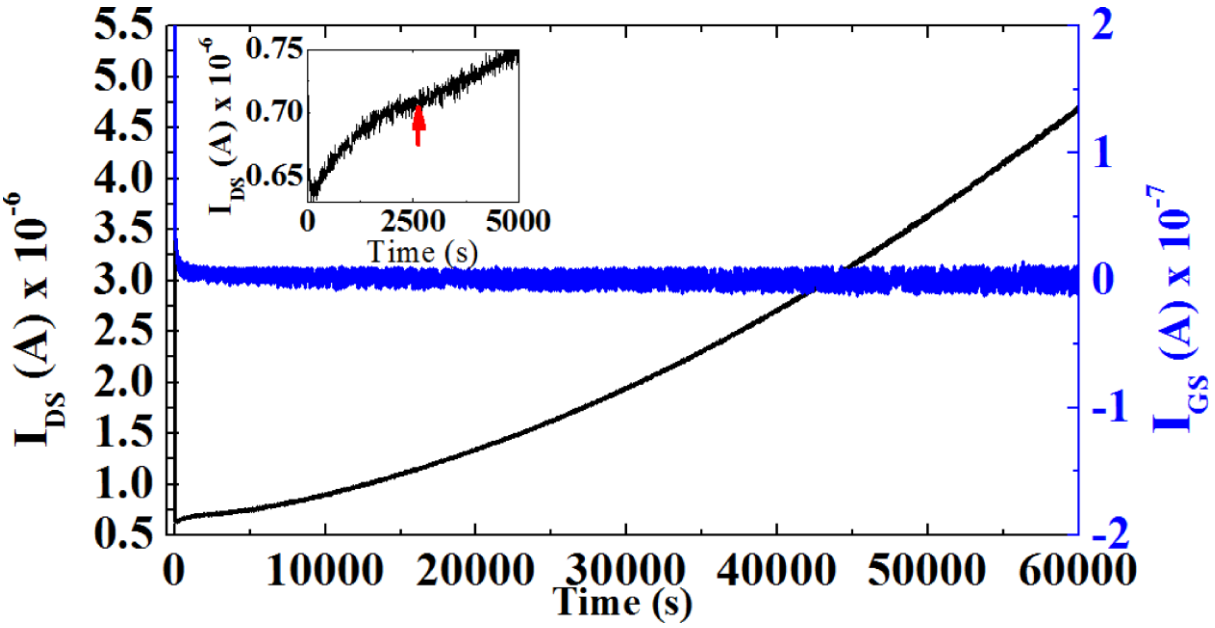

Figure SI 6-4 Transient characteristics (I_{DS} and I_{GS} versus time) for electrolyte gated WO_3 transistors making use of **[**BMIM**][**TFSI**]** (*L*=1000 µm and *W*=6000 µm) at V_{DS}=V_{GS}= 1 V.

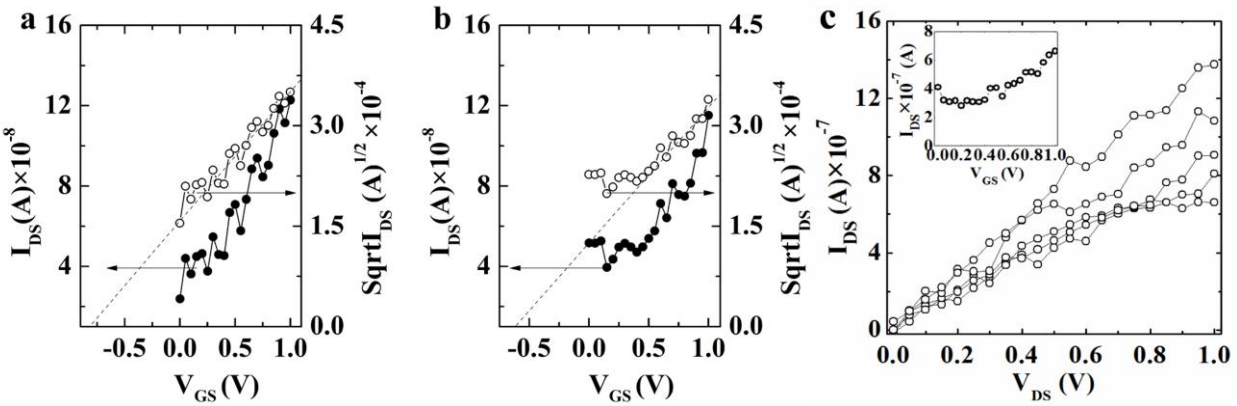

Figure SI 6-5 (a) Transfer characteristics of [EMIM][TFSI]-gated WO_3 transistors with V_{DS} = 1 V. (b) Transfer characteristics of [BMIM][PF6]-gated WO_3 transistors with V_{DS} = 1 V. V_{GS} sweeping rate is 0.8 mV/sec (*L*=1000 µm and *W*=6000 µm). (c) Output characteristics of [BMIM][TFSI]-gated WO_3 transistors with V_{GS} from 0 to 1 V with 0.2 V steps. Inset: transfer characteristics at V_{DS} =1 V. V_{GS} sweeping rate is 0.8 mV/sec; for each point the acquisition time is 60 sec. In the output curves, the hold time at a certain V_{GS} (before the measurement of the current at this same V_{GS}) is 600 sec.

6.2 Microfabrication of ITO microelectrodes

ITO is a commonly used conductive oxide due to its high transparency and high conductivity [276]. In this Ph.D. work, ITO was selected for the good matching between its Fermi energy level and the conduction band edge of WO_3 [148], [149]. For electrolyte gated WO_3 transistors, ITO (15 Ohm cm^{-1}, 125-130 nm-thick, dimensions 1.1 mm×30 mm×30 mm) source and drain electrodes were photolithographically patterned at LMF, Ecole Polytechnique de Montréal, by wet chemical etching in 5.5 M HCl:H_2O (45 cc:25 cc) for 9 min. Three different channel geometry were formed: width (6000 μm) and length (100 μm, 500 μm, 1000 μm).

Mask Design: The mask for the photolithography was designed by L-Edit or Libre-CAD and produced on a plastic sheet by printing at the Polygram laboratory (Electrical Engineering department, Ecole Polytechnique de Montreal). The minimum feature used for the mask layout was 100 μm (Figure 6-5). The mask was designed to fit on 3 cm×3 cm ITO substrates.

Cleaning: The microfabrication process is resumed in Table 6-1. Small particles or other type of contaminants, i.e. grease on the ITO surface, might cause problems in the patterning of the substrates. Therefore, prior to the microfabrication, ITO substrates were cleaned sequentially by sonication in detergent (Alconox)-DI water solution, DI water, acetone and isopropanol and afterwards dried with N_2 jet. ITO substrates were heat treated on top of a hot-plate at least 2 hours at 115 °C to evaporate physically adsorbed water and subsequently treated with UV-Ozone system for about 18 minutes to enhance the photoresist adhesion and uniformity on the substrate surface.

Photolithography: A positive resist, SPR 220.3 (Megaposit), was used to define the etching windows on top of ITO substrate. The thickness of the photoresist deviates 15% from the thickness obtained on a silicon wafer (Figure 6-4 and 6-11). Eventually a photoresist thickness of 2.75 μm was obtained by spin coating at 3000 rpm for 30 sec. After spin coating, the photoresist was soft-baked at 115 °C for 1.5 min on a hot plate as suggested by the manufacturer, for the photoresist to gain mechanical stability. Afterwards, the substrate was exposed to the i-line (365 nm) of the MA-4 aligner with intensity×time ~ 54 mW sec. Post-exposure bake was done at 115 °C for 1.5 min, similar to the soft-bake conditions. Post-exposure bake is useful to stop further reactions in the photoresist.

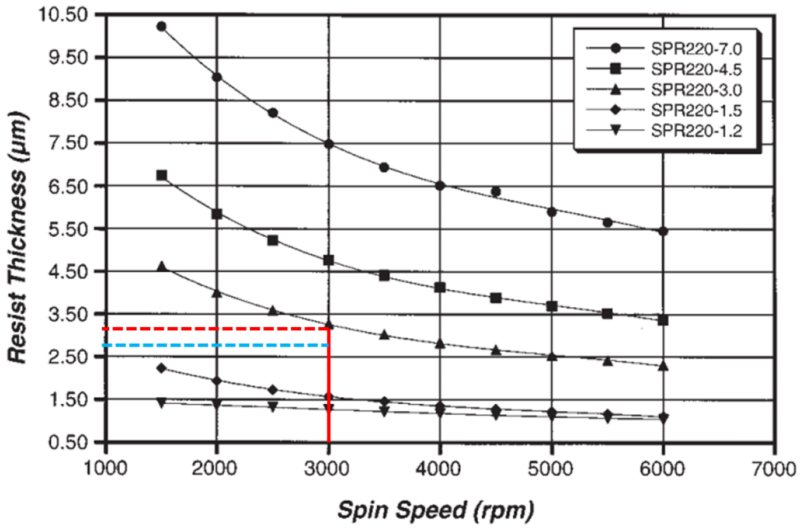

Figure 6-4 Spin speed versus thickness curves for 4 inch Si-wafers spin coated with SPR 220 photoresists. The difference in the photoresist thickness for the Si wafer (red dashed line) and the ITO substrate (blue dashed line)

Development: Development of the exposed photoresist was done using MF-319 developer. Development of the photoresist was followed with a Nikon microscope, with 30 sec intervals. The development is completed after 3.40 min (Figure 6-10).

Wet chemical etching: Etching was carried out with hydrochloric acid (HCl %70) diluted in DI water with two different concentrations, 9 and 5.5 M. A hot plate equipped with a thermal controller was used and set to 35 °C. The ITO glass was immersed vertically in the etching solution and etching was followed step-by-step by control of the substrate surface with the optical microscope, an amperometer and a Dektak profilometer (Figure 6-12). Since the 9 M solution quickly attacked the ITO, 5.5 M was finally chosen: patterned ITO substrates were successfully prepared in 9 min, at 35 °C.

Characterization: Prior to the wet chemical etching the channel between ITO electrodes was characterized for the surface morphology by scanning electron microscopy (SEM), chemical composition by energy dispersive X-ray spectroscopy (EDS), and conductivity with electrical measurements.

Table 6-1 Process steps for photolithography and etching of ITO substrates.

Step #	Process	Illustration
1	Mask preparation L-edit Libre-CAD	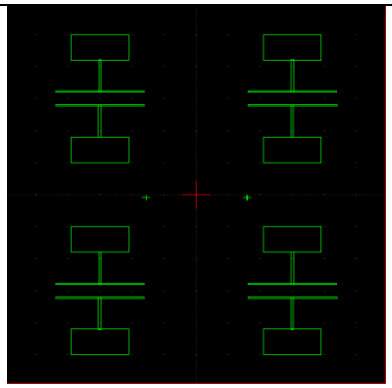 Figure 6-5 Mask layouts used for ITO patterning.
2	Cleaning Ultrasonic bath	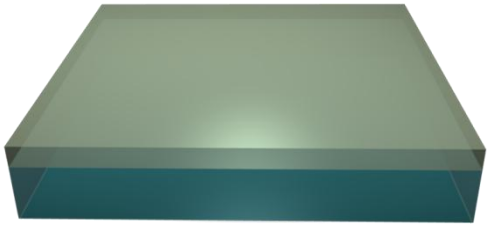 Figure 6-6 ITO substrate
3	Dehydrate Hot plate	120 °C, 2 hr
4	Organic removal UV-Ozone cleaner	18 min exposure
5	Photoresist (positive) Spin coater	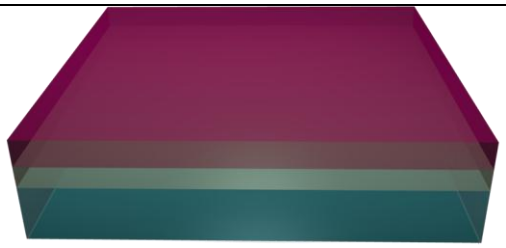 Figure 6-7 Photoresist coated ITO substrate, thickness ~2,75 µm

6	Soft Bake Hot plate	115 °C 1.5 min
7	UV-exposure Intensity×time=54 MA4- aligner	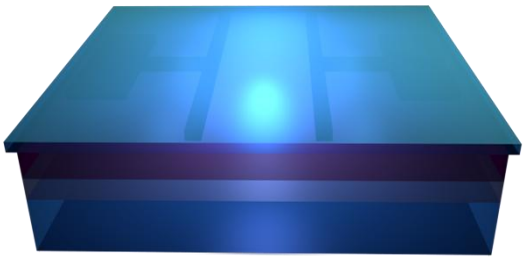 Figure 6-8 Hard contact (i-line, 365nm, exposure)
8	Post Bake Hot plate	115 °C, 1.5 min
9	Develop MF-319	3.40 min
10	Acid etching	5.5M HCl solution at 35 °C, 9 min
11	FINAL	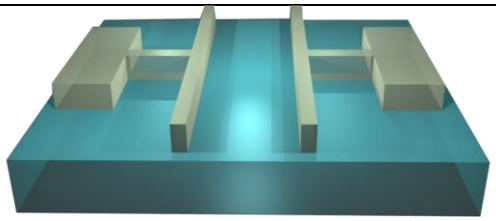 Figure 6-9 Patterned ITO glass

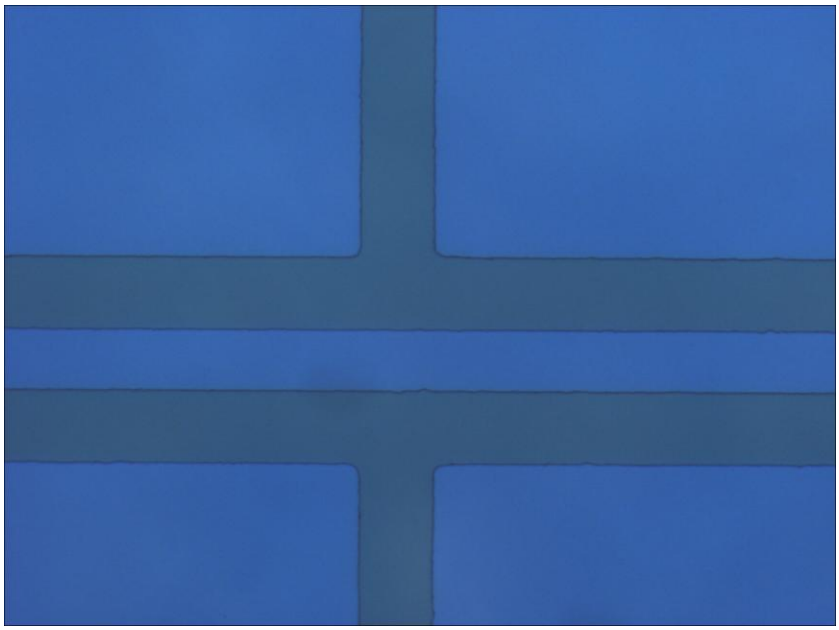

Figure 6-10 100 μm channel and developed 100 μm features of photoresist on ITO. Image taken under polarized light after 3 min 40 sec development, no photoresist was observed.

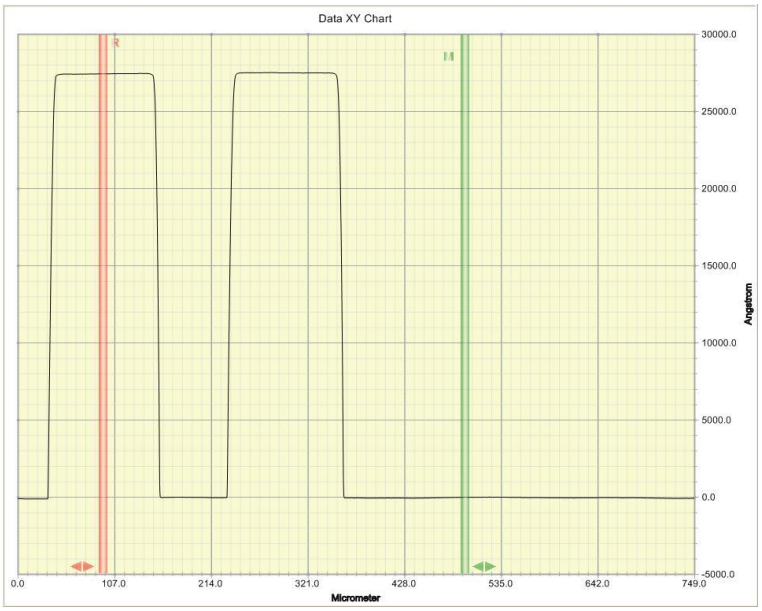

Figure 6-11 Developed photoresist cross section after 3 min 40 sec. Calibration correction 43% giving ~2.75 μm depth.

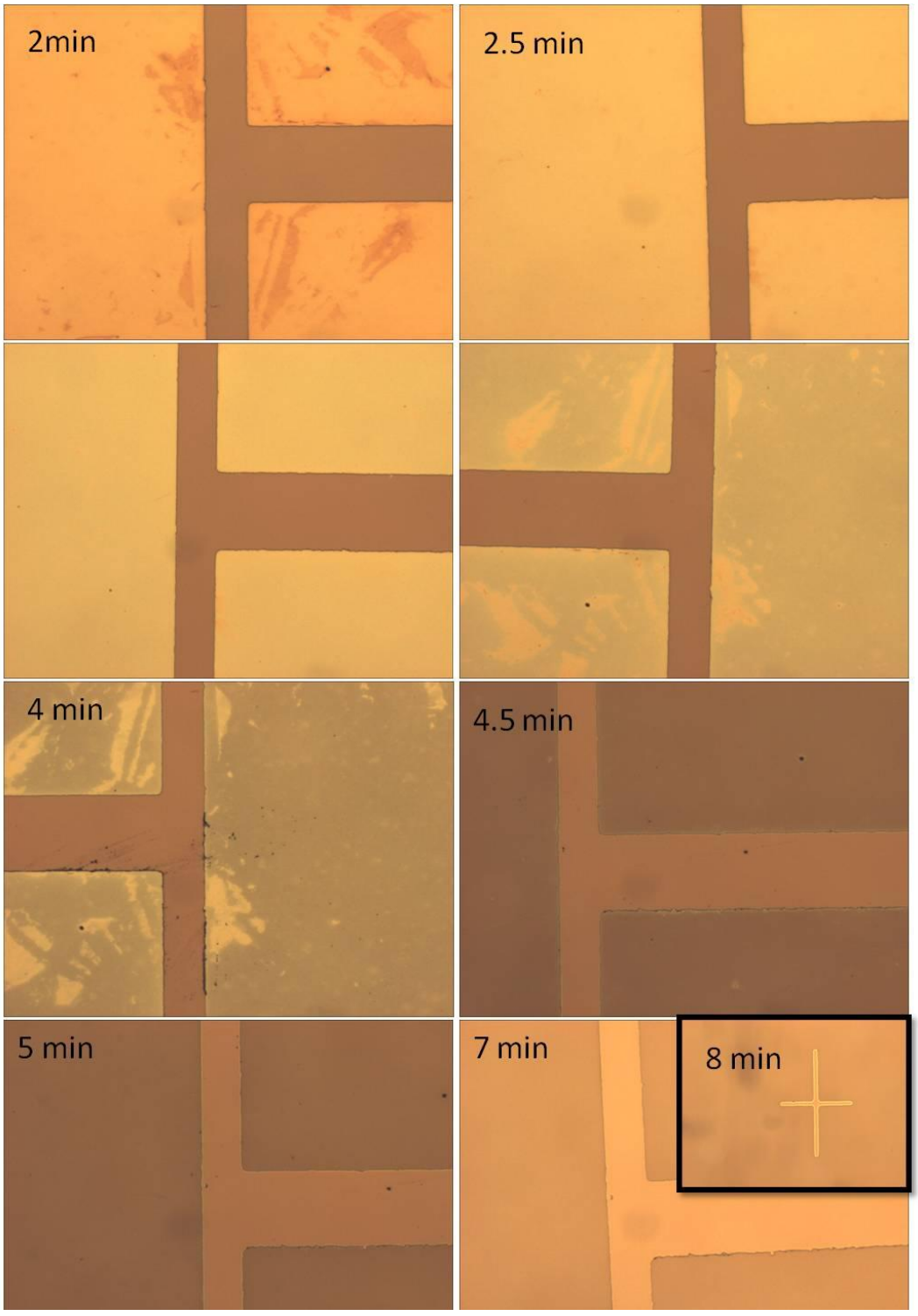

Figure 6-12 Optical images of step-by-step wet chemical etching.

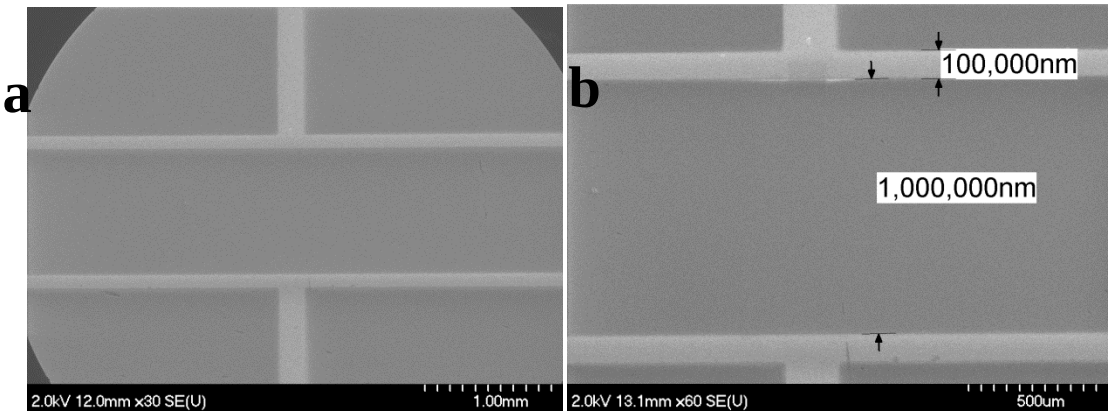

Figure 6-13 SEM Images showing the fabricated (a) ITO electrodes, (b) 1000 µm channel.

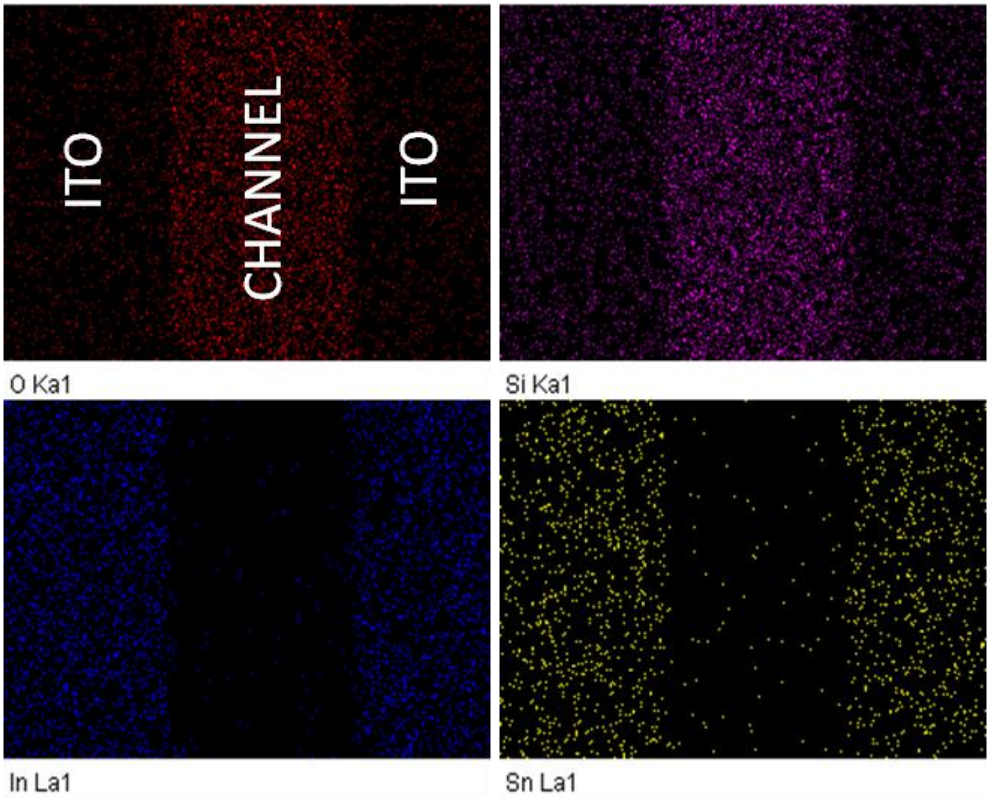

Figure 6-14 A portion of the transistor substrate showing the chemical distribution of elements in and around the channel, as obtained from a EDX survey. After etching In and Sn are replaced by Si and O, i.e. ITO was etched and glass substrate was reached.

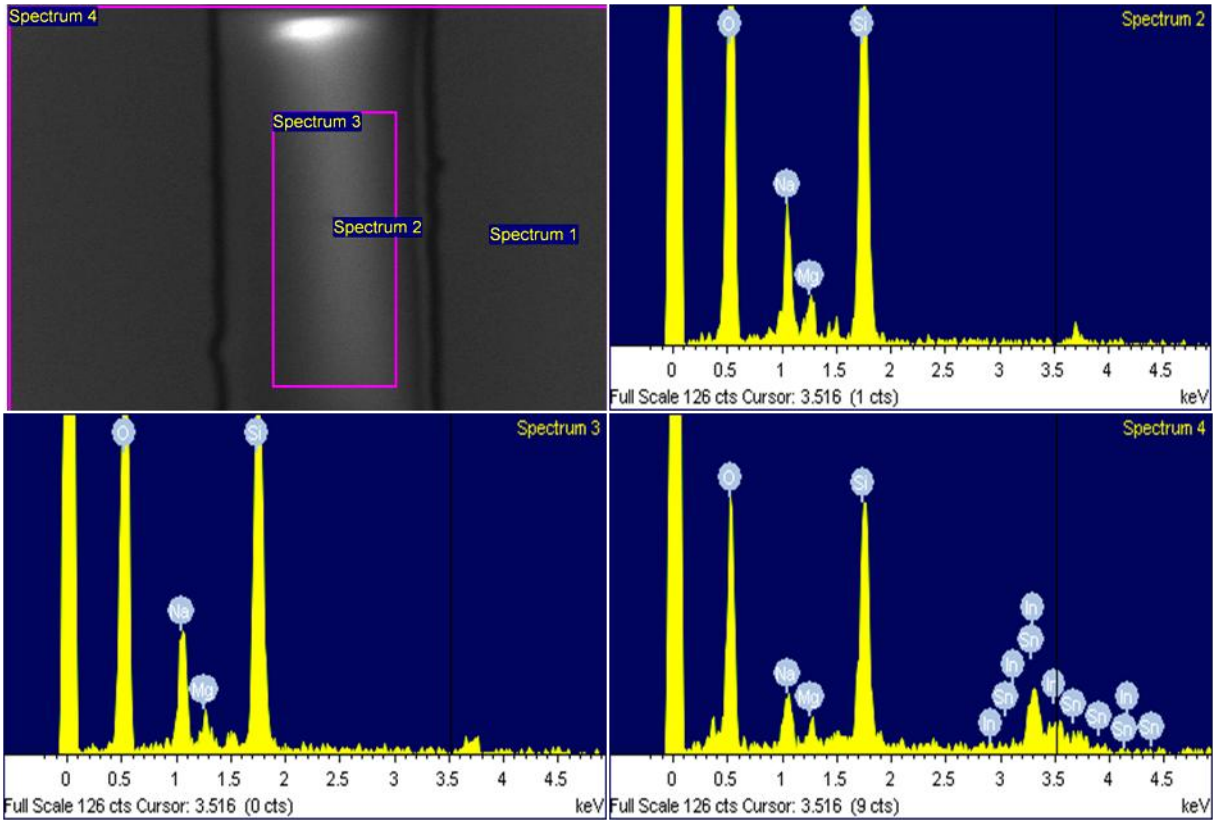

Figure 6-15 Spectra taken from different regions of the sample showing the presence of different elements in and near the transistor channel. These spectra clearly shows that no In or Sn residues were left in the channel after etching.

CHAPTER 7 CONCLUSIONS, PERSPECTIVES AND GENERAL DISCUSSION

The work described in this thesis is focused on solution processable organic and inorganic semiconductor thin films hosted in transistor configuration.

Primarily, in this Ph.D. work, the effect of the molecular structure and the supramolecular arrangement of the π-conjugated molecules in thin film form on the final charge transport properties was studied. The systematic investigations carried out on the thin film deposition conditions (substrate surface modification, solution concentration, and thermal treatment conditions of the films) for the organic semiconductors are reported in Chapters 4 and 5. The results we obtained using novel acene- and thiophene-based materials confirmed the key role played by the molecular structure on the functional properties of the films as well as the validity of the film engineering approach to further control such properties, before incorporation of the materials into device structures of technological interest.

In Chapter 4, solution deposited ambipolar and n-type thin film transistors based on pentacene derivatives were studied. Balanced e^- and h^+ mobility, on the order of 2×10^{-3} $cm^2/V\cdot sec$, were obtained for 2,3-CN2-TIPS-Pn films. On the other hand, electron mobility on the order of 10^{-3} $cm^2/V\cdot sec$ was obtained for TES-F8 and TIPS-F8 pentacene derivatives. The charge transport properties of thin films of 2,3-CN2-TIPS-Pn, TES-F8 and TIPS-F8 show the effectiveness of functionalization of the pentacene backbone with cyano- and fluoro- electron withdrawing groups to promote electron transport. In 2,3-CN2-TIPS-Pn hole transport was maintained. The GIXRD characterization made on thermally treated thin films of 2,3-CN2-TIPS-Pn revealed a favorable arrangement of the molecules in the transistor channel. Spin coating was found to produce molecular arrangements (π-π stacking) more favorable for the charge transport in the thin film transistor configuration compared to the dropcasting.

In Chapter 5, new soluble organic semiconductors making use of azomethine (-C=C-) couplings were reported and their electronic and optical properties were compared to those of an analogous oligomer based on more conventional vinylene couplings (-C=C-). Although poor,

results show that thin films of azomethines are electroactive and that there is room to improve such electroactivity by further work on their molecular structure and their processing conditions.

In Chapters 4 and 5 the matching between the HOMO and LUMO levels of the organic semiconductor molecule and the Fermi level of the gold metal electrodes employed in the corresponding thin film transistors explained the experimental results on the p-type, n-type and ambipolar charge carrier transport properties of the films.

With the aim of decreasing the operating voltages of solution processable transistors, the electrolyte gating approach was explored. Imidazolium-based room temperature ionic liquids were selected due to their good ionic conductivity. Nanostructured WO_3 thin films deposited by the sol-gel method where interfaced with the ionic liquids to fabricate transistors operating at about 1 V. Electron mobility for [EMIM][TFSI]- and [BMIM][PF6]-gated WO_3 transistors were 1.9×10^{-3} $cm^2/V\cdot sec$ and 2.1×10^{-3} $cm^2/V\cdot sec$, calculated considering the capacitance of the ionic liquid/WO_3 electrical double layers (C_{EDL}= 6.63×10^{-6} and 5.28×10^{-6} F/cm^2 for the [EMIM][TFSI] and [BMIM][PF6]) obtained after electrochemical impedance spectroscopy measurements.

To conclude, depending on the expertise gained, the work on the electrolyte gating can be further extended by exploring the effect of reduced channel lengths on the charge transport process. In this Ph.D. work the channel length investigated was relatively long (1 mm). Shorter channel lengths are expected to decrease the charge trap sites within the transistor channel (e.g. grain boundaries) thus improving transport.

The research carried out in this Ph.D. focused on thin films of solution processable semiconductors, formed by spin coating technique. However, printing technologies are attracting more and more interest for the production of electronic devices [277]. Today, printing technologies offer feature sizes on the order of 10-100 μm with 1-20 μm registration (overlay) accuracy [72], [277]. Considering the resolution, ease in handling of the materials and increasing capabilities of the printing technologies, efforts can be leveraged into this direction.

Secondly, to improve the yield and reproducibility of the solution processable organic and inorganic semiconductors controlled processing methods can be employed. This goal would be achieved by controlling the accuracy of each production step with care. Special care should be

directed on the surface modification methods by self assembling monolayers as described in Chapter 2 and surface patterning.

From a more fundamental point of view, the interaction between ionic liquids and relatively rough surfaces are not well understood. Understanding the ionic liquid/ semiconductor interface is important. Comparisons between atomically flat substrates and rough surfaces can yield useful information in modeling and better understanding of the interfaces. Relatively new methods such as electrowetting test where the contact angle of the ionic liquid is measured as a function of the applied potential would help us in understanding the formed interface [278], [279]. Collecting force curves at the ionic liquid/ semiconductor interfaces by use of atomic force microscopy is another way of exploring the electrical double layer and the interfacial features [169], [170], [280], [281], [282], [283].*

* Molecular structures and illustrations used in this thesis were created by use of Avogadro v 1.1 [284], Blender 3D v2.65[285], Inkscape v0.48[286], GIMP v2.8[287] and Paint.Net v3.5[288] computer programs

REFERENCES

[1] G. Malliaras and R. Friend, “An Organic Electronics Primer,” *Physics Today*, vol. 58, no. 5, pp. 53–58, 2005.

[2] H. Klauk, *Organic Electronics: Materials, Manufacturing, and Applications*. John Wiley & Sons, 2006.

[3] J. E. Anthony, “Functionalized Acenes and Heteroacenes for Organic Electronics,” *Chemical Reviews*, vol. 106, no. 12, pp. 5028–5048, Dec. 2006.

[4] C. Santato, L. Favaretto, M. Melucci, A. Zanelli, M. Gazzano, M. Monari, D. Isik, D. Banville, S. Bertolazzi, S. Loranger, and F. Cicoira, “Influence of the oxidation level on the electronic, morphological and charge transport properties of novel dithienothiophene S-oxide and S,S-dioxide inner core oligomers,” *J. Mater. Chem.*, vol. 20, no. 4, pp. 669–676, 2010.

[5] D. Işık, Y. Shu, G. Tarabella, N. Coppedè, S. Iannotta, L. Lutterotti, F. Cicoira, J. E. Anthony, and C. Santato, “Ambipolar organic thin film transistors based on a soluble pentacene derivative,” *Applied Physics Letters*, vol. 99, p. 023304, 2011.

[6] J. D. Plummer, M. D. Deal, and P. B. Griffin, *Silicon VLSI Technology: Fundamentals, Practice and Modeling*. Prentice Hall, 2000.

[7] Neamen, *Semiconductor Physics And Devices*. McGraw-Hill Education (India) Pvt Limited.

[8] S. A. Stauth and B. A. Parviz, “Self-assembled single-crystal silicon circuits on plastic,” *PNAS*, vol. 103, no. 38, pp. 13922–13927, Sep. 2006.

[9] E. Fortunato, P. Barquinha, and R. Martins, “Oxide Semiconductor Thin-Film Transistors: A Review of Recent Advances,” *Adv. Mater.*, vol. 24, no. 22, pp. 2945–2986, 2012.

[10] M. J. Powell, “The physics of amorphous-silicon thin-film transistors,” *IEEE Transactions on Electron Devices*, vol. 36, no. 12, pp. 2753 –2763, Dec. 1989.

[11] J. . Schön, C. Kloc, and B. Batlogg, “On the intrinsic limits of pentacene field-effect transistors,” *Organic Electronics*, vol. 1, no. 1, pp. 57–64, Dec. 2000.

[12] Y.-Y. Lin, D. J. Gundlach, S. F. Nelson, and T. N. Jackson, "Stacked pentacene layer organic thin-film transistors with improved characteristics," *IEEE Electron Device Letters*, vol. 18, no. 12, pp. 606–608, Dec. 1997.

[13] J. H. Schön, C. Kloc, and B. Batlogg, "Perylene: A promising organic field-effect transistor material," *Applied Physics Letters*, vol. 77, no. 23, pp. 3776–3778, Dec. 2000.

[14] K. Nomura, H. Ohta, A. Takagi, T. Kamiya, M. Hirano, and H. Hosono, "Room-temperature fabrication of transparent flexible thin-film transistors using amorphous oxide semiconductors," *Nature*, vol. 432, no. 7016, pp. 488–492, Nov. 2004.

[15] E. M. C. Fortunato, P. M. C. Barquinha, A. C. M. B. G. Pimentel, A. M. F. Gonçalves, A. J. S. Marques, L. M. N. Pereira, and R. F. P. Martins, "Fully Transparent ZnO Thin-Film Transistor Produced at Room Temperature," *Advanced Materials*, vol. 17, no. 5, pp. 590–594, 2005.

[16] D. Paret, *RFID at Ultra and Super High Frequencies: Theory and application*. John Wiley & Sons, 2009.

[17] S. G. Lim, S. Kriventsov, T. N. Jackson, J. Haeni, D. Schlom, A. Balbashov, R. Uecker, P. Reiche, J. Freeouf, and G. Lucovsky, "Dielectric functions and optical bandgaps of high-[bold K] dielectrics for metal-oxide-semiconductor field-effect transistors by far ultraviolet spectroscopic ellipsometry," *Journal of applied physics*, vol. 91, p. 4500, 2002.

[18] P. D. Ye, G. D. Wilk, B. Yang, J. Kwo, S. N. G. Chu, S. Nakahara, H.-J. L. Gossmann, J. P. Mannaerts, M. Hong, K. K. Ng, and J. Bude, "GaAs metal–oxide–semiconductor field-effect transistor with nanometer-thin dielectric grown by atomic layer deposition," *Applied Physics Letters*, vol. 83, no. 1, pp. 180–182, Jul. 2003.

[19] W. M. Tang, M. T. Greiner, M. G. Helander, Z. H. Lu, and W. T. Ng, "Effects of interfacial oxide layers of the electrode metals on the electrical characteristics of organic thin-film transistors with HfO2 gate dielectric," *Journal of Applied Physics*, vol. 110, no. 4, p. 044108, 2011.

[20] H. Klauk, U. Zschieschang, J. Pflaum, and M. Halik, "Ultralow-power organic complementary circuits," *Nature*, vol. 445, no. 7129, pp. 745–748, Feb. 2007.

[21] P. P. Konorov, A. M. Yafyasov, and V. B. Bogevolnov, *Field Effect in Semiconductor-Electrolyte Interfaces: Application to Investigations of Electronic Properties of Semiconductor Surfaces*. Princeton University Press, 2006.

[22] Y. Xia and C. D. Frisbie, "Low-Voltage Electrolyte-Gated OTFTs and Their Applications," in in *Organic Electronics II*, H. Klauk, Ed. Wiley-VCH Verlag GmbH & Co. KGaA, 2012, pp. 197–233.

[23] H. Y. Hwang, Y. Iwasa, M. Kawasaki, B. Keimer, N. Nagaosa, and Y. Tokura, "Emergent phenomena at oxide interfaces," *Nature Materials*, vol. 11, no. 2, pp. 103–113, Jan. 2012.

[24] W. H. Brattain and C. G. B. Garrett, "Experiments on the interface between germanium and an electrolyte," *Bell Syst. Tech. J*, vol. 34, no. 1, pp. 129–176, 1955.

[25] M. J. Natan, D. Bélanger, M. K. Carpenter, and M. S. Wrighton, "pH-sensitive Ni(OH)2-based microelectrochemical transistors," *Journal of Physical Chemistry*, vol. 91, no. 7, pp. 1834–1842, 1987.

[26] M. J. Natan, T. E. Mallouk, and M. S. Wrighton, "pH-sensitive WO3-based microelectrochemical transistors," *Journal of Physical Chemistry*, vol. 91, no. 3, pp. 648–654, 1987.

[27] S. Chao and M. S. Wrighton, "Characterization of a 'solid-state' polyaniline-based transistor: Water vapor dependent characteristics of a device employing a poly(vinyl alcohol)/phosphoric acid solid-state electrolyte," *Journal of the American Chemical Society*, vol. 109, no. 22, pp. 6627–6631, 1987.

[28] J. W. Thackeray, H. S. White, and M. S. Wrighton, "Poly(3-methylthiophene)-coated electrodes: Optical and electrical properties as a function of redox potential and amplification of electrical and chemical signals using poly(3-methylthiophene)-based microelectrochemical transistors," *Journal of Physical Chemistry*, vol. 89, no. 23, pp. 5133–5140, 1985.

[29] S. Chao and M. S. Wrighton, "Solid-state microelectrochemistry: Electrical characteristics of a solid-state microelectrochemical transistor based on poly(3-methylthiophene)," *Journal of the American Chemical Society*, vol. 109, no. 7, pp. 2197–2199, 1987.

[30] I. Kymissis, *Organic Field Effect Transistors*. Springer, 2011.

[31] S. Dasgupta, S. Gottschalk, R. Kruk, and H. Hahn, "A nanoparticulate indium tin oxide field-effect transistor with solid electrolyte gating," *Nanotechnology*, vol. 19, p. 435203, 2008.

[32] H. Yuan, H. Shimotani, J. Ye, S. Yoon, H. Aliah, A. Tsukazaki, M. Kawasaki, and Y. Iwasa, "Electrostatic and Electrochemical Nature of Liquid-Gated Electric-Double-Layer Transistors Based on Oxide Semiconductors," *J. Am. Chem. Soc.*, vol. 132, no. 51, pp. 18402–18407, Dec. 2010.

[33] C. J. Drury, C. M. J. Mutsaers, C. M. Hart, M. Matters, and D. M. De Leeuw, "Low-cost all-polymer integrated circuits," *Applied Physics Letters*, vol. 73, no. 1, pp. 108–110, 1998.

[34] V. Subramanian, P. C. Chang, J. B. Lee, S. E. Molesa, and S. K. Volkman, "Printed organic transistors for ultra-low-cost RFID applications," *IEEE Transactions on Components and Packaging Technologies*, vol. 28, no. 4, pp. 742 – 747, Dec. 2005.

[35] E. Cantatore, T. C. T. Geuns, G. H. Gelinck, E. van Veenendaal, A. F. A. Gruijthuijsen, L. Schrijnemakers, S. Drews, and D. M. de Leeuw, "A 13.56-MHz RFID System Based on Organic Transponders," *IEEE Journal of Solid-State Circuits*, vol. 42, no. 1, pp. 84 –92, Jan. 2007.

[36] S. H. Park, A. Roy, S. Beaupre, S. Cho, N. Coates, J. I. S. U. . Moon, D. Moses, M. Leclerc, K. Lee, And A. J. Heeger, "Bulk heterojunction solar cells with internal quantum efficiency approaching 100%," *Nature photonics*, vol. 3, no. 5, pp. 297–303, 2009.

[37] C. Longo, A. F. Nogueira, M.-A. De Paoli, and H. Cachet, "Solid-State and Flexible Dye-Sensitized TiO2 Solar Cells: a Study by Electrochemical Impedance Spectroscopy," *J. Phys. Chem. B*, vol. 106, no. 23, pp. 5925–5930, Jun. 2002.

[38] Y. Sun, G. C. Welch, W. L. Leong, C. J. Takacs, G. C. Bazan, and A. J. Heeger, "Solution-processed small-molecule solar cells with 6.7% efficiency," *Nat Mater*, vol. 11, no. 1, pp. 44–48, Jan. 2012.

[39] K. Tsakmakidis, “Molecular energy transfer,” *Nat Mater*, vol. 11, no. 12, pp. 1002–1002, Dec. 2012.

[40] G. P. Kittlesen, H. S. White, M. S. Wrighton, and E. Paul, “Opportunities For Electrochemical Sensors Using Microelectrode Devices.,” In *Electrochemical Society Extended Abstracts*, 1984, vol. 84–2, p. 800.

[41] M. Zirkl, A. Sawatdee, U. Helbig, M. Krause, G. Scheipl, E. Kraker, P. A. Ersman, D. Nilsson, D. Platt, P. Bodö, S. Bauer, G. Domann, and B. Stadlober, “An All-Printed Ferroelectric Active Matrix Sensor Network Based on Only Five Functional Materials Forming a Touchless Control Interface,” *Advanced Materials*, vol. 23, no. 18, pp. 2069–2074, 2011.

[42] Y. Miyahara, K. Tsukada, and H. Miyagi, “Field-effect transistor using a solid electrolyte as a new oxygen sensor,” *Journal of Applied Physics*, vol. 63, p. 2431, 1988.

[43] A. C. Arias, J. D. MacKenzie, I. McCulloch, J. Rivnay, and A. Salleo, “Materials and applications for large area electronics: solution-based approaches,” *Chemical reviews*, vol. 110, no. 1, p. 3, 2010.

[44] L. Kergoat, B. Piro, M. Berggren, G. Horowitz, and M.-C. Pham, “Advances in organic transistor-based biosensors: from organic electrochemical transistors to electrolyte-gated organic field-effect transistors,” *Analytical and Bioanalytical Chemistry*, vol. 402, no. 5, pp. 1813–1826, Sep. 2011.

[45] S. K. Arya, S. Saha, J. E. Ramirez-Vick, V. Gupta, S. Bhansali, and S. P. Singh, “Recent advances in ZnO nanostructures and thin films for biosensor applications: Review,” *Analytica Chimica Acta*, vol. 737, pp. 1–21, 2012.

[46] B. Fraboni, A. Ciavatti, F. Merlo, L. Pasquini, A. Cavallini, A. Quaranta, A. Bonfiglio, and A. Fraleoni-Morgera, “Organic Semiconducting Single Crystals as Next Generation of Low-Cost, Room-Temperature Electrical X-ray Detectors,” *Advanced Materials*, vol. 24, no. 17, pp. 2289–2293, 2012.

[47] N. C. Greenham, S. C. Moratti, D. D. C. Bradley, R. H. Friend, and A. B. Holmes, “Efficient light-emitting diodes based on polymers with high electron affinities,” *Nature*, vol. 365, no. 6447, pp. 628–630, Oct. 1993.

[48] R. R. Allison, V. S. Bagnato, and C. H. Sibata, “Future of oncologic photodynamic therapy,” *Future Oncology*, vol. 6, no. 6, pp. 929–940, Jun. 2010.

[49] R. Chesterfield, A. Johnson, C. Lang, M. Stainer, and J. Ziebarth, “Solution-Coating Technology for AMOLED Displays,” *Information Display*, vol. 1, no. 11, p. 11, 2011.

[50] I. Yagi, N. Hirai, Y. Miyamoto, M. Noda, A. Imaoka, N. Yoneya, K. Nomoto, J. Kasahara, A. Yumoto, and T. Urabe, “A flexible full-color AMOLED display driven by OTFTs,” *Journal of the Society for Information Display*, vol. 16, no. 1, pp. 15–20, 2008.

[51] A. Bedeloglu, A. Demir, Y. Bozkurt, and N. S. Sariciftci, “A flexible textile structure based on polymeric photovoltaics using transparent cathode,” *Synthetic Metals*, vol. 159, no. 19–20, pp. 2043–2048, Oct. 2009.

[52] M. Maccioni, E. Orgiu, P. Cosseddu, S. Locci, and A. Bonfiglio, “Towards the textile transistor: Assembly and characterization of an organic field effect transistor with a cylindrical geometry,” *Applied Physics Letters*, vol. 89, no. 14, pp. 143515–143515–3, Oct. 2006.

[53] C. Müller, M. Hamedi, R. Karlsson, R. Jansson, R. Marcilla, M. Hedhammar, and O. Inganäs, “Woven Electrochemical Transistors on Silk Fibers,” *Advanced Materials*, vol. 23, no. 7, pp. 898–901, 2011.

[54] W. Weng, T. Higuchi, M. Suzuki, T. Fukuoka, T. Shimomura, M. Ono, L. Radhakrishnan, H. Wang, N. Suzuki, H. Oveisi, and Y. Yamauchi, “A High-Speed Passive-Matrix Electrochromic Display Using a Mesoporous TiO2 Electrode with Vertical Porosity,” *Angewandte Chemie*, vol. 122, no. 23, pp. 4048–4051, 2010.

[55] C. K. Chiang, C. R. Fincher, Y. W. Park, A. J. Heeger, H. Shirakawa, E. J. Louis, S. C. Gau, and A. G. MacDiarmid, “Electrical Conductivity in Doped Polyacetylene,” *Phys. Rev. Lett.*, vol. 39, no. 17, pp. 1098–1101, Oct. 1977.

[56] A. J. Heeger, “Semiconducting and Metallic Polymers: The Fourth Generation of Polymeric Materials (Nobel Lecture),” *Angewandte Chemie International Edition*, vol. 40, no. 14, pp. 2591–2611, 2001.

[57] A. G. MacDiarmid, “Nobel Lecture: ‘Synthetic metals’: A novel role for organic polymers,” *Rev. Mod. Phys.*, vol. 73, no. 3, pp. 701–712, Sep. 2001.

[58] H. Shirakawa, “The Discovery of Polyacetylene Film: The Dawning of an Era of Conducting Polymers (Nobel Lecture),” *Angewandte Chemie International Edition*, vol. 40, no. 14, pp. 2574–2580, 2001.

[59] H. A. Klasens and H. Koelmans, “A tin oxide field-effect transistor,” *Solid-State Electronics*, vol. 7, no. 9, pp. 701–702, Sep. 1964.

[60] A. Aoki and H. Sasakura, “Tin Oxide Thin Film Transistors,” *Japanese Journal of Applied Physics*, vol. 9, no. 5, pp. 582–582, 1970.

[61] P. F. Carcia, R. S. McLean, M. H. Reilly, and G. Nunes, “Transparent ZnO thin-film transistor fabricated by rf magnetron sputtering,” *Applied Physics Letters*, vol. 82, no. 7, pp. 1117–1119, Feb. 2003.

[62] Y.-J. Chang, D.-H. Lee, G. S. Herman, and C.-H. Chang, “High-Performance, Spin-Coated Zinc Tin Oxide Thin-Film Transistors,” *Electrochem. Solid-State Lett.*, vol. 10, no. 5, pp. H135–H138, May 2007.

[63] R. L. Hoffman, B. J. Norris, and J. F. Wager, “ZnO-based transparent thin-film transistors,” *Applied Physics Letters*, vol. 82, no. 5, pp. 733 –735, Feb. 2003.

[64] L. L. Hench and J. K. West, “The sol-gel process,” *Chem. Rev.*, vol. 90, no. 1, pp. 33–72, Jan. 1990.

[65] C. Santato, M. Odziemkowski, M. Ulmann, and J. Augustynski, “Crystallographically Oriented Mesoporous WO3 Films: Synthesis, Characterization, and Applications,” *J. Am. Chem. Soc.*,, vol. 123, no. 43, pp. 10639–10649, Oct. 2001.

[66] D. Işık, M. Ak, and C. Durucan, “Structural, electrochemical and optical comparisons of tungsten oxide coatings derived from tungsten powder-based sols,” *Thin Solid Films*, vol. 518, no. 1, pp. 104–111, 2009.

[67] K. Shankar, G. K. Mor, H. E. Prakasam, S. Yoriya, M. Paulose, O. K. Varghese, and C. A. Grimes, “Highly-ordered TiO2 nanotube arrays up to 220 μm in length: use in water photoelectrolysis and dye-sensitized solar cells,” *Nanotechnology*, vol. 18, no. 6, p. 065707, 2007.

[68] M. Tomkiewicz, “The potential distribution at the TiO2 aqueous electrolyte interface,” *Journal of The Electrochemical Society*, vol. 126, no. 9, pp. 1505–1510, 1979.

[69] J. P. Randin, “Chemical and electrochemical stability of WO3 electrochromic films in liquid electrolytes,” *Journal of Electronic Materials*, vol. 7, no. 1, pp. 47–63, 1978.

[70] T. Tatsuma, S. Saitoh, Y. Ohko, and A. Fujishima, “TiO2-WO3 photoelectrochemical anticorrosion system with an energy storage ability,” *Chemistry of materials*, vol. 13, no. 9, pp. 2838–2842, 2001.

[71] W. Brütting, “Introduction to the Physics of Organic Semiconductors,” in in *Physics of Organic Semiconductors*, W. Brütting, Ed. Wiley-VCH Verlag GmbH & Co. KGaA, 2006, pp. 1–14.

[72] H. Klauk, *Organic Electronics II: More Materials and Applications*. John Wiley & Sons, 2012.

[73] N. Demirci Sankir, “Flexible electronics: Materials and device fabrication,” Ph.D., Virginia Polytechnic Institute and State University, United States -- Virginia, 2005.

[74] J.-M. Nunzi, “Organic photovoltaic materials and devices,” *Comptes Rendus Physique*, vol. 3, no. 4, pp. 523–542, 2002.

[75] M. Pope and C. E. Swenberg, *Electronic Processes in Organic Crystals and Polymers*, Second Edition. Oxford University Press, 1999.

[76] C. Goh and M. D. McGehee, “Organic Semiconductors for Low-Cost Solar Cells,” *The Bridge*, vol. 35, no. 4, pp. 33–39, 2005.

[77] I. Hisao, S. Kiyoshi, I. Eisuke, and S. Kazuhiko, “Energy Level Alignment and Interfacial Electronic Structures at Organic/Metal and Organic/Organic Interfaces,” *Advanced Materials*, vol. 11, no. 8, pp. 605–625, 1999.

[78] A. Troisi, “Prediction of the Absolute Charge Mobility of Molecular Semiconductors: the Case of Rubrene,” *Advanced Materials*, vol. 19, no. 15, pp. 2000–2004, 2007.

[79] A. Troisi and G. Orlandi, “Charge-Transport Regime of Crystalline Organic Semiconductors: Diffusion Limited by Thermal Off-Diagonal Electronic Disorder,” *Phys. Rev. Lett.*, vol. 96, no. 8, p. 086601, Mar. 2006.

[80] H. Klauk, “Organic thin-film transistors,” *Chemical Society Reviews*, vol. 39, no. 7, p. 2643, 2010.

[81] G. Paasch and S. Scheinert, “Charge carrier density of organics with Gaussian density of states: Analytical approximation for the Gauss–Fermi integral,” *Journal of Applied Physics*, vol. 107, no. 10, p. 104501, 2010.

[82] H. Bässler, “Charge Transport in Disordered Organic Photoconductors a Monte Carlo Simulation Study,” *physica status solidi (b)*, vol. 175, no. 1, pp. 15–56, 1993.

[83] T. Sakanoue and H. Sirringhaus, “Band-like temperature dependence of mobility in a solution-processed organic semiconductor,” *Nat Mater*, vol. 9, no. 9, pp. 736–740, Sep. 2010.

[84] O. D. Jurchescu, J. Baas, and T. T. M. Palstra, “Effect of impurities on the mobility of single crystal pentacene,” *Applied Physics Letters*, vol. 84, no. 16, pp. 3061–3063, Apr. 2004.

[85] O. Ostroverkhova, D. G. Cooke, S. Shcherbyna, R. F. Egerton, F. A. Hegmann, R. R. Tykwinski, and J. E. Anthony, “Bandlike transport in pentacene and functionalized pentacene thin films revealed by subpicosecond transient photoconductivity measurements,” *Phys. Rev. B*, vol. 71, no. 3, p. 035204, Jan. 2005.

[86] V. C. Sundar, J. Zaumseil, V. Podzorov, E. Menard, R. L. Willett, T. Someya, M. E. Gershenson, and J. A. Rogers, "Elastomeric Transistor Stamps: Reversible Probing of Charge Transport in Organic Crystals," *Science*, vol. 303, no. 5664, pp. 1644–1646, 2004.

[87] H. Bässler, "Localized states and electronic transport in single component organic solids with diagonal disorder," *physica status solidi (b)*, vol. 107, no. 1, pp. 9–54, 1981.

[88] H. Bässler, "Charge transport in molecularly doped polymers," *Philosophical Magazine Part B*, vol. 50, no. 3, pp. 347–362, 1984.

[89] C. V. Uglea and I. I. Negulescu, *Synthesis and characterization of oligomers*. CRC Press, 1991.

[90] J. Roncali, "Molecular Engineering of the Band Gap of π-Conjugated Systems: Facing Technological Applications," *Macromolecular Rapid Communications*, vol. 28, no. 17, pp. 1761–1775, 2007.

[91] C. J. Yang and S. A. Jenekhe, "Conjugated aromatic poly(azomethines). 1. Characterization of structure, electronic spectra, and processing of thin films from soluble complexes," *Chem. Mater.*, vol. 3, no. 5, pp. 878–887, Sep. 1991.

[92] I. F. Perepichka and D. F. Perepichka, *Handbook of Thiophene-Based Materials: Applications in Organic Electronics and Photonics, 2 Volume Set*. John Wiley & Sons, 2009.

[93] J. L. Bredas, R. Silbey, D. S. Boudreaux, and R. R. Chance, "Chain-length dependence of electronic and electrochemical properties of conjugated systems: polyacetylene, polyphenylene, polythiophene, and polypyrrole," *J. Am. Chem. Soc.*, vol. 105, no. 22, pp. 6555–6559, Oct. 1983.

[94] H. Meier, U. Stalmach, and H. Kolshorn, "Effective conjugation length and UV/vis spectra of oligomers," *Acta Polymerica*, vol. 48, no. 9, pp. 379–384, 1997.

[95] D. Işık, C. Santato, S. Barik, and W. G. Skene, "Charge-Carrier Transport in Thin Films of π-Conjugated Thiopheno-Azomethines," *Organic Electronics*, 2012.

[96] C. R. Swartz, S. R. Parkin, J. E. Bullock, J. E. Anthony, A. C. Mayer, and G. G. Malliaras, "Synthesis and characterization of electron-deficient pentacenes," *Organic Letters*, vol. 7, no. 15, pp. 3163–3166, 2005.

[97] O. L. Griffith, J. E. Anthony, A. G. Jones, and D. L. Lichtenberger, "Electronic Properties of Pentacene versus Triisopropylsilylethynyl-Substituted Pentacene: Environment-Dependent Effects of the Silyl Substituent," *Journal of the American Chemical Society*, vol. 132, no. 2, pp. 580–586, 2009.

[98] T. Okamoto, M. L. Senatore, M. M. Ling, A. B. Mallik, M. L. Tang, and Z. Bao, "Synthesis, Characterization, and Field-Effect Transistor Performance of Pentacene Derivatives," *Advanced Materials*, vol. 19, no. 20, pp. 3381–3384, 2007.

[99] A. Maliakal, K. Raghavachari, H. Katz, E. Chandross, and T. Siegrist, "Photochemical stability of pentacene and a substituted pentacene in solution and in thin films," *Chem. Mater*, vol. 16, no. 24, pp. 4980–4986, 2004.

[100] W. Osikowicz, M. P. de Jong, S. Braun, C. Tengstedt, M. Fahlman, and W. R. Salaneck, "Energetics at Au top and bottom contacts on conjugated polymers," *Appl. Phys. Lett.*, vol. 88, no. 19, pp. 193504–3, May 2006.

[101] B. Linkletter, "Molecular Orbital Tutorial." .

[102] M. Grigoras and N. Antonoaia, "Synthesis and characterization of some carbazole-based imine polymers," *European Polymer Journal*, vol. 41, no. 5, pp. 1079–1089, May 2005.

[103] M. Grigoras and C. O. Catanescu, "Imine oligomers and polymers," *Polymer Reviews*, vol. 44, no. 2, pp. 131–173, 2004.

[104] M. T. Greiner, M. G. Helander, W.-M. Tang, Z.-B. Wang, J. Qiu, and Z.-H. Lu, "Universal energy-level alignment of molecules on metal oxides," *Nat Mater*, vol. 11, no. 1, pp. 76–81, Jan. 2012.

[105] C. G. Granqvist, *Handbook of inorganic electrochromic materials*. Elsevier Science, 1995.

[106] S. Berglund and W. Sahle, "Accommodation of oxygen loss in WO3 equilibrated with CO + CO2 buffers," *Journal of Solid State Chemistry*, vol. 36, no. 1, pp. 66–73, Jan. 1981.

[107] W. Sahle, “Electron microscopy studies of W18O49. 1. Crystals formed by gaseous reduction of WO3,” *Journal of Solid State Chemistry*, vol. 45, no. 3, pp. 324–333, Dec. 1982.

[108] W. Sahle and M. Nygren, “Electrical conductivity and high resolution electron microscopy studies of WO3−x crystals with $0 \leq x \leq 0.28$,” *Journal of Solid State Chemistry*, vol. 48, no. 2, pp. 154–160, Jul. 1983.

[109] O. F. Schirmer and E. Salje, “Conduction bipolarons in low-temperature crystalline WO3-x,” *J. Phys. C: Solid State Phys.*, vol. 13, no. 36, p. L1067, Dec. 1980.

[110] J. M. Berak and M. J. Sienko, “Effect of oxygen-deficiency on electrical transport properties of tungsten trioxide crystals,” *Journal of Solid State Chemistry*, vol. 2, no. 1, pp. 109–133, Jun. 1970.

[111] Fenggong Wang, C. Di Valentin, and G. Pacchioni, “Semiconductor-to-metal transition in WO3-x: Nature of the oxygen vacancy,” *Physical Review B (Condensed Matter and Materials Physics)*, vol. 84, no. 7, p. 073103 (5 pp.), 2011.

[112] V. Wittwer, O. F. Schirmer, and P. Schlotter, “Disorder dependence and optical detection of the Anderson transition in amorphous HxWO3 bronzes,” *Solid State Communications*, vol. 25, no. 12, pp. 977–980, Mar. 1978.

[113] P. Lightsey, D. Lilienfeld, and D. Holcomb, “Transport properties of cubic Na_{x}WO_{3} near the insulator-metal transition,” *Physical Review B*, vol. 14, no. 10, pp. 4730–4732, Nov. 1976.

[114] R. Crandall and B. Faughnan, “Electronic Transport in Amorphous HxWO3,” *Physical Review Letters*, vol. 39, pp. 232–235, Jul. 1977.

[115] J. Molenda and A. Kubik, “Electrical Properties of Nonstoichiometric WO3−y at Temperatures 77 to 300 K,” *physica status solidi (b)*, vol. 191, no. 2, pp. 471–478, 1995.

[116] A. Coucou, A. Driouiche, M. Figlarz, M. Touboul, and G. Chevrier, “On the lacunar structure of pyrochlore-type WO3,” *Journal of Solid State Chemistry*, vol. 99, no. 2, pp. 283–289, Aug. 1992.

[117] S. K. Deb, “Opportunities and challenges in science and technology of WO3 for electrochromic and related applications,” *Solar Energy Materials and Solar Cells*, vol. 92, no. 2, pp. 245–258, Feb. 2008.

[118] H. Zheng, J. Z. Ou, M. S. Strano, R. B. Kaner, A. Mitchell, and K. Kalantar-zadeh, “Nanostructured Tungsten Oxide - Properties, Synthesis, and Applications,” *Advanced Functional Materials*, vol. 21, pp. 2175–2196, Jun. 2011.

[119] C. Balázsi, L. Wang, E. O. Zayim, I. M. Szilágyi, K. Sedlacková, J. Pfeifer, A. L. Tóth, and P.-I. Gouma, “Nanosize hexagonal tungsten oxide for gas sensing applications,” *Journal of the European Ceramic Society*, vol. 28, no. 5, pp. 913–917, 2008.

[120] R.-I. Stefan, J. F. van Staden, and H. Y. Aboul-Enein, “Electrochemical Sensor Arrays,” *Critical Reviews in Analytical Chemistry*, vol. 29, no. 2, pp. 133–153, 1999.

[121] M. Seibert, T. Flynn, D. Benson, E. Tracy, and M. Ghirardi, “Development of selection and screening procedures for rapid identification of H 2-producing algal mutants with increased O 2 tolerance,” *Biohydrogen*, pp. 227–234, 1999.

[122] M. L. Ghirardi, L. Zhang, J. W. Lee, T. Flynn, M. Seibert, E. Greenbaum, and A. Melis, “Microalgae: a green source of renewable H2,” *Trends in Biotechnology*, vol. 18, no. 12, pp. 506–511, Dec. 2000.

[123] M. Sadakane, K. Sasaki, H. Kunioku, B. Ohtani, W. Ueda, and R. Abe, “Preparation of nano-structured crystalline tungsten(VI) oxide and enhanced photocatalytic activity for decomposition of organic compounds under visible light irradiation,” *Chem. Commun.*, no. 48, pp. 6552–6554, Nov. 2008.

[124] R. Solarska, C. Santato, C. Jorand-Sartoretti, M. Ulmann, and J. Augustynski, “Photoelectrolytic oxidation of organic species at mesoporous tungsten trioxide film electrodes under visible light illumination,” *Journal of applied electrochemistry*, vol. 35, no. 7, pp. 715–721, 2005.

[125] C. Santato, M. Ulmann, and J. Augustynski, “Photoelectrochemical properties of nanostructured tungsten trioxide films,” *Journal of Physical Chemistry B*, vol. 105, no. 5, pp. 936–940, 2001.

[126] S.-H. Lee, R. Deshpande, P. A. Parilla, K. M. Jones, B. To, A. H. Mahan, and A. C. Dillon, "Crystalline WO3 Nanoparticles for Highly Improved Electrochromic Applications," *Advanced Materials*, vol. 18, no. 6, pp. 763–766, 2006.

[127] S. Tanisaki, "Crystal Structure of Monoclinic Tungsten Trioxide at Room Temperature," *Journal of the Physical Society of Japan*, vol. 15, no. 4, pp. 573–581, 1960.

[128] D. Bullett, "Bulk and surface electron states in WO3 and tungsten bronzes," *Journal of Physics C: Solid State Physics*, vol. 16, p. 2197, 1983.

[129] D. Gupta, M. Katiyar, and D. Gupta, "An analysis of the difference in behavior of top and bottom contact organic thin film transistors using device simulation," *Organic Electronics*, vol. 10, no. 5, pp. 775–784, Aug. 2009.

[130] I. Kymissis, C. D. Dimitrakopoulos, and S. Purushothaman, "High-performance bottom electrode organic thin-film transistors," *IEEE Transactions on Electron Devices*, vol. 48, no. 6, pp. 1060–1064, Jun.

[131] I. G. Hill, A. Rajagopal, A. Kahn, and Y. Hu, "Molecular level alignment at organic semiconductor-metal interfaces," *Applied Physics Letters*, vol. 73, no. 5, pp. 662–664, Aug. 1998.

[132] I. G. Hill, A. J. Makinen, and Z. H. Kafafi, "Initial stages of metal/organic semiconductor interface formation," *Journal of Applied Physics*, vol. 88, no. 2, pp. 889–895, 2000.

[133] F. Amy, C. Chan, and A. Kahn, "Polarization at the gold/pentacene interface," *Organic Electronics*, vol. 6, no. 2, pp. 85–91, Apr. 2005.

[134] H. Ishii, K. Sugiyama, E. Ito, and K. Seki, "Energy Level Alignment and Interfacial Electronic Structures at Organic/Metal and Organic/Organic Interfaces," *Advanced Materials*, vol. 11, no. 8, pp. 605–625, 1999.

[135] H. Ishii and K. Seki, "Energy level alignment at organic/metal interfaces studied by UV photoemission: breakdown of traditional assumption of a common vacuum level at the interface," *IEEE Transactions on Electron Devices*, vol. 44, no. 8, pp. 1295–1301, Aug.

[136] H. Vazquez, F. Flores, R. Oszwaldowski, J. Ortega, R. Perez, and A. Kahn, "Barrier formation at metal–organic interfaces: dipole formation and the charge neutrality level," *Applied surface science*, vol. 234, no. 1, pp. 107–112, 2004.

[137] L. Yan, N. J. Watkins, S. Zorba, Y. Gao, and C. W. Tang, "Thermodynamic equilibrium and metal-organic interface dipole," *Applied physics letters*, vol. 81, no. 15, pp. 2752–2754, 2002.

[138] Y. Shen, A. R. Hosseini, M. H. Wong, and G. G. Malliaras, "How To Make Ohmic Contacts to Organic Semiconductors," *ChemPhysChem*, vol. 5, no. 1, pp. 16–25, 2004.

[139] J. Zaumseil and H. Sirringhaus, "Electron and ambipolar transport in organic field-effect transistors," *Chemical reviews*, vol. 107, no. 4, pp. 1296–1323, 2007.

[140] Y.-Y. Liu, C.-L. Song, W.-J. Zeng, K.-G. Zhou, Z.-F. Shi, C.-B. Ma, F. Yang, H.-L. Zhang, and X. Gong, "High and Balanced Hole and Electron Mobilities from Ambipolar Thin-Film Transistors Based on Nitrogen-Containing Oligoacences," *J. Am. Chem. Soc.*, vol. 132, no. 46, pp. 16349–16351, Nov. 2010.

[141] M. L. Tang, A. D. Reichardt, N. Miyaki, R. M. Stoltenberg, and Z. Bao, "Ambipolar, High Performance, Acene-Based Organic Thin Film Transistors," *J. Am. Chem. Soc.*, vol. 130, no. 19, pp. 6064–6065, May 2008.

[142] J. E. Anthony, A. Facchetti, M. Heeney, S. R. Marder, and X. Zhan, "n-Type Organic Semiconductors in Organic Electronics," *Advanced Materials*, vol. 22, no. 34, pp. 3876–3892, 2010.

[143] J. Meyer, T. Winkler, S. Hamwi, S. Schmale, H.-H. Johannes, T. Weimann, P. Hinze, W. Kowalsky, and T. Riedl, "Transparent Inverted Organic Light-Emitting Diodes with a Tungsten Oxide Buffer Layer," *Advanced Materials*, vol. 20, no. 20, pp. 3839–3843, 2008.

[144] C. Tao, S. Ruan, G. Xie, X. Kong, L. Shen, F. Meng, C. Liu, X. Zhang, W. Dong, and W. Chen, "Role of tungsten oxide in inverted polymer solar cells," *Applied Physics Letters*, vol. 94, no. 4, pp. 043311–043311–3, Jan. 2009.

[145] M. Y. Chan, C. S. Lee, S. L. Lai, M. K. Fung, F. L. Wong, H. Y. Sun, K. M. Lau, and S. T. Lee, "Efficient organic photovoltaic devices using a combination of exciton blocking layer and anodic buffer layer," *Journal of Applied Physics*, vol. 100, no. 9, pp. 094506–094506–4, Nov. 2006.

[146] C. S. Beleznai, D. Vouagner, and J. P. Girardeau-Montaut, "Work function variation during UV laser-induced oxide removal," *Applied Surface Science*, vol. 138–139, pp. 6–11, Jan. 1999.

[147] J. Meyer, S. Hamwi, T. Bulow, H.-H. Johannes, T. Riedl, and W. Kowalsky, "Highly efficient simplified organic light emitting diodes," *Applied Physics Letters*, vol. 91, no. 11, pp. 113506 –113506–3, Sep. 2007.

[148] M. Gratzel, "Photoelectrochemical cells," *Nature*, vol. 414, no. 6861, pp. 338–344, Nov. 2001.

[149] L. Weinhardt, M. Blum, M. Bar, C. Heske, B. Cole, B. Marsen, and E. L. Miller, "Electronic Surface Level Positions of WO3 Thin Films for Photoelectrochemical Hydrogen Production," *J. Phys. Chem. C*, vol. 112, no. 8, pp. 3078–3082, Feb. 2008.

[150] G. D. Wilk, R. M. Wallace, and J. M. Anthony, "High-κ gate dielectrics: Current status and materials properties considerations," *Journal of Applied Physics*, vol. 89, no. 10, pp. 5243–5275, May 2001.

[151] J. Robertson, "High dielectric constant gate oxides for metal oxide Si transistors," *Rep. Prog. Phys.*, vol. 69, no. 2, p. 327, Feb. 2006.

[152] J. Wünsche, G. Tarabella, S. Bertolazzi, M. Bocoum, N. Coppedè, L. Barba, G. Arrighetti, L. Lutterotti, S. Iannotta, F. Cicoira, and C. Santato, "The correlation between gate dielectric, film growth, and charge transport in organic thin film transistors: the case of vacuum-sublimed tetracene thin films," *Journal of Materials Chemistry C*, vol. 1, no. 5, p. 967, 2013.

[153] H. Sirringhaus, P. J. Brown, R. H. Friend, M. M. Nielsen, K. Bechgaard, B. M. W. Langeveld-Voss, A. J. H. Spiering, R. A. J. Janssen, E. W. Meijer, P. Herwig, and D. M.

de Leeuw, “Two-dimensional charge transport in self-organized, high-mobility conjugated polymers,” *Nature*, vol. 401, no. 6754, pp. 685–688, 1999.

[154] D. T. Duong, M. F. Toney, and A. Salleo, “Role of confinement and aggregation in charge transport in semicrystalline polythiophene thin films,” *Phys. Rev. B*, vol. 86, no. 20, p. 205205, Nov. 2012.

[155] J. Rivnay, L. H. Jimison, J. E. Northrup, M. F. Toney, R. Noriega, S. Lu, T. J. Marks, A. Facchetti, and A. Salleo, “Large modulation of carrier transport by grain-boundary molecular packing and microstructure in organic thin films,” *Nature Materials*, vol. 8, no. 12, pp. 952–958, 2009.

[156] C. Wang, L. H. Jimison, L. Goris, I. McCulloch, M. Heeney, A. Ziegler, and A. Salleo, “Microstructural Origin of High Mobility in High-Performance Poly(thieno-thiophene) Thin-Film Transistors,” *Advanced Materials*, vol. 22, no. 6, pp. 697–701, 2010.

[157] J. Rivnay, M. F. Toney, Y. Zheng, I. V. Kauvar, Z. Chen, V. Wagner, A. Facchetti, and A. Salleo, “Unconventional Face-On Texture and Exceptional In-Plane Order of a High Mobility n-Type Polymer,” *Advanced Materials*, vol. 22, no. 39, pp. 4359–4363, 2010.

[158] A. Salleo, R. J. Kline, D. M. DeLongchamp, and M. L. Chabinyc, “Microstructural Characterization and Charge Transport in Thin Films of Conjugated Polymers,” *Advanced Materials*, vol. 22, no. 34, pp. 3812–3838, 2010.

[159] C. Tanase, E. J. Meijer, P. W. M. Blom, and D. M. de Leeuw, “Local charge carrier mobility in disordered organic field-effect transistors,” *Organic Electronics*, vol. 4, no. 1, pp. 33–37, Jun. 2003.

[160] S. Bertolazzi, J. Wnsche, F. Cicoira, and C. Santato, “Tetracene thin film transistors with polymer gate dielectrics,” *Applied Physics Letters*, vol. 99, no. 1, 2011.

[161] R. Ruiz, A. Papadimitratos, A. C. Mayer, and G. G. Malliaras, “Thickness Dependence of Mobility in Pentacene Thin-Film Transistors,” *Advanced Materials*, vol. 17, no. 14, pp. 1795–1798, 2005.

[162] A. Facchetti, M.-H. Yoon, and T. J. Marks, “Gate dielectrics for organic field-effect transistors: new opportunities for organic electronics,” *Advanced Materials*, vol. 17, no. 14, pp. 1705–1725, 2005.

[163] J. Veres, S. Ogier, G. Lloyd, and D. De Leeuw, “Gate insulators in organic field-effect transistors,” *Chemistry of materials*, vol. 16, no. 23, pp. 4543–4555, 2004.

[164] M.-H. Yoon, C. Kim, A. Facchetti, and T. J. Marks, “Gate dielectric chemical structure-organic field-effect transistor performance correlations for electron, hole, and ambipolar organic semiconductors,” *Journal of the American Chemical Society*, vol. 128, no. 39, pp. 12851–12869, 2006.

[165] S. C. Lim, S. H. Kim, J. H. Lee, M. K. Kim, D. J. Kim, and T. Zyung, “Surface-treatment effects on organic thin-film transistors,” *Synthetic Metals*, vol. 148, no. 1, pp. 75–79, Jan. 2005.

[166] S. K. Park, T. N. Jackson, J. E. Anthony, and D. A. Mourey, “High mobility solution processed 6,13-bis(triisopropyl-silylethynyl) pentacene organic thin film transistors,” *Appl. Phys. Lett.*, vol. 91, no. 6, pp. 063514–3, 2007.

[167] H. Sirringhaus, “Device Physics of Solution-Processed Organic Field-Effect Transistors,” *Advanced Materials*, vol. 17, no. 20, pp. 2411–2425, 2005.

[168] L.-L. Chua, J. Zaumseil, J.-F. Chang, E. C.-W. Ou, P. K.-H. Ho, H. Sirringhaus, and R. H. Friend, “General observation of n-type field-effect behaviour in organic semiconductors,” *Nature*, vol. 434, no. 7030, pp. 194–199, Mar. 2005.

[169] R. Atkin, S. Z. E. Abedin, R. Hayes, L. H. S. Gasparotto, N. Borisenko, and F. Endres, “AFM and STM Studies on the Surface Interaction of [BMP]TFSA and [EMIm]TFSA Ionic Liquids with Au(111),” *J. Phys. Chem. C*, vol. 113, no. 30, pp. 13266–13272, Jul. 2009.

[170] X. Zhang, Y.-X. Zhong, J.-W. Yan, Y.-Z. Su, M. Zhang, and B.-W. Mao, “Probing double layer structures of Au (111)–BMIPF6 ionic liquid interfaces from potential-dependent AFM force curves,” *Chem. Commun.*, vol. 48, no. 4, pp. 582–584, Dec. 2011.

[171] M. M. Islam, M. T. Alam, T. Okajima, and T. Ohsaka, “Electrical Double Layer Structure in Ionic Liquids: An Understanding of the Unusual Capacitance−Potential Curve at a Nonmetallic Electrode,” *J. Phys. Chem. C*, vol. 113, no. 9, pp. 3386–3389, Mar. 2009.

[172] S. Perkin, “Ionic liquids in confined geometries,” *Physical Chemistry Chemical Physics*, vol. 14, no. 15, p. 5052, 2012.

[173] E. Paek and G. S. Hwang, “Electrochemical Double Layer Structure at the Graphene/[BMIM][PF6] Interface: A Molecular Dynamics Study,” *ECS Transactions*, vol. 35, no. 34, pp. 217–226, 2011.

[174] M. Sha, G. Wu, Q. Dou, Z. Tang, and H. Fang, “Double-Layer Formation of [Bmim][PF6] Ionic Liquid Triggered by Surface Negative Charge,” *Langmuir*, vol. 26, no. 15, pp. 12667–12672, Aug. 2010.

[175] E. A. Meulenkamp, “Electron Transport in Nanoparticulate ZnO Films,” *J. Phys. Chem. B*, vol. 103, no. 37, pp. 7831–7838, 1999.

[176] H. Yuan, H. Shimotani, A. Tsukazaki, A. Ohtomo, M. Kawasaki, and Y. Iwasa, “High-Density Carrier Accumulation in ZnO Field-Effect Transistors Gated by Electric Double Layers of Ionic Liquids,” *Advanced Functional Materials*, vol. 19, no. 7, pp. 1046–1053, 2009.

[177] M. S. Kang, J. Lee, D. J. Norris, and C. D. Frisbie, “High Carrier Densities Achieved at Low Voltages in Ambipolar PbSe Nanocrystal Thin-Film Transistors,” *Nano Letters*, vol. 9, pp. 3848–3852, Nov. 2009.

[178] M. J. Panzer and C. D. Frisbie, “Exploiting Ionic Coupling in Electronic Devices: Electrolyte-Gated Organic Field-Effect Transistors,” *Advanced Materials*, vol. 20, no. 16, pp. 3177–3180, Aug. 2008.

[179] L. Herlogsson, Y.-Y. Noh, N. Zhao, X. Crispin, H. Sirringhaus, and M. Berggren, “Downscaling of Organic Field-Effect Transistors with a Polyelectrolyte Gate Insulator,” *Advanced Materials*, vol. 20, no. 24, pp. 4708–4713, 2008.

[180] J. N. Haddock, X. Zhang, S. Zheng, Q. Zhang, S. R. Marder, and B. Kippelen, "A comprehensive study of short channel effects in organic field-effect transistors," *Organic Electronics*, vol. 7, no. 1, pp. 45–54, Feb. 2006.

[181] W. Brütting, *Physics of Organic Semiconductors*. Weinheim: WILEY-VCH Verlag GmbH & Co. KGaA,, 2005.

[182] H. Klauk, M. Halik, U. Zschieschang, G. Schmid, W. Radlik, and W. Weber, "High-mobility polymer gate dielectric pentacene thin film transistors," *Journal of Applied Physics*, vol. 92, no. 9, pp. 5259–5263, Nov.

[183] C. D. Dimitrakopoulos, S. Purushothaman, J. Kymissis, A. Callegari, and J. M. Shaw, "Low-voltage organic transistors on plastic comprising high-dielectric constant gate insulators," *Science*, vol. 283, no. 5403, pp. 822–824, 1999.

[184] M. J. Panzer, C. R. Newman, and C. D. Frisbie, "Low-voltage operation of a pentacene field-effect transistor with a polymer electrolyte gate dielectric," *Applied Physics Letters*, vol. 86, p. 103503, 2005.

[185] H. Shimotani, H. Asanuma, A. Tsukazaki, A. Ohtomo, M. Kawasaki, and Y. Iwasa, "Insulator-to-metal transition in ZnO by electric double layer gating," *Applied Physics Letters*, vol. 91, no. 8, 2007.

[186] H. Ji, J. Wei, and D. Natelson, "Modulation of the Electrical Properties of VO2 Nanobeams Using an Ionic Liquid as a Gating Medium," *Nano Lett.*, vol. 12, no. 6, pp. 2988–2992, 2012.

[187] H. Shimotani, H. Suzuki, K. Ueno, M. Kawasaki, and Y. Iwasa, "P -type field-effect transistor of NiO with electric double-layer gating," *Applied Physics Letters*, vol. 92, no. 24, 2008.

[188] "IEEE Standard for Test Methods for the Characterization of Organic Transistors and Materials," *IEEE Std 1620-2008*, pp. 1 –14, 2008.

[189] D. K. Schroder, *Semiconductor Material and Device Characterization*. John Wiley & Sons, 2006.

[190] H. Ohno, *Electrochemical Aspects of Ionic Liquids*. John Wiley & Sons, 2011.

[191] Iolitec Inc., "Viscosities, electrochemical windows and ionic conductivities of the ILs were provided by Iolitec Inc: The viscosity of [EMIM][TFSI] is 39×10-2 Poise, at 20 °C, for [BMIM][TFSI] 49×10-2 Poise at 20 °C, and for [BMIM][PF6] it is 310×10-2 Poise at 20 °C.The ionic conductivity of [EMIM][TFSI] is 6.63 mS/cm, at 20 °C, for [BMIM][TFSI] 3.41 mS/cm at 20 °C, and for [BMIM][PF6] it is 1.37 mS/cm at 20 °C. Electrochemical windows for [EMIM][TFSI] it is 2.5 V /- 2.1 V, for [BMIM][TFSI] it is 2.6 V / - 2.1 V and for [BMIM][PF6] it is 2.2 V / - 1.8 V and vs Ag+/AgCl reference electrode."

[192] J. Leger, M. Berggren, and S. Carter, *Iontronics: Ionic Carriers in Organic Electronic Materials and Devices*. CRC Press, 2010.

[193] S. M. Sze and K. K. Ng, *Physics of Semiconductor Devices*. John Wiley & Sons, 2006.

[194] Y. Suzue, T. Manaka, and M. Iwamoto, "Current-Voltage Characteristics of Pentacene Films: Effect of UV/Ozone Treatment on Au Electrodes," *Japanese Journal of Applied Physics*, vol. 44, no. 1B, pp. 561–565, 2005.

[195] S. Y. Kim, J.-L. Lee, K.-B. Kim, and Y.-H. Tak, "Effect of ultraviolet–ozone treatment of indium–tin–oxide on electrical properties of organic light emitting diodes," *Journal of Applied Physics*, vol. 95, no. 5, pp. 2560–2563, Mar. 2004.

[196] B. D. Cullity, *Elements of X-ray diffraction*. Addison-Wesley Pub. Co., 1956.

[197] D. Basu, "Charge transport in polymer semiconductors," Ph.D., The University of Texas at Austin, United States -- Texas, 2007.

[198] J. Rivnay, R. Steyrleuthner, L. H. Jimison, A. Casadei, Z. Chen, M. F. Toney, A. Facchetti, D. Neher, and A. Salleo, "Drastic Control of Texture in a High Performance n-Type Polymeric Semiconductor and Implications for Charge Transport," *Macromolecules*, vol. 44, no. 13, pp. 5246–5255, Jul. 2011.

[199] L. Lutterotti and P. Scardi, "Simultaneous structure and size-strain refinement by the Rietveld method," *Journal of applied Crystallography*, vol. 23, no. 4, pp. 246–252, 1990.

[200] N. Petkov, S. Mintova, B. Jean, T. Metzger, and T. Bein, “Functionalized cubic mesostructured silica films,” *Materials Science and Engineering: C*, vol. 23, no. 6–8, pp. 827–831, Dec. 2003.

[201] Veeco Instruments Inc., “A Practical Guide to Scanning Probe Microscopy (SPM),” 2005. [Online]. Available: http://www.veeco.com/pdfs/library/SPM_Guide_0829_05_166.pdf. [Accessed: 02-Jan-2013].

[202] J. M. Lerner, “Imaging spectrometer fundamentals for researchers in the biosciences—a tutorial,” *Cytometry Part A*, vol. 69, no. 8, pp. 712–734, 2006.

[203] J. Goldstein, D. Newbury, D. Joy, C. Lyman, P. Echlin, E. Lifshin, L. Sawyer, and J. Michael, *Scanning Electron Microscopy and X-ray Microanalysis*, 3rd ed. 2003. Corr. 4th printing. Springer, 2003.

[204] J. Chen, J. Anthony, and D. C. Martin, “Thermally Induced Solid-State Phase Transition of Bis(triisopropylsilylethynyl) Pentacene Crystals,” *The Journal of Physical Chemistry B*, vol. 110, no. 33, pp. 16397–16403, 2006.

[205] Z. Bao and J. Locklin, *Organic Field-Effect Transistors*. CRC Press, 2007.

[206] R. Y. C. Shin, P. Sonar, P. S. Siew, Z.-K. Chen, and A. Sellinger, “Electron-Accepting Conjugated Materials Based on 2-Vinyl-4,5-dicyanoimidazoles for Application in Organic Electronics,” *J. Org. Chem.*, vol. 74, no. 9, pp. 3293–3298, May 2009.

[207] C. Santato, I. Manunza, A. Bonfiglio, F. Cicoira, P. Cosseddu, R. Zamboni, and M. Muccini, “Tetracene light-emitting transistors on flexible plastic substrates,” *Applied Physics Letters*, vol. 86, no. 14, pp. 141106–141106–3, 2005.

[208] Z. Liang, Q. Tang, J. Xu, and Q. Miao, “Soluble and Stable N-Heteropentacenes with High Field-Effect Mobility,” *Advanced Materials*, vol. 23, no. 13, pp. 1535–1539, 2011.

[209] D. J. Gundlach, L. Zhou, J. A. Nichols, T. N. Jackson, P. V. Necliudov, and M. S. Shur, “An experimental study of contact effects in organic thin film transistors,” *Journal of Applied Physics*, vol. 100, no. 2, pp. 024509 –024509–13, Jul. 2006.

[210] M. Ling, Z. Bao, P. Erk, M. Koenemann, and M. Gomez, “Complementary inverter using high mobility air-stable perylene di-imide derivatives,” *Applied Physics Letters*, vol. 90, no. 9, pp. 093508 –093508–3, Feb. 2007.

[211] Y.-F. Lim, Y. Shu, S. R. Parkin, J. E. Anthony, and G. G. Malliaras, “Soluble n-type pentacene derivatives as novel acceptors for organic solar cells,” *Journal of Materials Chemistry*, vol. 19, no. 19, pp. 3049–3056, 2009.

[212] M.-Y. Kuo, H.-Y. Chen, and I. Chao, “Cyanation: Providing a Three-in-One Advantage for the Design ofn-Type Organic Field-Effect Transistors,” *Chem. Eur. J.*, vol. 13, no. 17, pp. 4750–4758, Jun. 2007.

[213] L. Lutterotti, “Total pattern fitting for the combined size-strain-stress-texture determination in thin film diffraction,” *Nuclear Instruments and Methods in Physics Research Section B: Beam Interactions with Materials and Atoms*, vol. 268, no. 3–4, pp. 334–340, 2010.

[214] “Electrochemical analyses were performed with a BAS i-Epsilon voltammetric analyzer in a three electrode cell configuration consisting of silver wire as a pseudo reference electrode, platinum button as the working electrode and platinum wire as counter electrode, using a 0.1M solution of tetrabutylammonium hexafluorophosphate in dichloromethane and a scan rate of 50 mV/s. Oxidation and reduction potentials were calibrated with respect to ferrocene/ferrocenium redox couple.” .

[215] M. L. Tang, A. D. Reichardt, P. Wei, and Z. Bao, “Correlating Carrier Type with Frontier Molecular Orbital Energy Levels in Organic Thin Film Transistors of Functionalized Acene Derivatives,” *Journal of the American Chemical Society*, vol. 131, no. 14, pp. 5264–5273, Apr. 2009.

[216] S. Milita, M. Servidori, F. Cicoira, C. Santato, and A. Pifferi, “Synchrotron X-ray investigation of tetracene thin films grown at different deposition fluxes,” *Nuclear Instruments and Methods in Physics Research, Section B: Beam Interactions with Materials and Atoms*, vol. 246, no. 1, pp. 101–105, 2006.

[217] F. Cicoira, C. M. Aguirre, and R. Martel, “Making Contacts to n-Type Organic Transistors Using Carbon Nanotube Arrays,” *ACS Nano*, vol. 5, no. 1, pp. 283–290, Jan. 2011.

[218] A. Salleo, “Charge transport in polymeric transistors,” *Materials Today*, vol. 10, no. 3, pp. 38–45, Mar. 2007.

[219] I. McCulloch, M. Heeney, M. L. Chabinyc, D. DeLongchamp, R. J. Kline, M. Cölle, W. Duffy, D. Fischer, D. Gundlach, B. Hamadani, R. Hamilton, L. Richter, A. Salleo, M. Shkunov, D. Sparrowe, S. Tierney, and W. Zhang, “Semiconducting Thienothiophene Copolymers: Design, Synthesis, Morphology, and Performance in Thin-Film Organic Transistors,” *Advanced Materials*, vol. 21, no. 10–11, pp. 1091–1109, 2009.

[220] L. H. Jimison, A. Salleo, M. L. Chabinyc, D. P. Bernstein, and M. F. Toney, “Correlating the microstructure of thin films of poly[5,5-bis(3-dodecyl-2-thienyl)-2,2-bithiophene] with charge transport: Effect of dielectric surface energy and thermal annealing,” *Phys. Rev. B*, vol. 78, no. 12, p. 125319, Sep. 2008.

[221] A. Zen, J. Pflaum, S. Hirschmann, W. Zhuang, F. Jaiser, U. Asawapirom, J. P. Rabe, U. Scherf, and D. Neher, “Effect of Molecular Weight and Annealing of Poly(3-hexylthiophene)s on the Performance of Organic Field-Effect Transistors,” *Advanced Functional Materials*, vol. 14, no. 8, pp. 757–764, 2004.

[222] A. Bolduc, S. Dufresne, and W. G. Skene, “EDOT-containing azomethine: An easily prepared electrochromically active material with tuneable colours,” *Journal of Materials Chemistry*, vol. 20, no. 23, pp. 4820–4826, 2010.

[223] A. Bolduc, V. Lachapelle, and W. G. Skene, “Snap Together Bonds for Amine Capturing – New Spectroscopic and Amperometric Sensors,” *Macromolecular Symposia*, vol. 297, no. 1, pp. 87–93, 2010.

[224] A. Bolduc, S. Dufresne, G. S. Hanan, and W. G. Skene, “Synthesis, photophysics, and electrochemistry of thiophene–pyridine and thiophene–pyrimidine dyad comonomers,” *Canadian Journal of Chemistry*, vol. 88, no. 3, pp. 236–246, 2010.

[225] S. Dufresne, A. Bolduc, and W. G. Skene, “Towards materials with reversible oxidation and tuneable colours using heterocyclic conjugated azomethines,” *Journal of Materials Chemistry*, vol. 20, no. 23, pp. 4861–4866, 2010.

[226] S. Barik, S. Bishop, and W. G. Skene, “Spectroelectrochemical and electrochemical investigation of a highly conjugated all-thiophene polyazomethine,” *Materials Chemistry and Physics*, vol. 129, no. 1–2, pp. 529–533, 2011.

[227] S. Dufresne and W. G. Skene, “Optoelectronic property tailoring of conjugated heterocyclic azomethines – the effect of pyrrole, thiophene and furans,” *Journal of Physical Organic Chemistry*, vol. 25, no. 3, pp. 211–221, 2012.

[228] T. Greene and P. G. M. Wuts, *Protective Groups in Organic Synthesis*, Second. New York: John Wiley and Sons, Inc., 1991.

[229] K.-H. Lee, K. Morino, A. Sudo, and T. Endo, “Preparation and properties of a novel polythiophene, poly[(3-hexyliminomethyl)thiophene] with a high regioregularity,” *Journal of Polymer Science Part A: Polymer Chemistry*, vol. 49, no. 5, pp. 1190–1194, 2011.

[230] J.-C. Chen, Y.-C. Liu, J.-J. Ju, C.-J. Chiang, and Y.-T. Chern, “Synthesis, characterization and hydrolysis of aromatic polyazomethines containing non-coplanar biphenyl structures,” *Polymer*, vol. 52, no. 4, pp. 954–964, 2011.

[231] L. Marin, E. Perju, and M. D. Damaceanu, “Designing thermotropic liquid crystalline polyazomethines based on fluorene and/or oxadiazole chromophores,” *European Polymer Journal*, vol. 47, no. 6, pp. 1284–1299, 2011.

[232] F.-C. Tsai, C.-C. Chang, C.-L. Liu, W.-C. Chen, and S. A. Jenekhe, “New Thiophene-Linked Conjugated Poly(azomethine)s: Theoretical Electronic Structure, Synthesis, and Properties,” *Macromolecules*, vol. 38, no. 5, pp. 1958–1966, Mar. 2005.

[233] F. B. L. Cougnon and J. K. M. Sanders, “Evolution of Dynamic Combinatorial Chemistry,” *Accounts of Chemical Research*, p. 10.1021/ar200240m, 2011.

[234] N. Giuseppone, G. Fuks, and J.-M. Lehn, “Tunable Fluorene-Based Dynamers through Constitutional Dynamic Chemistry,” *Chemistry - A European Journal*, vol. 12, no. 6, pp. 1723–1735, 2006.

[235] T. Ono, S. Fujii, T. Nobori, and J.-M. Lehn, “Optodynamers: expression of color and fluorescence at the interface between two films of different dynamic polymers,” *Chem. Commun.*, no. 42, pp. 4360–4362, 2007.

[236] J. F. Folmer-Andersen, E. Buhler, S. J. Candau, S. Joulie, M. Schmutz, and J. M. Lehn, “Cooperative, bottom-up generation of rigid-rod nanostructures through dynamic polymer chemistry,” *Polymer International*, vol. 59, no. 11, pp. 1477–1491, 2010.

[237] N. Kiriy, V. Bocharova, A. Kiriy, M. Stamm, F. C. Krebs, and H.-J. Adler, “Designing Thiophene-Based Azomethine Oligomers with Tailored Properties: Self-assembly and Charge Carrier Mobility,” *Chemistry of Materials*, vol. 16, no. 23, pp. 4765–4771, Kasım 2004.

[238] G. J. Ashwell, L. J. Phillips, B. J. Robinson, B. Urasinska-Wojcik, C. J. Lambert, I. M. Grace, M. R. Bryce, R. Jitchati, M. Tavasli, T. I. Cox, I. C. Sage, R. P. Tuffin, and S. Ray, “Molecular Bridging of Silicon Nanogaps,” *ACS Nano*, vol. 4, no. 12, pp. 7401–7406, Dec. 2010.

[239] S. H. Choi and C. D. Frisbie, “Enhanced Hopping Conductivity in Low Band Gap Donor−Acceptor Molecular Wires Up to 20 nm in Length,” *Journal of the American Chemical Society*, vol. 132, no. 45, pp. 16191–16201, Nov. 2010.

[240] S. H. Choi, C. Risko, M. C. R. Delgado, B. Kim, J.-L. Brédas, and C. D. Frisbie, “Transition from Tunneling to Hopping Transport in Long, Conjugated Oligo-imine Wires Connected to Metals,” *Journal of the American Chemical Society*, vol. 132, no. 12, pp. 4358–4368, Mar. 2010.

[241] A. Iwan, Z. Mazurak, B. Kaczmarczyk, B. Jarzabek, and D. Sek, “Synthesis and characterization of polyketanils with 3,8-diamino-6-phenylphenanthridine moieties exhibiting light emitting properties: Molecular and supramolecular engineering concept,” *Spectrochimica Acta Part A: Molecular and Biomolecular Spectroscopy*, vol. 69, no. 2, pp. 291–303, 2008.

[242] A. Iwan, M. Palewicz, A. Chuchmała, L. Gorecki, A. Sikora, B. Mazurek, and G. Pasciak, “Opto(electrical) properties of new aromatic polyazomethines with fluorene moieties in the

main chain for polymeric photovoltaic devices," *Synthetic Metals*, vol. 162, no. 1–2, pp. 143–153, 2012.

[243] M. Palewicz, A. Iwan, M. Sibinski, A. Sikora, and B. Mazurek, "Organic photovoltaic devices based on polyazomethine and fullerene," *Energy Procedia*, vol. 3, no. 0, pp. 84–91, 2011.

[244] T. Tshibaka, S. Bishop, I. U. Roche, S. Dufresne, W. D. Lubell, and W. G. Skene, "Conjugated 4-Methoxybipyrrole Thiophene Azomethines: Synthesis, Opto-Electronic Properties, and Crystallographic Characterization," *Chemistry - A European Journal*, vol. 17, no. 39, pp. 10879–10888, 2011.

[245] A. Bolduc, S. Dufresne, and W. G. Skene, "Chemical doping of EDOT azomethine derivatives: insight into the oxidative and hydrolytic stability," *J. Mater. Chem.*, vol. 22, pp. 5053–5064, 2012.

[246] W. G. Skene and S. Dufresne, "Easy One-Pot Synthesis of Energy Transfer Cassettes," *Organic Letters*, vol. 6, no. 17, pp. 2949–2952, 2004.

[247] M. Bourgeaux and W. G. Skene, "Photophysics and electrochemistry of conjugated oligothiophenes prepared by using azomethine connections," *Journal of Organic Chemistry*, vol. 72, no. 23, pp. 8882–8892, 2007.

[248] M. Bourgeaux and W. G. Skene, "A highly conjugated p- and n-type polythiophenoazomethine: Synthesis, spectroscopic, and electrochemical investigation," *Macromolecules*, vol. 40, no. 6, pp. 1792–1795, 2007.

[249] N. G. Connelly and W. E. Geiger, "Chemical Redox Agents for Organometallic Chemistry," *Chemical Reviews*, vol. 96, no. 2, pp. 877–910, 1996.

[250] R. B. K. Siram, K. Tandy, M. Horecha, P. Formanek, M. Stamm, S. Gevorgyan, F. C. Krebs, A. Kiriy, P. Meredith, P. L. Burn, E. B. Namdas, and S. Patil, "Synthesis and Self-Assembly of Donor–Acceptor–Donor Based Oligothiophenes and Their Optoelectronic Properties," *The Journal of Physical Chemistry C*, vol. 115, no. 29, pp. 14369–14376, Jul. 2011.

[251] S.-Y. Jang, B. Lim, B.-K. Yu, J. Kim, K.-J. Baeg, D. Khim, and D.-Y. Kim, "Synthesis and characterization of low-band-gap poly(thienylenevinylene) derivatives for polymer solar cells," *J. Mater. Chem.*, vol. 21, no. 32, pp. 11822–11830, Aug. 2011.

[252] J. R. Lakowicz, *Principles of Fluorescence Spectroscopy*, 4th Printing. Springer, 2006.

[253] S.-W. Hwang and Y. Chen, "Synthesis and Electrochemical and Optical Properties of Novel Poly(aryl ether)s with Isolated Carbazole and p-Quaterphenyl Chromophores," *Macromolecules*, vol. 34, no. 9, pp. 2981–2986, Apr. 2001.

[254] C. Wang, H. Dong, W. Hu, Y. Liu, and D. Zhu, "Semiconducting π-Conjugated Systems in Field-Effect Transistors: A Material Odyssey of Organic Electronics," *Chem. Rev.*, 2011.

[255] A. Facchetti, "π-Conjugated Polymers for Organic Electronics and Photovoltaic Cell Applications†," *Chem. Mater.*, vol. 23, no. 3, pp. 733–758, 2010.

[256] Y. Li, S. P. Singh, and P. Sonar, "A High Mobility P-Type DPP-Thieno[3,2-b]thiophene Copolymer for Organic Thin-Film Transistors," *Advanced Materials*, vol. 22, no. 43, pp. 4862–4866, 2010.

[257] H. Pan, Y. Li, Y. Wu, P. Liu, B. S. Ong, S. Zhu, and G. Xu, "Low-Temperature, Solution-Processed, High-Mobility Polymer Semiconductors for Thin-Film Transistors," *Journal of the American Chemical Society*, vol. 129, no. 14, pp. 4112–4113, Apr. 2007.

[258] X. Guo, R. P. Ortiz, Y. Zheng, Y. Hu, Y.-Y. Noh, K.-J. Baeg, A. Facchetti, and T. J. Marks, "Bithiophene-Imide-Based Polymeric Semiconductors for Field-Effect Transistors: Synthesis, Structure−Property Correlations, Charge Carrier Polarity, and Device Stability," *Journal of the American Chemical Society*, vol. 133, no. 5, pp. 1405–1418, 2011.

[259] S. Wen, J. Pei, P. Li, Y. Zhou, W. Cheng, Q. Dong, Z. Li, and W. Tian, "Synthesis and photovoltaic properties of low-bandgap 4,7-dithien-2-yl-2,1,3-benzothiadiazole-based poly(heteroarylenevinylene)s," *Journal of Polymer Science Part A: Polymer Chemistry*, vol. 49, no. 12, pp. 2715–2724, 2011.

[260] F. C. Krebs and M. Jorgensen, "The effect of fluorination in semiconducting polymers of the polyphenyleneimine type," *Synthetic Metals*, vol. 142, no. 1–3, pp. 181–185, 2004.

[261] N. Karl, “Charge carrier transport in organic semiconductors,” *Synthetic Metals*, vol. 133–134, no. 0, pp. 649–657, 2003.

[262] M. Turbiez, P. Frère, M. Allain, C. Videlot, J. Ackermann, and J. Roncali, “Design of Organic Semiconductors: Tuning the Electronic Properties of π-Conjugated Oligothiophenes with the 3,4-Ethylenedioxythiophene (EDOT) Building Block,” *Chemistry - A European Journal*, vol. 11, no. 12, pp. 3742–3752, 2005.

[263] C. Santato, F. Rosei, and others, “Organic/metal interfaces: seeing both sides.,” *Nature chemistry*, vol. 2, no. 5, p. 344, 2010.

[264] S. H. Kim, K. Hong, W. Xie, K. H. Lee, S. Zhang, T. P. Lodge, and C. D. Frisbie, “Electrolyte-Gated Transistors for Organic and Printed Electronics,” *Adv. Mater.*, vol. 25, no. 13, pp. 1822–1846, 2013.

[265] T. Fujimoto and K. Awaga, “Electric-Double-Layer Field-Effect Transistors with Ionic Liquids,” *Phys. Chem. Chem. Phys.*, vol. in Press, Apr. 2013.

[266] G. Tarabella, F. M. Mohammadi, N. Coppedè, F. Barbero, S. Iannotta, C. Santato, and F. Cicoira, “New opportunities for organic electronics and bioelectronics: ions in action,” *Chem. Sci.*, vol. 4, p. 1395, 2013.

[267] S. Thiemann, S. Sachnov, S. Porscha, P. Wasserscheid, and J. Zaumseil, “Ionic Liquids for Electrolyte-Gating of ZnO Field-Effect Transistors,” *The Journal of Physical Chemistry C*, vol. 116, no. 25, pp. 13536–13544, 2012.

[268] W. H. Brattain and J. Bardeen, “Surface Properties of Germanium,” *Bell Sys.Tech.*, vol. 32, pp. 1–41, 1953.

[269] S. Baldelli, “Surface Structure at the Ionic Liquid−Electrified Metal Interface,” *Acc. Chem. Res.*, vol. 41, no. 3, pp. 421–431, Mar. 2008.

[270] See supplementary material for morphological and structural properties of WO_3 thin films and of transistor characteristics.

[271] M. Galiński, A. Lewandowski, and I. Stepniak, “Ionic liquids as electrolytes,” *Electrochim. Acta*, vol. 51, no. 26, pp. 5567–5580, 2006.

[272] Electrochemical windows for [EMIM][TFSI] is 2.5 V/- 2.1 V, for [BMIM][TFSI] is 2.6 V/- 2.1 V and for [BMIM][PF6] is 2.2 V/-1.8 V vs Ag/AgCl reference electrode. Data provided by Iolitec Inc.

[273] B. E. Conway, *Electrochemical supercapacitors: scientific fundamentals and technological applications (POD)*. Kluwer Academic/plenum. New York, 1999.

[274] M. Lazzari, C. Arbizzani, F. Soavi, and M. Mastragostino, "EDLCs Based on Solvent-Free Ionic Liquids," in in *Supercapacitors*, F. Béguin and E. Frąckowiak, Eds. Wiley-VCH Verlag GmbH & Co. KGaA, 2013, pp. 289–306.

[275] $\mu_{Sat} = \frac{2L}{WC}\left(\frac{\partial\sqrt{I_{DS}}}{\partial V_{GS}}\right)^2_{V_{DS}=const>V_{GS}-V_{Th}}$

[276] J. Li, M. Yahiro, K. Ishida, H. Yamada, and K. Matsushige, "Enhanced performance of organic light emitting device by insertion of conducting/insulating WO3 anodic buffer layer," *Synthetic Metals*, vol. 151, no. 2, pp. 141–146, Jun. 2005.

[277] D. Lupo, W. Clemens, S. Breitung, and K. Hecker, "OE-A Roadmap for Organic and Printed Electronics," in in *Applications of Organic and Printed Electronics*, E. Cantatore, Ed. Springer US, 2013, pp. 1–26.

[278] Y. S. Nanayakkara, S. Perera, S. Bindiganavale, E. Wanigasekara, H. Moon, and D. W. Armstrong, "The Effect of AC Frequency on the Electrowetting Behavior of Ionic Liquids," *Anal. Chem.*, vol. 82, no. 8, pp. 3146–3154, Apr. 2010.

[279] E. Wanigasekara, X. Zhang, Y. Nanayakkara, T. Payagala, H. Moon, and D. W. Armstrong, "Linear Tricationic Room-Temperature Ionic Liquids: Synthesis, Physiochemical Properties, and Electrowetting Properties," *ACS Appl. Mater. Interfaces*, vol. 1, no. 10, pp. 2126–2133, Oct. 2009.

[280] J. J. Segura, A. Elbourne, E. J. Wanless, G. G. Warr, K. Voïtchovsky, and R. Atkin, "Adsorbed and near surface structure of ionic liquids at a solid interface," *Physical Chemistry Chemical Physics*, vol. 15, no. 9, p. 3320, 2013.

[281] V. Lockett, R. Sedev, J. Ralston, M. Horne, and T. Rodopoulos, "Differential Capacitance of the Electrical Double Layer in Imidazolium-Based Ionic Liquids: Influence of Potential,

Cation Size, and Temperature," *J. Phys. Chem. C*, vol. 112, no. 19, pp. 7486–7495, May 2008.

[282] M. V. Fedorov, N. Georgi, and A. A. Kornyshev, "Double layer in ionic liquids: The nature of the camel shape of capacitance," *Electrochemistry Communications*, vol. 12, no. 2, pp. 296–299, Feb. 2010.

[283] M. Z. Bazant, B. D. Storey, and A. A. Kornyshev, "Double Layer in Ionic Liquids: Overscreening versus Crowding," *Phys. Rev. Lett.*, vol. 106, no. 4, p. 046102, Jan. 2011.

[284] M. D. Hanwell, D. E. Curtis, D. C. Lonie, T. Vandermeersch, E. Zurek, and G. R. Hutchison, "Avogadro: an advanced semantic chemical editor, visualization, and analysis platform," *Journal of Cheminformatics*, vol. 4, no. 1, p. 17, Aug. 2012.

[285] Blender Foundation, *Blender 3D Animation Program*. 2013.

[286] B. Harrington, D. Yip, M. Albert, J. Andler, T. Bah, and P. Barbry-Blot, *Inkscape*. 2012.

[287] Spencer Kimball and Peter Mattis, *GIMP - The GNU Image Manipulation Program*. 2012.

[288] R. Brewster, E. Harvey, T. Jackson, Z. Walker, and D. Issel, *Paint.NET - Free Software for Digital Photo Editing*. 2011.